



UNIVERSITÀ DI PISA

Facoltà di Ingegneria

Dipartimento di Ingegneria Civile ed Industriale

**Numerical study on the blending of Immiscible  
Liquids in static mixer**

Supervisors :

Prof. Elisabetta Brunazzi

Prof. Mark Simmons

Prof. Chiara Galletti

Candidate :

Domenico Daraio

Master's Degree in Chemical Engineering

Academic Year 2015/2016



*“Most people say that it is the intellect which makes a great scientist. They are wrong: it is character”*

Albert Einstein

Equipped with his five senses, man explores the universe around him and calls the adventure Science.

Edwin Powell Hubble

# Abstract

Department of Civil and Industrial Engineering

Master Thesis in Chemical Engineering

## **Numerical study on the blending of Immiscible Liquids in static mixer**

Domenico Daraio

The present work is focused on a better understanding of both mixing processes in static mixer for immiscible liquids (oil-in-water emulsion) and the most important parameters affecting the mixing performance. In particular, the goals of this work were to obtain information about the break up of oil drops in water from a 2D multiphase model and to obtain information both on the velocity field and the shear stress field, from a 3D single-phase model with 6 Kenics static mixer (KM). To this purpose, numerical simulations were performed for a simple 2D model and a more complex 3D model, by using RANS ( Reynolds Averaged Navier-Stokes) model. Salome 7.5.1 an open source software has been used to draw and mesh the geometries while Parafoam (OpenFoam tool) and Matlab have been used for the post-processing of the numerical solution. Three Reynolds Number have been tested, with the continuous phase velocity ranging from 0.1m/s to 0.9 m/s and by using as input into the numerical models density, viscosity and the surface tension for both the phases.

# Contents

<b>Abstract</b> .....	iv
<b>Contents</b> .....	v
<b>List of Figures</b> .....	viii
<b>List of Tables</b> .....	x
<b>Symbols</b> .....	xi
<b>Introduction</b> .....	<b>1</b>
1.1 Objectives and aims .....	1
1.2 Structure of the thesis.....	3
<b>Literature Review</b> .....	<b>4</b>
2.1 Introduction .....	4
2.2 Immiscible Liquid-Liquid Systems .....	4
2.2.1 Fundamentals .....	4
2.2.2 Emulsions.....	5
2.2.3 Droplet breakup mechanism .....	12
2.2.3.1 Breakup in a laminar flow.....	13
2.2.3.2 Breakup in a turbulence flow .....	14
2.3 Mixing equipment.....	16
2.3.1 Introduction.....	16
2.3.2 Mixing of immiscible liquids in Stirred Tank.....	17
2.3.3 Mixing of immiscible liquids in Static Mixer .....	18
2.4 Computational fluid dynamic for mixing .....	23
2.4.1 Introduction .....	23
2.4.2 Conservation Equations .....	24
2.4.2.1 Continuity Equation.....	24
2.4.2.2 Momentum Equation .....	25
2.4.2.3 Species Equation.....	26
2.4.2.4 Energy Equation.....	26
2.4.3 Numerical Methods .....	27
2.4.3.1 Discretization of the domain : Grid generation .....	28
2.4.3.2 Discretization of the Equations .....	30

2.4.3.3 Discretization schemes .....	31
2.4.3.4 Final Discretized Equation .....	34
2.4.3.5 Solution Methods .....	34
2.4.4 Structure of OpenFoam .....	35
<b>Materials &amp; Methods .....</b>	<b>37</b>
3.1 Introduction .....	37
3.2 Geometry and Mesh .....	37
3.2.1 2D Geometry .....	38
3.2.2 3D Geometry .....	39
3.3 Grid Independence .....	41
3.3.1 Flow field Independence .....	42
3.3.2 Numerical diffusion .....	45
3.4 Settings 2D Multi-phase Model .....	47
3.4.1 Choice of the Solver .....	47
3.4.2 Choice of the turbulence Model.....	47
3.4.3 Set-up of the Initial Conditions & Physical properties in input .....	49
3.4.4 Utility SetFields .....	49
3.5 Settings 3D Single-phase Model .....	50
3.5.1 Choice of the Solver .....	50
3.5.2 Choice of the turbulence Model.....	50
3.5.3 Set-up of the Initial Conditions & Physical properties in input .....	51
3.6 Cluster BlueBear .....	51
<b>Results .....</b>	<b>53</b>
4.1 Introduction .....	53
4.2 2D Multi-phase Results .....	53
4.2.1 Analysis of the oil drop surface.....	55
4.2.2 Streamlines analysis.....	63
4.3 3D Single-phase Results .....	74
4.3.1 3D Streamlines analysis .....	74
4.3.2 Analysis of the coefficient of variation (CoV) .....	81
4.3.3 3D flow field.....	85
<b>Conclusions.....</b>	<b>92</b>
5.1 Future work .....	94
<b>Appendix A .....</b>	<b>95</b>

OpenFoam Turbulence Model ( 2D Multi-phase model) .....	95
OpenFoam Turbulence Properties ( 2D Multi-phase model) .....	95
OpenFoam RAS Properties ( 2D Multi-phase model) .....	96
ControlDict file ( 2D Multi-phase model) .....	97
FvSchemes file ( 2D Multi-phase model) .....	98
FvSolution file ( 2D Multi-phase model).....	99
SetFields file ( 2D Multi-phase model) .....	101
ControlDict file ( 3D Single-phase model) .....	102
DecomposeParDict file ( 3D Single-phase model) .....	103
FvSchemes file ( 3D Single-phase model).....	104
FvSchemes file ( 3D Single-phase model).....	105
Job submitted for BlueBear .....	107
<b>REFERENCES.....</b>	<b>108</b>
<b>Ringraziamenti .....</b>	<b>113</b>

# List of Figures

Figure 1	Energy gap in the emulsification process.....	7
Figure 2	Overview of the main breakdown processes.....	8
Figure 3	Schematics of Eletrostatic stabilization.....	10
Figure 4	Schematics of steric stabilization (left) , Schematics of depletion stabilization (right) .....	11
Figure 5	Schematics of electrosteric stabilization.....	11
Figure 6	Elements of different commercial static mixers .....	20
Figure 7	Conservation equation .....	225
Figure 8	Element types for computational grids.....	28
Figure 9	Types of meshes: (a) structured, (b) unstructured, and (c) block-structured.....	29
Figure 12	OpenFoam structure .....	35
Figure 13	2D Geometry .....	38
Figure 14	2D Mesh (a) , (b) .....	39
Figure 15	Section pipe + static mixer .....	40
Figure 16	Kenics static mixer.....	40
Figure 17	Kenics static mixer mesh .....	41
Figure 18	Skewness error on the face .....	42
Figure 19	Points for the grid independence.....	43
Figure 20	Grid Independence for velocity of 0.1m/s.....	44
Figure 21	Numerical diffusion for cells with $0 < C < 1$ .....	46
Figure 22	Flow field for 0.1m/s .....	54
Figure 23	Drop re-built with Matlab (a) , Drop image from simulation (b).....	56
Figure 24	Steps of the Matlab Script.....	56
Figure 25	Shear stress (a) and energy dissipation (b) on the oil drop surface.....	58
Figure 26	Link between shear stress , energy dissipation and deformation.....	60
Figure 27	Global analysis on the shear stress .....	61
Figure 28	Local approach vs Global approach.....	62
Figure 29	Streamlines studied (a) , all the streamlines (b).....	64
Figure 30	Distributions of shear stress (a) and energy turbulence dissipation (b) .....	65
Figure 31	Energy turbulence dissipation distribution at different velocity .....	66
Figure 32	Shear stress distribution at different velocity.....	67
Figure 33	Drop path (a) , Matlab reconstruction for a specific time (b) at velocity of 0.1m/s .....	68
Figure 34	Drop path (a) , Matlab reconstruction for a specific time (b) at velocity of 0.5m/s .....	69
Figure 35	Drop path (a) , Matlab reconstruction for a specific time (b) at velocity of 0.9m/s .....	70
Figure 36	Energy profile for the streamlines, changing the continuous phase velocity .....	71
Figure 37	Residence time profile changing the continuous phase velocity.....	72
Figure 38	Residence time profile for different velocity, changing the streamlines.....	73
Figure 39	ZY pipe section, seeding points to create the streamlines.....	75
Figure 40	Streamlines paths for 0.1m/s (a) , for 0.5m/s (b) and for 0.9m/s (c).....	76

Figure 41 Velocity on X direction for 0.1m/s (a) , for 0.5m/s (b) , for 0.9m/s (c) .....	77
Figure 42 3D Energy profile for different velocity with 6 Kenics static mixer .....	78
Figure 43 3D shear stress trend for different velocity with 6 Kenics static mixer .....	78
Figure 44 3D residence time profile with 6 Kenics static mixer .....	79
Figure 45 Residence Time profile for all the velocity, by using 2000 streamlines .....	80
Figure 46 Energy CoV by using 6 Kenics static mixer .....	82
Figure 47 Shear stress CoV for 0.1m/s (a) , for 0.5m/s (b) , for 0.9m/s (c) .....	83
Figure 48 The velocity CoV by using 6 Kenics static mixer .....	85
Figure 49 3D velocity field with 6 Kenics static mixer (Magnitude of the velocity) .....	87
Figure 50 Streamlines on the ZY pipe section for all the velocities (with 6 Kenics static mixer) .....	90

# List of Tables

Table 1	Classification of emulsion types .....	5
Table 2	Comparison between features of static mixer and stirred tank .....	17
Table 3	Lists manufacturers .....	19
Table 4	Values of $K_L$ and $K_T$ for different static mixer (Streiff 1997).....	22
Table 5	Summary of Discretization Schemes .....	33
Table 6	Grid characteristics.....	42
Table 7	New Grid to avoid the numerical diffusion .....	46
Table 8	Reynolds number .....	48
Table 9	Physical Properties .....	49
Table 10	Study of the drop break up .....	57
Table 11	Drop re-building with Matlab.....	57
Table 12	Comparison between the $K_T$ parameters.....	91

# Symbols

U	Surface Energy
A	Surface area
$\sigma$	Interface tension
T	Temperature
$\Delta S$	Entropy variation
$\Delta G$	Gibbs Energy variation
$\Delta P$	Pressure drop
$\Delta W$	Work to expand the interface
R	Radius of a sphere
$\tau$	External stress
Re	Reynolds number
$\rho$	Density
v	Superficial velocity
D	Diameter of a pipe
$\mu_c$	Dynamic viscosity of the continuous phase
$\nu_c$	Kinematic viscosity of the continuous phase
Ca	Capillary number
We	Weber number
$\dot{\gamma}$	shear strain
$\varepsilon$	Energy turbulence dissipation rate
$\dot{\varepsilon}$	Extensional rate
$P_L$	Capillary pressure
L	Pipe length
d	Diameter of a drop
$\lambda_K$	Kolmogorov scale
$C_K$	Kolmogorov constant
f	Fanning friction factor

$J_{i,j}$	Diffusion flux of species i in the mixture
$R_i$	Consumption or production term for reactions
$S_i$	General source term
$m_i$	Mass of the i- species
$K_{eff}$	Effective conductivity
$\phi$	Generic scalar property
$\Gamma$	Diffusion coefficient
$A_i$	Coefficient in the discretized equation
$C$	Fraction function for the VOF method
Cov	Coefficient of variance

Alla mia famiglia

# Chapter 1

---

## Introduction

### 1.1 Objectives and aims

The purpose of the present thesis is to deepen the knowledge about mixing of immiscible fluids in static mixer. These devices are important in several industrial processes and their use has become increasingly widespread thanks to their versatility and the low running costs. Mixing is the most fundamental process among all industrial chemical processes, ranging from simple blending, to mixing of complex multiphase reaction systems. In many cases static or dynamic mixers are widely used for mixing immiscible liquids. However, static mixers are applied more often than stirrers due to lower operating costs.

Experimental studies of the two-phase flow field are difficult because intrusive techniques can disturb the flow. On the other hand, enormous capability of Computational Fluid Dynamics (CFD) codes has been exploited in modern investigations of two-phase liquid-liquid flow. However, despite of the high potential of CFD and increasing number of papers on liquid-liquid flows, the flows are yet not sufficiently studied. This is due to the complexity of two-phase liquid-liquid flows.

This thesis is the following step of a previous experimental work (Giuseppe Forte 2015 :“Use of PLIF to investigate of immiscible liquids in static mixer”) where Planar Laser Induced Fluorescence (PLIF) technique has been used to characterize the drop size of the emulsion after passing through the mixing elements. During the experimental work a strange behaviour of the droplet diameter distributions has been found. Indeed for low values of the continuous phase velocity ranging from 0.16m/s to 0.5m/s the size of the droplets has been found decreases, hence a better dispersion is obtained. While increasing the continuous phase velocity from 0.5m/s to 0.9m/s the droplet diameter distributions change behaviour with the droplet size that increases with the velocity.

Hence, the purpose of this work is to clarify the dependence of the mixing performance in term of droplet break up with the continuous phase velocity, by means of numerical simulations. Indeed the numerical tool allows for computing flow structure, local flow and turbulence of both phases and their interaction. Basically, the objective of the research is to create a numerical model for a deeper understanding of the mixing process and the main parameters affecting the mixing performance.

For achieving this purpose a software called OpenFoam has been used (OpenFOAM®). The OpenFOAM® (Open Field Operation and Manipulation) CFD Toolbox is a free, open source CFD software package which has a large user base across most areas of engineering and science. OpenFOAM has an extensive range of features to solve anything from complex fluid flows involving chemical reactions, turbulence and heat transfer, to solid dynamics and electromagnetics. Several steps are necessary to build a numerical model, such as the choice of the solver, the choice of the turbulence model, the creation of the geometry and the mesh. The first performed model is a 2D multiphase model, where the continuous phase is water and the disperse phase is oil. In this case the geometry is a simple pipe with baffles, to balance the numerical complexity of the multi-phase model. Basically, local information on the velocity field and the shear stress field come from this model, which can follow an oil droplet to study the break up phenomenon. This preliminary step is fundamental to generalize the droplet's behaviour and link it to the continuous phase velocity and make energy considerations. The second performed model is a 3D single-phase model which simulates the flow in a real geometry, 6 Kenics static mixer. This equipment has been used during a previous experimental work. In this case, the idea is to obtain the flow field in presence of static mixer and try to understand what can happen if we have an oil droplet in these conditions of velocity and shear stress.

## 1.2 Structure of the thesis

This dissertation consists of five chapters:

In the present chapter, the motivation and the goal of this work are discussed. The topic of the research is introduced and the outline of the numerical simulations briefly illustrated.

Chapter 2 presents the state of the art in this field. Basic but fundamental information are provided for the development of the study. First, basic emulsion stability principles, including information about emulsification processes, surfactants, and the most important emulsion breakdown mechanisms are discussed. Then the most employed mixing equipment are presented enlightening the advantages of continuous motionless devices. Finally, the keys concept of a numerical simulations are explained.

In the Chapter 3 the numerical approach is described. The setting, procedures and software employed in this work are presented in details.

Chapter 4 is about the analysis part of the research. In the first part the 2D results are presented and are compared with the experimental results come from a previous work, therefore Matlab post-processing is necessary to re-build the oil drop and study its surface. Then a streamlines analysis is carry on to explain and demonstrate some trends. In the second part the 3D results are presented and a study to characterize the flow field is showed. In this case, to generalise the final results a statistical approach is used, involving the coefficient of variation (CoV) .

Chapter 5 summarizes the conclusions of this study and suggests recommendations for further research.

# Chapter 2

---

## Literature Review

### 2.1 Introduction

This chapter contains a review of the current literature on the fundamentals of immiscible liquid liquid systems and in particular on the equipment and detection systems applied in the mixing processes. In the first section of this chapter, the emulsion nature is analysed focusing on the droplet breakup mechanism. In the following part, two different approaches to the dispersing process are shown: the batch stirred tank and the continuous devices. Amongst the latter the static mixers are described in detail presenting the several commercial models. At last, articles on CFD applications are reviewed focusing onto the structure of a numerical model.

### 2.2 Immiscible Liquid-Liquid Systems

#### 2.2.1 Fundamentals

The term *immiscible liquid-liquid system* refers to two or more mutually insoluble liquids present as separate phases. When the two phases are liquids, the system itself is named emulsion. In an emulsion is possible to identify a dispersed or drop phase and a continuous or matrix phase, in which the dispersed phase is commonly smaller in volume than the continuous phase (Lemenand, Habchi et al. 2014). Emulsions are meta-stable systems (Cramer, Fischer et al. 2004) well known in the manufacture industry. Applications are found extensively throughout the chemical, petroleum, and pharmaceutical industries. Examples include nitration, sulfonation, alkylation, hydrogenation, and halogenation. The petroleum industry depends on efficient coalescence processing to remove aqueous brine drops in crude refinery feed streams to prevent severe corrosion of processing equipment. Control of mean drop size and drop size distribution (DSD) is vital to emulsification and suspension polymerization

applications. Unfortunately, fundamental research on emulsions is not easy because model systems are difficult to produce (Das, Legrand et al. 2005). In many cases, theories on emulsion stability are not exact and semi-empirical approaches are used.

## 2.2.2 Emulsions

Emulsions are a class of disperse systems consisting of two immiscible liquids. As Tadros summarizes in his overview (Tadros, Th.F. and Vincent, B. (1983) in *Encyclopedia of Emulsion Technology*), several emulsion classes may be distinguished: oil-in-water (O/W), water-in-oil (W/O), and oil-in-oil (O/O). The latter class may be exemplified by an emulsion consisting of a polar oil (e.g., propylene glycol) dispersed in a nonpolar oil (paraffinic oil) and vice versa. To disperse two immiscible liquids, one needs a third component, namely, the emulsifier. The choice of the emulsifier is crucial in the formation of the emulsion and its long-term stability. Other two classifications of emulsions can be done. Accordingly to the nature of emulsifier :

---

Nature of emulsifier	Structure of the system
Simple molecules and ions W/O	Nature of internal and external phase: O/W,
Nonionic surfactants	—
Surfactant mixtures	Micellar emulsions (microemulsions)
Ionic surfactants	Macroemulsions
Nonionic polymers	Bilayer droplets
Polyelectrolytes	Double and multiple emulsions
Mixed polymers and surfactants	Mixed emulsions
Liquid crystalline phases	—
Solid particles	—

---

**Table 1 Classification of emulsion types**

The third classification accordingly to the drop size of the dispersed phase:

- O/W and W/O macroemulsions: size range of 0.1–5  $\mu\text{m}$  with an average of 1–2  $\mu\text{m}$ ;
- Nanoemulsions: size range of 20–100 nm. Similar to macroemulsions, they are only kinetically stable;
- Micellar emulsions or microemulsions: these usually have the size range of 5–50 nm. They are thermodynamically stable;

- Double and multiple emulsions: these are emulsions-of-emulsions, W/O/W, and O/W/O systems;
- Mixed emulsions: these are systems consisting of two different disperse droplets that do not mix in a continuous medium.

The two fundamental processes occurring during emulsification are drop breakup and drop coalescence (Rueger and Calabrese 2013). These are concurrent processes, and the relative rates of the two mechanisms determine the final drop size (Tcholakova, Denkov et al. 2004). Surfactants can influence both these processes: by reducing the interfacial tension and interfacial energy, thereby promoting rupture, and by providing a barrier to coalescence via interactions between the adsorbed layers on two colliding drops (Lobo and Svereika 2003).

When two incompatible components forming an interface upon mixing, if a stable interface is formed the free energy of formation must be positive. This behavior finds its expression in a special form of the Gibbs-Helmholtz equation :

$$U^S = \sigma - T \cdot \left(\frac{\partial \sigma}{\partial T}\right)_S, \quad \text{for most systems } \left(\frac{\partial \sigma}{\partial T}\right)_S < 0 \quad (1)$$

Where  $U^S$  is the total surface energy for a given interface (S),  $\sigma$  is the interfacial tension, and T is the absolute temperature. This leads to conclude that the preparation of emulsions requires energy to disperse the organic phase (solvent or solution) in water (Tadros, Izquierdo et al. 2004). The increase in the energy of an emulsion compared to the nonemulsified components is equal to  $\Delta W$ , where  $\Delta W$  is the work required to expand the interfacial area. This amount of energy can be considered as a measure of the thermodynamic instability of an emulsion.

$$\Delta W = \sigma \cdot \Delta A \quad (2)$$

Where  $\Delta A$  is the increase of the interfacial area when the drop with surface A1 splits producing a large number of drops with total area A2; and  $\Delta W$  is the free energy of the interface and corresponds to the reversible work brought permanently into the system during the emulsification process. This makes an emulsion very prone to coalescence processes which lead to a decrease in  $\Delta A$  and subsequently in  $\Delta W$ . The conclusion is straightforward that ultimate stability against coalescence processes is only achieved if  $\sigma$  approaches zero. Once again it is important to underline that in the absence of any stabilization mechanism, the emulsion has a high probability to break by one of the phenomena discussed later.

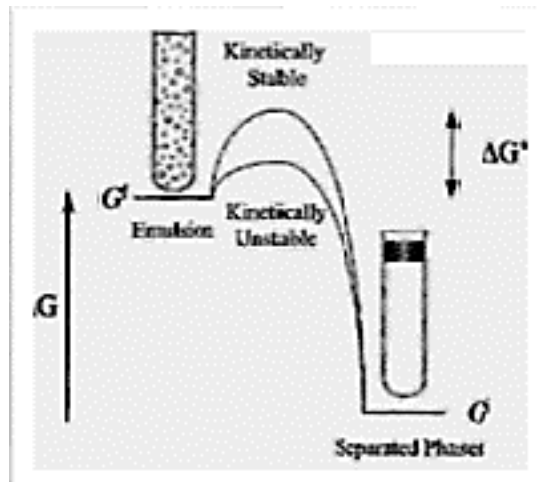


**Figure 1** Energy gap in the emulsification process

In Figure 1 the energy gap between the separate phases condition and the dispersed condition is represented. In the chart,  $\Delta G^*$  is the energetic barrier due to the eventual presence of the emulsifier that has the role of avoiding the return to the low energy condition. It is a well-known phenomenon that surfactants, even at low concentration, influence strongly the droplet formation (Fischer and Erni 2007). They help to control the oil droplet size by reducing the interfacial tension and decreasing coalescence by affecting interfacial mobility. The drop formation in the actual process is due mainly to the Kelvin-Helmholtz instability (Kiss, Brenn et al. 2011), a phenomenon that takes place when two fluids, with different densities, move in parallel flows (Thomson 1871). This mechanism was also found in spray formation by pre-filming atomizers (Dorfner et al., 1995).

But several processes relating to the breakdown of emulsions may occur on storage, depending on:

- the particle size distribution and the density difference between the droplets and the medium; .
- the magnitude of the attractive versus repulsive forces, which determines flocculation;
- the solubility of the disperse droplets and the particle size distribution, which in turn determines Ostwald ripening;
- The stability of the liquid film between the droplets, which determines coalescence; and phase inversion.

The various breakdown processes are illustrated schematically in Figure 2. The physical phenomena involved in each breakdown process are not simple, and require an analysis to be

made of the various surface forces involved. In addition, the breakdown processes may take place simultaneously rather than consecutively, which in turn complicates the analysis.

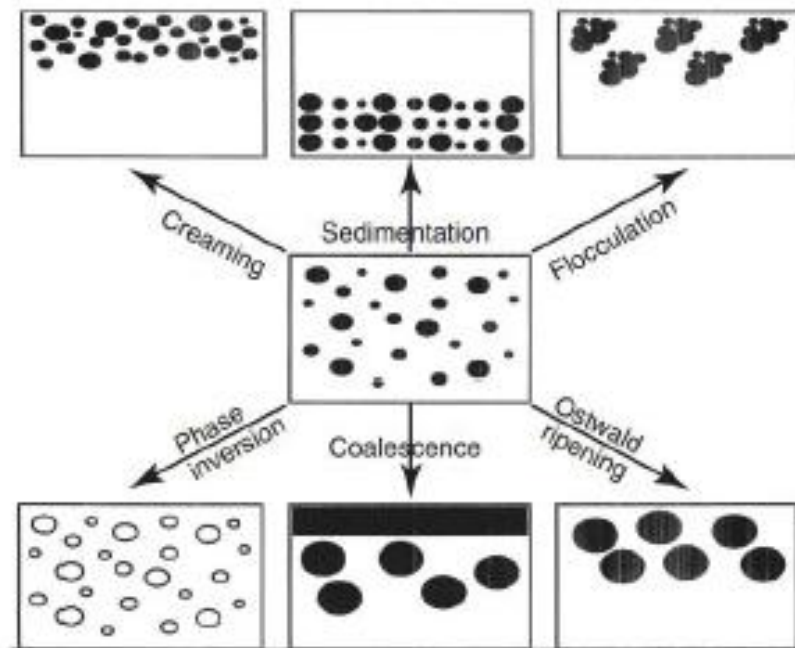


**Figure 2** Overview of the main breakdown processes

A summary of each of the above breakdown processes is provided in the following sections, together with details of each process and methods for its prevention.

### **Creaming and Sedimentation**

This process results from external forces, usually gravitational or centrifugal. When such forces exceed the thermal motion of the droplets (Brownian motion), a concentration gradient builds up in the system such that the larger droplets move more rapidly either to the top (if their density is less than that of the medium) or to the bottom (if their density is greater than that of the medium) of the container. In the limiting cases, the droplets may form a close-packed (random or ordered) array at the top or bottom of the system, with the remainder of the volume occupied by the continuous liquid phase.

### **Flocculation**

This process refers to aggregation of the droplets (without any change in primary droplet size) into larger units. It is the result of the van der Waals attractions, which are universal with all

disperse systems. Flocculation occurs when there is not sufficient repulsion to keep the droplets apart at distances where the van der Waals attraction is weak. Flocculation may be either 'strong' or 'weak', depending on the magnitude of the attractive energy involved.

### **Ostwald Ripening (Disproportionation)**

This effect results from the finite solubility (etc.) of the liquid phases. Liquids that are referred to as being 'immiscible' often have mutual solubilities which are not negligible. With emulsions, which are usually polydisperse, the smaller droplets will have a greater solubility when compared to larger droplets (due to curvature effects). With time, the smaller droplets disappear and their molecules diffuse to the bulk and become deposited on the larger droplets. With time, the droplet size distribution shifts to larger values.

### **Coalescence**

This refers to the process of thinning and disruption of the liquid film between the droplets, with the result that fusion of two or more droplets occurs to form larger droplets. The limiting case for coalescence is the complete separation of the emulsion into two distinct liquid phases. The driving force for coalescence is the surface or film fluctuations; this results in a close approach of the droplets whereby the van der Waals forces are strong and prevent their separation.

### **Phase Inversion**

This refers to the process whereby there will be an exchange between the disperse phase and the medium. For example, an O/W emulsion may with time or change of conditions invert to a W/O emulsion. In many cases, phase inversion passes through a transition state whereby multiple emulsions are produced.

Preventing the occurrence of those phenomena is crucial for the long term stability of the emulsion, in this, adsorbed surfactants exert their role. Since there are always strong, long-range attractive forces between similar colloidal particles, it is necessary to provide a long range repulsion between the particles to impart stability.

Stability can be obtained with several mechanisms :

- With an electrical double layer (electrostatic or charge stabilization).
- With adsorbed or chemically attached polymeric molecules (steric stabilization).
- With free polymer in the dispersion medium (depletion stabilization).

Combination of the first two stabilization mechanisms lead to electrosteric stabilization. The latter two types of stabilization are often realized by the addition of polymers to stabilize dispersions and are called polymeric stabilization.

**Electrostatic stabilization** consists in ionic groups that can adsorb to the surface of a colloidal particle through different mechanisms to form a charged layer. The idea is to counterbalance the Van der Waals attraction between colloidal particles in polar liquids providing the particles with Coulombic repulsion. In liquid dispersion media, to maintain electroneutrality, an equal number of counterions with the opposite charge will surround the colloidal particles and give rise to overall charge-neutral double layers. In charge stabilization, it is the mutual repulsion of these double layers surrounding particles that provides stability. But one great disadvantage of charge stabilization of particles is its great sensitivity to the ionic strength of the dispersion medium. In addition it only works in polar liquid which can dissolve electrolytes. However, due to the advantages in simplicity and cost price, charge stabilization is still widely used in stabilizing dispersions in aqueous media. (D.H. Napper, Academic Press, London, 1983.)

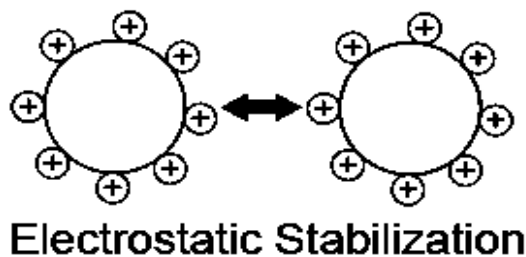


**Figure 3** Schematics of Electrostatic stabilization

Steric stabilization and depletion stabilization are two different mechanisms accepted for polymeric stabilization of colloidal dispersion. For polymers with molecular weights  $>10000$  D, the chain dimensions are comparable to, or in excess of, the range of the Van der Waals attraction. Hence, as long as they can generate repulsion, these polymer molecules can be used to impart colloid stability (D.H. Napper, Academic Press, London, 1983.) .

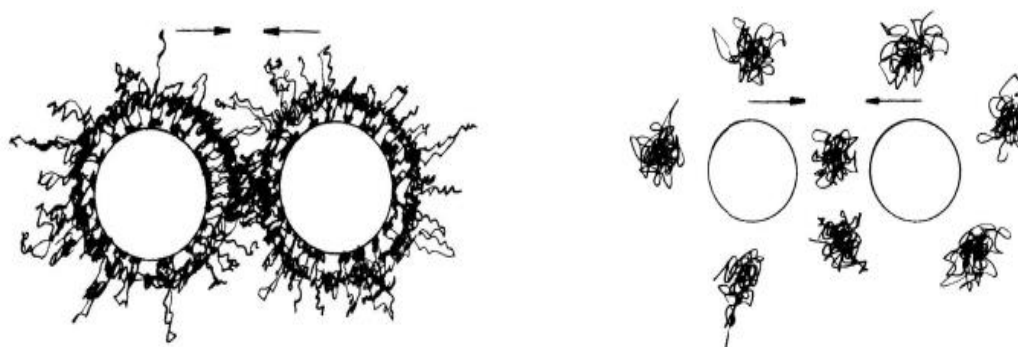


**Figure 4** Schematics of steric stabilization (left) , Schematics of depletion stabilization (right)

**Steric stabilization** of colloidal particles is achieved by attaching (grafting or chemisorption) macromolecules to the surfaces of the particles (figure 1.1). The stabilization due to the adsorbed layers on the dispersed particle is generally called steric stabilization.

**Depletion stabilization** of colloidal particles is imparted by macromolecules that are free in solution (figure 1.2). The study of this type of stabilization is still in its initial stage. Electrostatic and steric stabilization can be combined as *electrosteric stabilization*. The origin of the electrostatic component may be a net charge on the particle surface (Figure 1.3a) and/or charges associated with the polymer attached to the surface (i.e. through an attached polyelectrolyte) (Figure 1.3b).

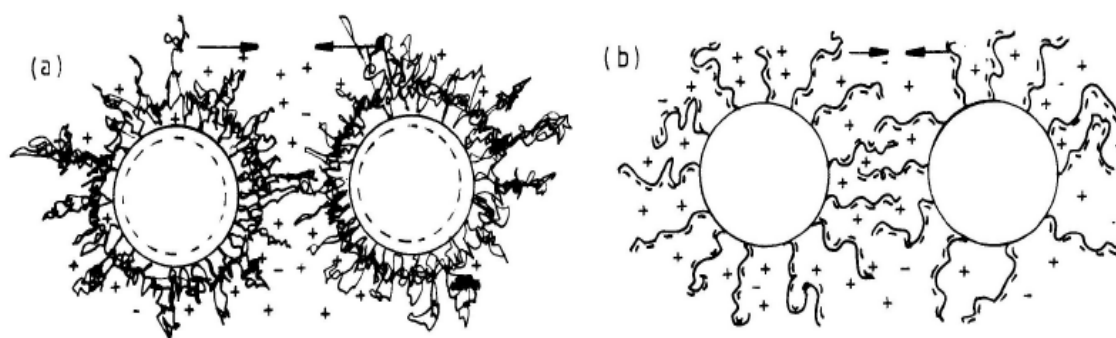


**Figure 5** Schematics of electrosteric stabilization: (a) charged particles with nonionic polymers; (b) polyelectrolytes attached to uncharged particles.

### 2.2.3 Droplet breakup mechanism

The prediction and the control of the final drop size of the dispersed phase require a deep analysis of the droplet breakup mechanisms. Since this difficulty in achieving the satisfying final dimension, the processes are commonly conducted in turbulent regime. Turbulent particles breakup has been the subject of an ongoing investigation, beginning with the pioneering work of Kolmogorov (1949) and Hinze (1955). Many efforts have been done in this field for understanding the turbulent dispersions in stirred tanks and pipelines (Shinnar 1961, Sleicher 1962, Arai 1977, Calabrese 1986a, Calabrese, Wang et al. 1986b, Wang and Calabrese 1986b, Berkman and Calabrese 1988, Hesketh, Etchells et al. 1991, Cabaret, Rivera et al. 2007). Other research has focused on the study of particle breakup frequency developing models to predict the final drop size distribution (Coulaloglou and Tavlarides 1977, Konno, Matsunaga et al. 1980, Prince and Blanch 1990, Tsouris and Tavlarides 1994, Luo and Svendsen 1996, Eastwood, Armi et al. 2004).

In general the principle of break-up can be looked upon as the interaction between two types of forces (Hinze, 1955). An external disturbing force, induced by the flow field, tries to deform the droplet and an internal restoring force tries to keep the droplet in its original shape. As a first approximation the restoring force can be represented by the interfacial tension which is proportional to  $\sigma/d$ , where  $\sigma$  is the interfacial tension and  $d$  the droplet diameter. The disturbing force,  $\tau$ , can be either an inertial or a viscous force, exerted by the surrounding continuous phase on the dispersed droplet. The ratio between the disturbing and the restoring forces,  $\tau d/\sigma$ , is often used for the description of the break-up process. Depending on whether the disturbing force is inertial or viscous, the ratio is called Weber number ( $We$ ) or Capillary number ( $Ca$ ), respectively. If this ratio exceeds a certain value, the droplet will break up. This critical number depends on the ratio between the viscosities of the dispersed and continuous phases and the geometry of the flow field around the droplet (Janssen, 1993).

### 2.2.3.1 Breakup in a laminar flow

Viscous shear forces in the continuous phase cause a velocity gradient around the interface that deforms the fluid particle and can lead to breakup. Shear stresses also appear due to the wake effect downstream of an obstacle. The canonical laminar flow fields are simple shear flow and, for the elongational component, uniaxial, planar or equibiaxialflow (Windhab et al., 2005). This means that in laminar flow two different cases should be analysed:

- Simple shear: when the velocity gradient and the flow direction are parallel;
- Simple extensional: when the elongation is present and the stretching is on a single axis.

In **simple shear flow** the deforming viscous stresses  $\tau_v$  acting on the surface of emulsion drops are generated proportional to the acting shear rates and the related viscosity of the continuous fluid phase:  $\tau_v = \mu_c \cdot |\dot{\gamma}|$ ;

With  $\mu_c$  the continuous-phase viscosity and  $|\dot{\gamma}|$  the shear rate. The capillary pressure  $P_L$  acting against the deforming stresses is given by the Laplace equation leading to a spherical drop:

$$P_L = \frac{4\sigma}{d} \quad (3)$$

with  $\sigma$  the interfacial tension and  $d$  the diameter of the spherical droplet. The dimensionless stress ratio  $\frac{\tau_v}{P_L}$  is denoted by the shear capillary number  $Ca^S$  :

$$Ca^S = \frac{\mu_c \cdot |\dot{\gamma}| \cdot d}{2\sigma} \quad (4)$$

with  $d$  the droplet size. Drop breakup occurs if the critical capillary number is exceeded. Hence the maximum drop diameter surviving under shear flow conditions  $d_{s \max}$  is given by the critical shear capillary number  $Ca^S$  from Eq. (4) as :

$$d_{\max} = \frac{2 \cdot Ca_{Cr}^S \cdot \sigma}{\mu_c \cdot |\dot{\gamma}|} \quad (5)$$

As the breakup proceeds with the flow, of course the  $d_{\max}$  obtained from Eq. (5) is valid if the residence time of the drop in the shear breakage zone is much greater than the deformation

time scale of the drop. Note that recent numerical simulations (Windhab et al., 2005) can reproduce the interface deformation and splitting at the scale of a few numbers of drops.

In presence of elongational flow ( laminar flow) , drops can also be deformed when the fluid elements accelerate and induce a normal strain and stress. The highest accelerating rates in the flow controls  $d_{max}$ . The drops are convected along the streamlines, and so from a Lagrangian point of view the drops experience a non-uniform strain rate due to the spatial heterogeneity of the velocity field. The analysis developed for the case of shear flows is also valid for the extensional laminar steady flows, in which the extensional rate  $\dot{\epsilon}$  is included in the definition of the capillary number in place of the shear rate. In practice, the generalized shear rate can be used (second invariant of the strain rate tensor) in the capillary number, as it takes into account both the extensional and shear components.

$$Ca^e = \frac{\mu_c \cdot |\dot{\epsilon}| \cdot d}{2\sigma} \quad (6)$$

With  $|\dot{\epsilon}|$  the extensional rate.

As for the shear stress case, from Eq. (6), the maximum drop diameter due to elongation  $d_{max}$  can be expressed as :

$$d_{max} = \frac{2 \cdot Ca_{Cr}^e \cdot \sigma}{\mu_c \cdot |\dot{\epsilon}|} \quad (7)$$

Eq. (7) can be used to predict  $d_{max}$ , with the same remark on the drop residence time in the high-elongation rate zone.

### 2.2.3.2 Breakup in a turbulence flow

In a turbulent flow field, the breakup of fluid particles is caused mainly by turbulent pressure fluctuations on the drop surface, sometime called particle-eddy collisions. The particle can be assumed to modify its spherical form with the fluctuation of the surrounding fluid. When the amplitude of the oscillation is close to that required to make the particle surface unstable, it starts to deform and fragments into two (or more) daughter particles. The breakup mechanism can then be expressed as a balance between the dynamic pressure  $\tau_i$  and the capillary force  $\tau_s$ . The viscous stresses of the fluid inside the particle are usually neglected in a coarse

approach. Whether or not the particle breaks depends on the extent of the deformation, characterized by the Weber number  $We = \frac{\tau_i}{\tau_s}$ . Concerning this criterion for breakup, Liao and Lucas (2009) distinguish some mechanisms, the most significant being that the turbulent kinetic energy of the particle is greater than a critical value (Chatzi and Kiparissides, 1992; Coulaloglou and Tavlarides, 1977) and that the turbulent kinetic energy of the eddy is greater than a critical value (Martínez-Bazán et al., 1999a,b; Luo and Svendsen, 1996; Tsouris and Tavlarides, 1994). The critical energy is arbitrarily defined by the above authors as the surface energy of the parent particle (Martínez-Bazán et al., 1999a,b), the increase in surface energy before and after breakup (Luo and Svendsen, 1996), or the mean value of the surface energy increase for breakup into two equal-size daughters and into a smaller and a larger one (Tsouris and Tavlarides, 1994).

In turbulent flow fields, all flow parameters fluctuate locally, resulting in an eddy size distribution ranging from the macroscale  $L$  to the Kolmogorov length scale  $\lambda_K$ . The Kolmogorov and Hinze theory, suggested independently by Kolmogorov (1949) and Hinze (1955), is based on the idea of an energy cascade. It is the main contribution to a physical understanding and provides a universal model for droplet breakup in turbulent flow. The Kolmogorov scale  $\lambda_K$  is characterized by a Reynolds number of about unity :

$$\lambda_K = \nu_c^{3/4} \cdot \varepsilon^{-1/4} \quad (8)$$

where  $\nu_c$  is the kinematic viscosity of the continuous phase and  $\varepsilon$  the energy dissipation rate per mass unit. The size of the largest stable drop in the emulsion is determined by the equilibrium between the turbulent pressure fluctuations, which tend to deform and break up the drop, and the surface tension, which resists these deformations and holds the drop together. From previous considerations, the ratio of these two constraints defines the droplet Weber number:

$$We = \frac{\rho_c \cdot \overline{\delta u(d)^2} \cdot d}{\sigma} \quad (9)$$

where  $\rho_c$  is the continuous phase density and  $\overline{\delta u(d)^2}$  the spatial longitudinal autocorrelation of instantaneous velocities at the distance  $d$  equal to the drop diameter. In the inertial field for isotropic turbulence in the drop length scale,  $\overline{\delta u(d)^2}$  is given by Batchelor (1953) as:

$$\overline{\delta u(d)^2} = C_K \cdot \varepsilon^{2/3} \cdot d^{2/3} \quad (10)$$

where  $C_K$  is known as the Kolmogorov constant in physical space (there is a related constant in spectral space). As previously mentioned, droplet breakup occurs when the Weber number reaches a critical value  $We_{cr}$ . So the maximum diameter  $d_{max}$  of drops that resist further breakup by the turbulent fluctuations is obtained as:

$$d_{max} = \left( \frac{We_{cr}}{C_K} \right)^{3/5} \cdot \left( \frac{\sigma}{\rho} \right)^{3/5} \cdot \epsilon^{-2/5} \quad (11)$$

This approach leads to the conclusion that the viscosity forces in the dispersed phase are negligible, a statement that could be justified for drop sizes much larger than the Kolmogorov length scale.

The application of this model to “non-coalescing” systems has been tested over a wide range of processes: stirred vessels, emulsifiers with ultrasound, and homogenizers. Many authors (Eastwood et al., 2004; Hesketh et al., 1991; Martínez-Bazán et al., 1999a; Risso and Fabre, 1998; Streiff et al., 1997) report good predictions of the maximum droplet diameter, despite some discrepancies in the constant value  $(We_{cr}/C_K)^{3/5}$ .

## 2.3 Mixing equipment

### 2.3.1 Introduction

“Characterizing mixing in industrial processes is an important issue for various economic and environmental considerations since it governs byproduct effluents and consequently process efficiency. (Anxionnaz et al., 2008; Lobry et al., 2011; Stankiewicz and Moulijn, 2000) “

The mixing of liquids is a unit operation in which two or more miscible or immiscible liquids are mixed together to reach a certain degree of homogeneity or dispersion (Paul 2003). Mixing is a common operation for the manufacture of a wide range of products such as food, personal care, home care and catalysts industry. When the mixing involves immiscible fluids the operation is called dispersion. Stirred vessels, rotor-stator mixers, static mixers, decanters, settlers, centrifuges, homogenizers, extraction columns, and electrostatic coalescers are examples of industrial process equipment used to handle liquid-liquid systems. All these operations can be classified as batch or continuous processes (Hall, Cooke et al. 2011). In batch

processes, stirred tanks and similar devices are used to blend fluids, employing an impeller for generating the fluid motion. The amount of time required to reach the degree of homogeneity desired is known as the blend time or residence time, which is the time spent by the fluid inside the tank before reaching the desired level of mixing. Static mixers and similar devices are used for continuous processes where fluids are pumped through mixing elements installed inside pipes. In the following table the main characteristics of static mixers compared with stirred tanks are reported (Thakur, Vial et al. 2003).

Static Mixer	CSTR
Small space requirement	Large space requirement
Low equipment cost	High equipment cost
No power required except pumping	High power consumption
No moving parts except pump	Agitator drive and seals
Short residence times	Long residence times
Approaches plug flow	Exponential distribution of residence times
Good mixing at low shear rates	Locally high shear rates can damage sensitive materials
Fast product grade changes	Product grade changes may generate waste
Self-cleaning, interchangeable mixers or disposable mixers	Large vessels to be cleaned

**Table 2** Comparison between features of static mixer and stirred tank

### 2.3.2 Mixing of immiscible liquids in Stirred Tank

Stirred vessels are among the most commonly used pieces of equipment in the chemical and biochemical processes. They are used for the homogenization of single or several phases. There are at least two kinds of agitation commonly employed in stirred vessels: pneumatic and mechanical. The former type uses an air stream in order to achieve bulk mixing. The latter method is based on the use of rotating impellers driven usually by electrical motors. Mixing and contacting in agitated tanks can be accomplished in continuous, batch, or fed-batch mode. A good mixing result is important for minimizing investment and operating costs, providing high yields when mass transfer is limiting, and thus enhancing profitability. Processing with mechanical mixers occurs under either laminar or turbulent flow conditions, depending on the impeller Reynolds number, defined as  $Re = \rho ND^2/\mu$ .

Stirred vessels are still powerful tools in process industry and find vast applications especially for process in highly viscous products (Aubin and Xuereb, 2006; Cabaret et al., 2007). Numerous recent studies investigate their hydro-dynamics with Newtonian as well as rheologically complex fluids (Alliet-Gaubert et al., 2006; Aubin et al., 2000, 2001; Fangary et al., 2000; Torr  et al., 2007). New impeller and mixing vessel configurations and innovative operating methods are being introduced to enhance their mixing efficiency, safety, and overall productivity (Aubin et al., 2006; Fentiman et al., 1998; Torr  et al., 2008).

The quality of mixing mainly depends upon the relative distribution of mean and turbulent kinetic energy. Power draw is a very important variable in chemical and bioprocess engineering. It is defined as the amount of energy necessary in a period of time, in order to generate the movement of the fluid within a container (e.g. bioreactor, mixing tank, chemical reactor, etc.) by means of mechanical or pneumatic agitation. The costs associated with power draw contribute significantly to the overall operation costs of industrial plants. Therefore, it is desired that the mixing process is performed efficiently and with a minimum expense of energy required to achieve the objective established a priori (Bader, 1987). Power draw influences heat and mass transfer processes, mixing and circulation times. Power draw has been used as a criterion for process scale-up and bioreactor design (Charles, 1985). Commonly, it is referred as the volumetric power draw ( $P=V$ ).

In view of such an immense importance of the knowledge of quality of flow, vigorous research efforts have been made during the last 50 years using various flow measurement techniques and computational fluid dynamics (CFD). The on going demand for the improved impeller designs usually comes from the users of industrial mixing equipment when the vessels are to be designed for new plants or improvement in the existing design is desired for enhancing quality, capacity, process efficiency and energy efficiency.

### **2.3.3 Mixing of immiscible liquids in Static Mixer**

Static mixers, also known as motionless mixers, have become standard equipment in the process industries. However, new designs are being developed and new applications are being explored. Static mixers are employed inline in a once-through process or in a recycle loop where they supplement or even replace a conventional agitator. Their use in continuous processes is

an attractive alternative to conventional agitation since similar and sometimes better performance can be achieved at lower cost. Motionless mixers typically have lower energy consumptions and reduced maintenance requirements because they have no moving parts. They offer a more controlled and scaleable rate of dilution in fed batch systems and can provide homogenization of feed streams with a minimum residence time. They are available in most materials of construction.

Although static mixers did not become generally established in the process industries until the 1970s, the patent is much older. An 1874 patent describes a single element, multilayer motionless mixer used to mix air with a gaseous fuel (Sutherland, 1874). Nowadays there are approximately 2000 US patents and more than 8000 literature articles that describe motionless mixers and their applications. More than 30 commercial models are currently available. The prototypical design of a static mixer is a series of identical, motionless inserts that are called *elements* and that can be installed in pipes, columns or reactors. The purpose of the elements is to redistribute fluid in the directions transverse to the main flow, i.e. in the radial and tangential directions. The effectiveness of this redistribution is a function of the specific design and number of elements. Commercial static mixers have a wide variety of basic geometries and many adjustable parameters that can be optimized for specific applications. Table 3 lists manufacturers, and Figure 6 illustrates commercial designs.

Company	Mixers
Chemineer-Kenics	Chemineer-Kenics Kenics mixer (KM), HEV (high efficiency vortex mixer)
Koch-Sulzer	Sulzer mixer SMF, SMN, SMR, SMRX, SMV, SMX, SMXL
Charles Ross & Son	ISG (interfacial surface generator), LPD (low pressure drop), LLPD
Wymbs Engineering	HV (high viscosity), LV (low viscosity)
Lightnin	Inliner Series 45, Inliner Series 50
EMI	Cleveland
Komax	Komax
Brann and Lubbe	N-form
Toray	Hi-Toray Mixer
Prematechnik	PMR (pulsating mixer reactor)
UET	Heli_o (Series, I, II and III)

**Table 3** Lists manufacturers

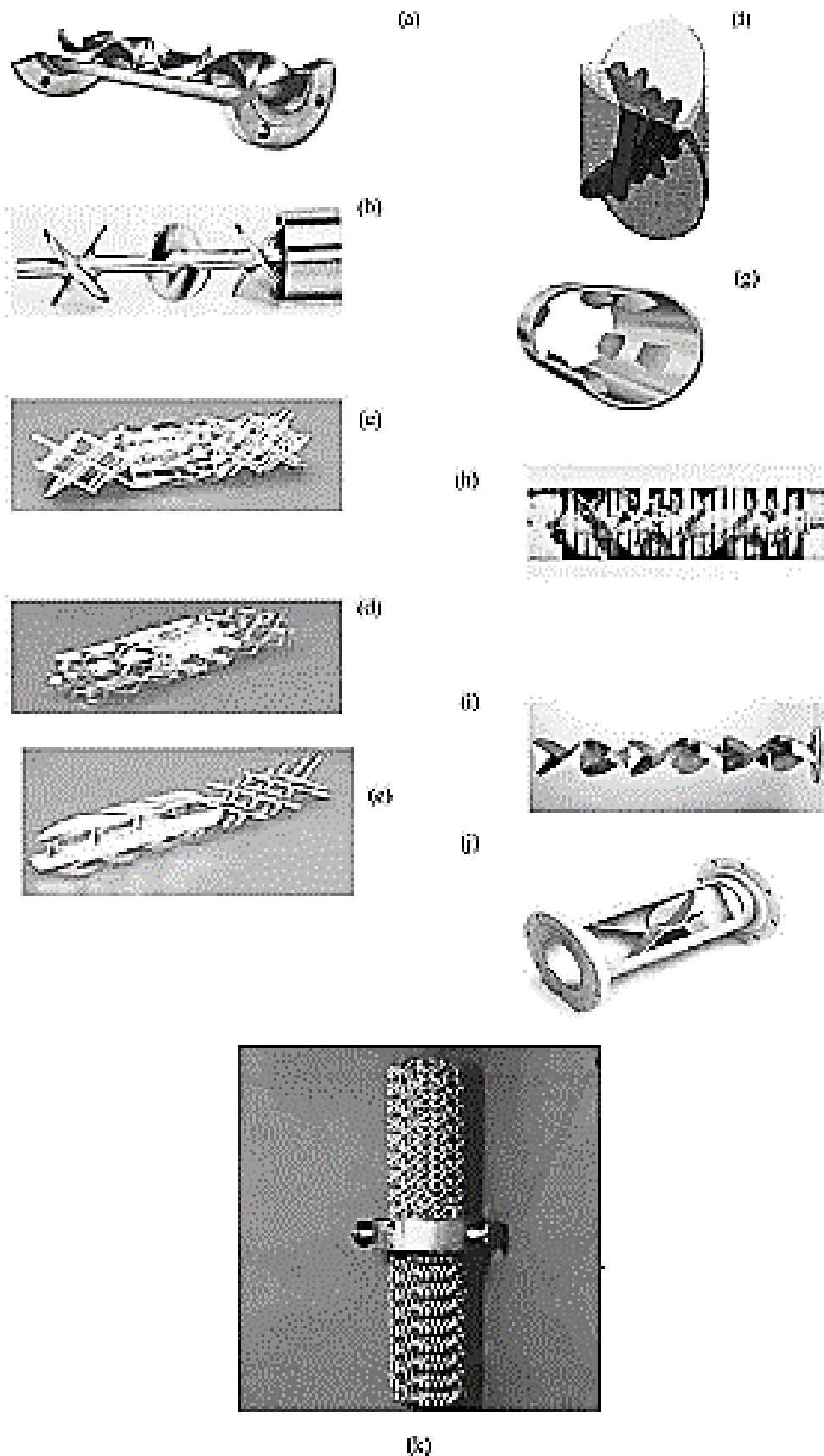


**Figure 6** Elements of different commercial static mixers: (a) Kenics (Chemineer Inc.); (b) low pressure drop (Ross Engineering Inc.); (c) SMV (Koch-Glitsch Inc.); (d) SMX (Koch-Glitsch Inc.); (e) SMXL (Koch-Glitsch Inc.); (f) Interfacial Surface Generator-ISG (Ross Engineering Inc.); (g) HEV (Chemineer Inc.);(h) Inliner series 50 Lightnin inc.); (i) Inliner series 45 (Lightnin Inc.); (j) Custody transfer mixer (Komax systems Inc.); (k) SMR (Koch-Glitsch, Inc.).

Mixing operations are essential in the process industries. They include the classical mixing of miscible fluids in single-phase flow as well as heat transfer enhancement, dispersion of gas into a liquid continuous liquid phase, dispersion of an immiscible organic phase as drops in a continuous aqueous phase, three-phase contacting and mixing of solids. Static mixers are now commonly used in the chemical and petrochemical industries to perform continuous operations. They have also found applications in the pharmaceutical, food engineering and pulp and paper industries .

In laminar flows, static mixers divide and redistribute streamlines in a sequential fashion using only the energy of the flowing fluid. In turbulent flows, they enhance turbulence and give intense radial mixing, even near the wall. In both cases, they can significantly improve heat and mass transfer operations.

Three different stages are introduced to describe the mixing mechanism: macromixing, mesomixing and micromixing (Fournier, Falk et al. 1996, Baldyga and Bourne 1999). In all these cases, the key parameters to compare the different available static mixer at the same performance (drop size distribution) are the energy consumption or pressure drop and the number of elements necessary.

The pressure drop in a static mixer of fixed geometry is expressed as the ratio of the pressure drop through the mixer to the pressure drop through the same diameter and length of open pipe , by using a K factor ( $K_L$  for laminar and  $K_T$  for turbulent flow) determined empirically.

$$\Delta P_{SM} = \begin{cases} K_L \cdot \Delta P_{EmptyPipe} \\ K_T \cdot \Delta P_{EmptyPipe} \end{cases} \quad (12)$$

Where the standard pressure drop for an empty smooth pipe are:

$$\Delta P = 4f \cdot \frac{L}{D} \cdot \rho \cdot \frac{V^2}{2} \quad (13)$$

And the Fanning friction factor is given by the Blasius equation for turbulent flow:

$$f = \frac{0.079}{Re^{0.25}} \quad (14)$$

and in laminar flow by:

$$f = \frac{16}{Re} \quad (15)$$

In Tables 7-5 values of  $K_L$  and  $K_T$  are given. These values are considered good to about 15%.

Device	$K_L$	$K_T$
Empty pipe	1	1
KMS	6.9	150
SMX	37.5	500
SMXL	7.8	100
SMR	46.9	-
SMV	-	100-200

**Table 4** Values of  $K_L$  and  $K_T$  for different static mixer (Streiff 1997)

Most vendors have more accurate correlations that take into account a slight Reynolds number effect in transitional and turbulent flow, and the volume fraction occupied by the mixer, which varies with mixer diameter and pressure rating. A more detailed approach is necessary for some designs that have the option for variable but similar geometry. For the most accurate pressure drop predictions, the manufacturer should always be consulted.

There is still, of course, substantial room for further improvement and new designs and principles for these devices. Even the most widely studied geometries can still be further optimized. Fouling resistance, corrosion, maintenance, and cleaning operations are at present problems in such devices. Academia seems overly obsessed with theoretical gains in mixing and heat transfer, and the tools to address technical complications in the implementation and production phases are still immature and need extensive development. Moreover, laboratory-scale optimization processes are leading to new designs but sometimes it can take years for research prototypes to become available in the markets, if ever.

## 2.4 Computational fluid dynamic for mixing

### 2.4.1 Introduction

Computational fluid dynamics (CFD) is the numerical simulation of fluid motion. While the motion of fluids in mixing is an obvious application of CFD, there are hundreds of others, ranging from blood flow through arteries, to supersonic flow over an airfoil, to the extrusion of rubber in the manufacture of automotive parts. While in 1975 numerical results were only making their entrance into the arena of fluid flow and heat/mass transfer and they were not considered serious competition to experimental data (Chapman et al. 1975), thirty years later, computational projects and results constitute the major source of useful and reliable information in most engineering and physical disciplines. The combination of significant improvements and advances in computational speed and accuracy, and the affordability of computational power have prompted most scientists to use numerical methods for the studies on the flow and heat/mass transfer processes associated with particles, bubbles and drops and, thus, develop the new field of Computational Fluid Dynamics (CFD). Numerous models and solution techniques have been developed over the years to help describe a wide variety of fluid motion. The fundamental equations for fluid flow are presented in detailed in the following paragraphs, but before advantages of CFD in obtaining scientific information rather than experimental methods are given :

- The rapid development of CFD methods has improved significantly the accuracy and reliability of the final results.
- The cost of CFD calculations in the simulation of realistic systems and conditions has dropped dramatically, while the cost of experimentation has constantly increased.
- CFD generates complete and easily accessible information. The results of a simulation may be viewed in different ways and from different points, thus providing the researcher with a complete depiction of the object of study.
- CFD has the ability to model and simulate idealized or desired conditions for a specific variable or effect, which are difficult or impossible to achieve in practice

## 2.4.2 Conservation Equations

If a small volume, or element of fluid in motion is considered, two changes to the element will probably take place: (1) the fluid element will translate and possibly rotate in space, and (2) it will become distorted, either by a simple stretching along one or more axes or by an angular distortion that causes it to change shape. The process of translation is often referred to as *convection*, and the process of distortion is related to the presence of gradients in the velocity field and a process called *diffusion*. In the simplest case, these processes govern the evolution of the fluid from one state to another. In more complicated systems, sources can also be present that give rise to additional changes in the fluid.

Many of the processes such as those that are involved in the description of generalized fluid motion are described by a set of conservation or transport equations. These equations track, over time, changes in the fluid that result from convection, diffusion, and sources or sinks of the conserved or transported quantity. Furthermore, these equations are coupled, meaning that changes in one variable (say, the temperature) can give rise to changes in other variables (say, the pressure). The conservation equations are:

- Continuity equation
- Momentum equation
- Species equation
- Energy equation

### 2.4.2.1 Continuity Equation

The continuity equation is a statement of conservation of mass. To understand its origin, consider the flow of a fluid of density  $\rho$  through the six faces of a rectangular block, as shown in **Figure 7**. The block has sides of length  $\Delta x_1$ ,  $\Delta x_2$ , and  $\Delta x_3$  and velocity components  $U_1$ ,  $U_2$ , and  $U_3$  in each of the three coordinate directions.

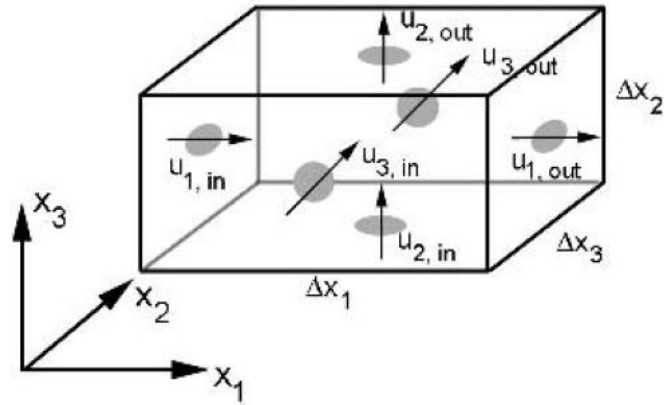


**Figure 7** A rectangular volume with inflow and outflow can be used to illustrate a conservation equation.

To ensure conservation of mass, the sum of the mass flowing through all six faces must be zero:

$$\begin{aligned} & \rho(U_{1,\text{out}} - U_{1,\text{in}}) \cdot (\Delta x_2 \cdot \Delta x_3) + \rho(U_{2,\text{out}} - U_{2,\text{in}}) \cdot (\Delta x_1 \cdot \Delta x_3) \\ & + \rho(U_{3,\text{out}} - U_{3,\text{in}}) \cdot (\Delta x_1 \cdot \Delta x_2) = 0 \end{aligned} \quad (16)$$

Dividing through by  $(\Delta x_1 \Delta x_2 \Delta x_3)$  the equation can be written as :

$$\rho \cdot \frac{\Delta U_1}{\Delta x_1} + \rho \cdot \frac{\Delta U_2}{\Delta x_2} + \rho \cdot \frac{\Delta U_3}{\Delta x_3} = 0 \quad (17)$$

or, in differential form :

$$\rho \cdot \frac{\partial U_1}{\partial x_1} + \rho \cdot \frac{\partial U_2}{\partial x_2} + \rho \cdot \frac{\partial U_3}{\partial x_3} = 0 \quad (18)$$

For more general cases, the density can vary in time and in space, and the continuity equation takes on the more familiar form :

$$\frac{\partial \rho}{\partial t} + \frac{\partial(\rho U_i)}{\partial x_i} = 0 \quad (19)$$

### 2.4.2.2 Momentum Equation

The momentum equation is a statement of conservation of momentum in each of the three component directions. The three momentum equations are collectively called the *Navier–Stokes equations*. In addition to momentum transport by convection and diffusion, several momentum sources are also involved:

$$\frac{\partial(\rho U_i)}{\partial t} + \frac{\partial(\rho U_i U_j)}{\partial x_j} = -\frac{\partial p}{\partial x_i} + \frac{\partial}{\partial x_j} \left[ \mu \left( \frac{\partial U_i}{\partial x_j} + \frac{\partial U_j}{\partial x_i} - \frac{2}{3} \cdot \frac{\partial U_k}{\partial x_k} \cdot \delta_{ij} \right) \right] + \rho g + F_i \quad (20)$$

In eq. (20) the convection terms are on the left. The terms on the right-hand side are the pressure gradient, a source term; the divergence of the stress tensor, which is responsible for the diffusion of momentum; the gravitational force, another source term; and other generalized forces (source terms), respectively.

### 2.4.2.3 Species Equation

The species equation is a statement of conservation of a single specie. Multiple-species equations can be used to represent fluids in a mixture with different physical properties. Solution of the species equations can predict how different fluids mix, but not how they will separate. For the species  $i$ , the conservation equation is for the mass fraction of that species,  $m_i$ , and has the following form:

$$\frac{\partial(\rho m_i)}{\partial t} + \frac{\partial(\rho U_i m_i)}{\partial x_i} = -\frac{\partial(J_{i,i})}{\partial x_i} + R_i + S_i \quad (21)$$

In eq. (21),  $J_{i,i}$  is the  $i$  component of the diffusion flux of species  $i$  in the mixture. For laminar flows,  $J_{i,i}$  is related to the diffusion coefficient for the species and local concentration gradients (Fick's law of diffusion). For turbulent flows,  $J_{i,i}$  includes a turbulent diffusion term, which is a function of the turbulent Schmidt number.  $R_i$  is the rate at which the species is either consumed or produced in one or more reactions, and  $S_i$  is a general source term for species. When two or more species are present, the sum of the mass fractions in each cell must add to 1.0. For this reason, if there are  $n$  species involved in a simulation, only  $n - 1$  species equations need to be solved. The mass fraction of the  $n$ th species can be computed from the required condition:

$$\sum_{i=1}^n m_i = 1 \quad (22)$$

### 2.4.2.4 Energy Equation

Heat transfer is often expressed as an equation for the conservation of energy, typically in the form of static or total enthalpy. Heat can be generated (or extracted) through many mechanisms, such as wall heating (in a jacketed reactor), cooling through the use of coils, and

chemical reaction. In addition, fluids of different temperatures may mix in a vessel, and the time for the mixture to come to equilibrium may be of interest. The equation for conservation of energy (total enthalpy) is :

$$\frac{\partial(\rho E)}{\partial t} + \frac{\partial[U_i(\rho E+p)]}{\partial x_i} = \frac{\partial}{\partial x_i} \left[ K_{\text{eff}} \frac{\partial T}{\partial x_i} + \sum h_j J_{i,j} + U_i (\tau_{ij})_{\text{eff}} \right] + S_h \quad (23)$$

In this equation, the energy,  $E$ , is related to the static enthalpy,  $h$ , through the following relationship involving the pressure,  $p$ , and velocity magnitude,  $U$ :

$$E = h - \frac{p}{\rho} + \frac{U^2}{2} \quad (24)$$

The first term on the right-hand side of eq. (24) represents heat transfer due to conduction, or the diffusion of heat, where the effective conductivity,  $k_{\text{eff}}$ , contains a correction for turbulent simulations. The second term represents heat transfer due to the diffusion of species, where  $J_{j,i}$  is the diffusion flux. The third term involves the stress tensor,  $(\tau_{ij})_{\text{eff}}$ , a collection of velocity gradients, and represents heat loss through viscous dissipation. The fourth term is a general source term that can include heat sources due to reactions, radiation, or other processes.

### 2.4.3 Numerical Methods

The differential equations presented above describe the continuous movement of a fluid in space and time. To be able to solve those equations numerically, all aspects of the process need to be discretized, or changed from a continuous to a discontinuous formulation. For example, the region where the fluid flows needs to be described by a series of connected control volumes, or computational cells. The equations themselves need to be written in an algebraic form. Advancement in time and space needs to be described by small, finite steps rather than the infinitesimal steps that are so familiar to students of calculus. All of these processes are collectively referred to as *discretization*. In the next paragraphs, discretization of the domain, or grid generation, and discretization of the equations are presented in detail.

### 2.4.3.1 Discretization of the domain : Grid generation

To break the domain into a set of discrete subdomains, or computational cells, or control volumes, a *grid* is used. Also called a *mesh*, the grid can contain elements of many shapes and sizes. In 2D domains, for example, the elements are usually either quadrilaterals or triangles. In 3D domains (Figure 8), they can be tetrahedra (with four sides), prisms (five sides), pyramids (five sides), or hexahedra (six sides). A series of line segments (2D) or planar faces (3D) connecting the boundaries of the domain are used to generate the elements.

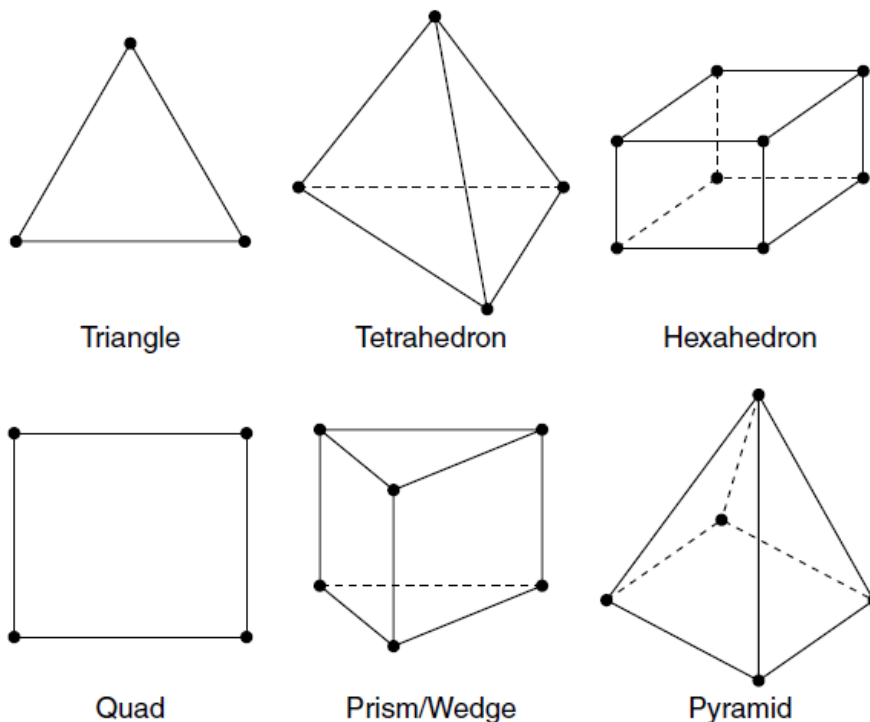


**Figure 8** Element types for computational grids.

There are several types of mesh (figure 9) :

- A **structured mesh** is one in which all interior vertices are topologically alike. In graphtheoretic terms, a structured mesh is an induced subgraph of an infinite periodic graph such as a grid.
- An **unstructured mesh** is one in which vertices may have arbitrarily varying local neighborhoods.
- A **block-structured or hybrid mesh** is formed by a number of small structured meshes combined in an overall unstructured pattern

In general, structured meshes offer simplicity and easy data access, while unstructured meshes offer more convenient mesh adaptivity (refinement/derefinement based on an initial solution) and a better fit to complicated domains. High-quality hybrid meshes enjoy the advantages of both approaches, but hybrid meshing is not yet fully automatic. We shall discuss unstructured mesh generation at greater length than structured or hybrid mesh generation, both because the unstructured approach seems to be gaining ground and because it is more closely connected to computational geometry. The division between structured and unstructured meshes usually extends to the shape of the elements: two-dimensional structured meshes typically use quadrilaterals, while unstructured meshes use triangles. There is, however, no essential reason for structured and unstructured meshes to use different element shapes. In fact it is possible to subdivide elements in order to convert between triangles and quadrilaterals (Figure 10) and between tetrahedral and hexahedra.

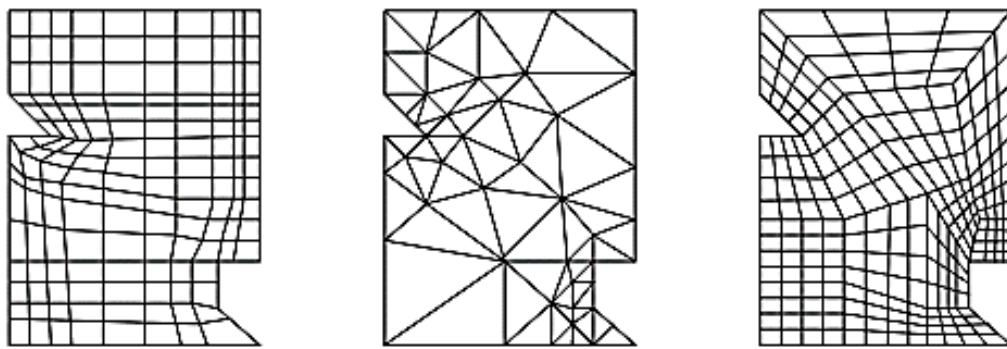


Figure 9 Types of meshes: (a) structured, (b) unstructured, and (c) block-structured.

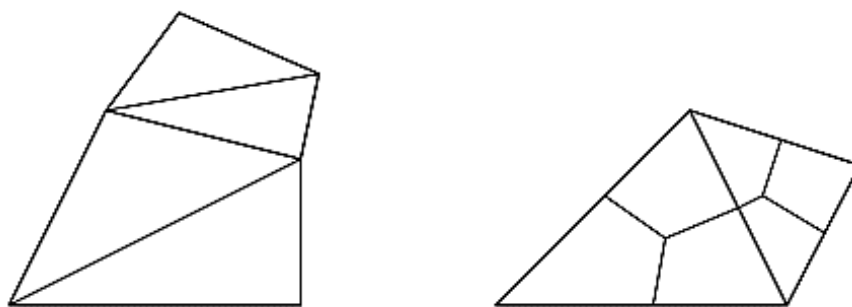


Figure 10 Element shape : (a) Triangulating quadrilaterals. (b) Subdividing triangles to form quadrilaterals.

In general, the density of cells in a computational grid needs to be fine enough to capture the flow details, but not so fine that the overall number of cells in the domain is excessively large, since problems described by large numbers of cells require more time to solve. Nonuniform

grids of any topology can be used to focus the grid density in regions where it is needed and to allow for expansion in other regions. In laminar flows, the grid near boundaries should be refined to allow the solution to capture the boundary layer flow detail. For turbulent flows, it is customary to use a wall function in the near-wall regions. This is due to the fact that the transport equation for the eddy dissipation has a singularity at the wall.

### 2.4.3.2 Discretization of the Equations

Several methods have been employed over the years to solve the Navier–Stokes equations numerically, including the finite difference, finite element, spectral element, and finite volume methods. The focus of this paragraph is on the finite volume method, which is described in detail below. To illustrate the discretization of a typical transport equation using the finite volume formulation (Patankar, 1980; Versteeg and Malalasekera, 1995), a generalized scalar equation can be used. The scalar equation has the form :

$$\frac{\partial(\rho\phi)}{\partial t} + \frac{\partial(\rho U_i \phi)}{\partial x_i} = \frac{\partial}{\partial x_i} \left( \Gamma \frac{\partial(\phi)}{\partial x_i} \right) + S' \quad (25)$$

The parameter  $\Gamma$  is used to represent the diffusion coefficient for the scalar  $\phi$ . If  $\phi$  is one of the components of velocity, for example,  $\Gamma$  would represent the viscosity. All sources are collected in the term  $S'$ . The control volume has a node, P, at its center where all problem variables are stored. The transport equation describes the flow of the scalar  $\phi$  into and out of the cell through the cell faces. To keep track of the inflow and outflow, the four faces are labeled with lowercase letters representing the east, west, north, and south borders. The neighboring cells also have nodes at their centers, and these are labeled with the capital letters E, W, N, and S. For the purpose of this example, flow in the one dimensional row of cells shown in **Figure 11-b** is considered.

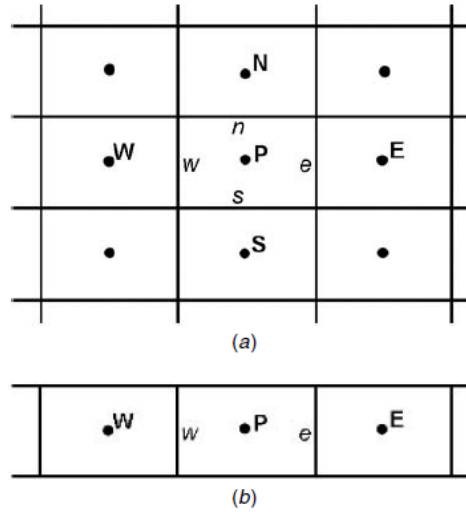


**Figure 11** (a) Simple 2D domain showing the cell centers and faces. (b) 1D rectangular simplification of the 2D domain.

The first step in the discretization of the transport equation is an integration over the control volume. The volume integral can be converted to a surface integral by applying the divergence theorem. Using a velocity in the positive  $x$ -direction, neglecting time dependence, and assuming that the faces  $e$  and  $w$  have area  $A$ , the integrated transport equation takes the following form:

$$(\rho_e U_e \phi_e - \rho_w U_w \phi_w)A = \left( \Gamma_e \left[ \frac{d\phi}{dx_e} \right] - \Gamma_w \left[ \frac{d\phi}{dx_w} \right] \right) + S \quad (26)$$

where  $S$  is the volume integral of the source terms contained in  $S'$ . This expression contains four terms that are evaluated at the cell faces. To obtain the face values of these terms as a function of values that are stored at the cell centers, a discretization scheme is required.

### 2.4.3.3 Discretization schemes

Since all of the problem variables are stored at the cell center, the face values (e.g., the derivatives) need to be expressed in terms of cell center values. To do this, consider a steady-state conservation equation in one dimension without source terms:

$$\frac{d(\rho\phi U)}{dx} = \frac{d}{dx} \left( \Gamma \frac{\partial(\phi)}{\partial x} \right) \quad (27)$$

This equation can be solved exactly. On a linear domain that extends from  $x = 0$  to  $x = L$ , corresponding to the locations of two adjacent cell nodes, with  $\phi = \phi_o$  at  $x = 0$  and  $\phi = \phi_L$  at  $x = L$ , the solution for  $\phi$  at any intermediate location (such as the face) has the form :

$$\phi = \phi_o + (\phi_L - \phi_o) \cdot \frac{\exp(Pe(\frac{x}{L})-1)}{\exp(Pe-1)} \quad (28)$$

The Peclet number,  $Pe$ , appearing in this equation is the ratio of the influence of convection to that of diffusion on the flow field:

$$Pe = \frac{\rho UL}{\Gamma} \quad (29)$$

Depending on the value of the Peclet number, different limiting behavior exists for the variation of  $\phi$  between  $x = 0$  and  $x = L$ . These limiting cases are discussed below, along with some more rigorous discretization or differencing schemes that are in popular use today. The principle discretization schemes are :

- *Central Differencing Scheme* : For  $Pe = 0$  (i.e.,  $U = 0$ ), there is no convection, and the solution is purely diffusive. the variable  $\phi$  varies linearly from cell center to cell center, so the value at the cell face can be found from linear interpolation. When linear interpolation is used in general, i.e., when both convection and diffusion are present, the discretization scheme is called *central differencing*. When used in this manner, as a general purpose discretization scheme, it can lead to errors and loss of accuracy in the solution. One way to reduce these errors is to use a refined grid, but the best way is to use another differencing scheme.
- *Upwind Differencing Schemes* : For  $Pe \gg 1$ , convection dominates, and the value at the cell face can be assumed to be identical to the upstream or upwind value (i.e.,  $\phi_w = \phi_W$ ). When the value at the upwind node is used at the face, independent of the flow conditions, the process is called *first-order upwind differencing*. A modified version of first-order upwind differencing makes use of multidimensional gradients in the upstream variable, based on the upwind neighbour and its neighbors. This scheme, which makes use of a Taylor series expansion to describe the upwind gradients, is called *second-order upwind differencing*. It offers greater accuracy than the first-order upwind method, but requires additional computational effort.

- *Power Law Differencing Scheme* : For intermediate values of the Péclet number,  $0 \leq Pe \leq 10$ , the face value can be computed as a function of the local Peclet number, as shown in eq. (7). This expression can be approximated by one that does not use exponentials, involving the Peclet number raised to an integral power. It is from this approximate form that the power law differencing scheme draws its name. This first-order scheme is identical to the first-order upwind differencing scheme in the limit of strong convection, but offers slightly improved accuracy for the range of Péclet numbers mentioned above.
- *QUICK Differencing Scheme*. The QUICK differencing scheme (Leonard and Mokhtari, 1990) is similar to the second-order upwind differencing scheme, with modifications that restrict its use to quadrilateral or hexahedral meshes. In addition to the value of the variable at the upwind cell center, the value from the next neighbor upwind is also used. Along with the value at the node P, a quadratic function is fitted to the variable at these three points and used to compute the face value. This scheme can offer improvements over the second-order upwind differencing scheme for some flows with high swirl.

In the following table there is a summary of these discretization schemes.

Discretization Scheme	Description, Advantages, and Disadvantages
Central	Good when diffusion dominates. Assumes that there is no convection and that variables vary linearly from cell center to cell center. For convective flows, errors can be reduced by the use of a refined grid. This scheme is recommended for LES simulations.
First-order upwind	Good when convection dominates and the flow is aligned with the grid. Assumes that the face value for each variable is equal to the upstream cell center value. Stable, and a good way to start off a calculation. A switch to a higher-order scheme is usually recommended once the solution has partially converged.
Second-order upwind	Good for full range of Peclet numbers. Computes the face value for each variable from gradients involving the upwind neighbor and its neighbors.
Power law	Good for intermediate values of Peclet number. Computes the face value for each variable from gradients expressed in the form of a power law function. For high Péclet numbers, results are equivalent to first-order upwind.
QUICK	Good for full range of Péclet numbers. Similar to second-order upwind, but restricted to quadrilateral and hexahedral meshes.

**Table 5** Summary of Discretization Schemes

### 2.4.3.4 Final Discretized Equation

Once the face values have been computed using one of the above differencing schemes, terms multiplying the unknown variable at each of the cell centres can be collected. Large coefficients multiply each of these terms. These coefficients contain information that includes the properties, local flow conditions, and results from previous iterations at each node. In terms of these coefficients,  $A_i$ , the discretized equation has the following form for the simple 2D grid shown in Figure 11 (above):

$$A_P\phi_P = A_N\phi_N + A_S\phi_S + A_E\phi_E + A_W\phi_W = \sum_{i,\text{neighbors}} A_i\phi_i \quad (30)$$

For a complex, or even a simple flow simulation, there will be one equation of this form for each variable solved, in each cell in the domain. Furthermore, the equations are coupled, since for example, the solution of the momentum equations will affect the transport of every other scalar quantity. It is the job of the solver to solve these equations collectively with the most accuracy in the least amount of time.

### 2.4.3.5 Solution Methods

The result of the discretization process is a finite set of coupled algebraic equations that need to be solved simultaneously in every cell in the solution domain. Because of the nonlinearity of the equations that govern the fluid flow and related processes, an iterative solution procedure is required. Two methods are commonly used. A segregated solution approach is one where one variable at a time is solved throughout the entire domain. Thus, the x-component of the velocity is solved on the entire domain, then the y-component is solved, and so on. One iteration of the solution is complete only after each variable has been solved in this manner. A coupled solution approach, on the other hand, is one where all variables, or at a minimum, momentum and continuity, are solved simultaneously in a single cell before the solver moves to the next cell, where the process is repeated. The segregated solution approach is popular for incompressible flows with complex physics, typical of those found in mixing applications. Typically, the solution of a single equation in the segregated solver is carried out on a subset of cells, using a Gauss–Seidel linear equation solver. In some cases the solution time can be improved (i.e., reduced) through the use of an algebraic multigrid correction scheme. Independent of the method used, however, the equations must be solved over and over again

until the collective error is reduced to a value that is below a preset minimum value. At this point, the solution is considered converged, and the results are most meaningful. Converged solutions should demonstrate overall balances in all computed variables, including mass, momentum, heat, and species, for example.

## 2.4.4 Structure of OpenFoam

In the present work has been decided to operate with a software called OpenFoam, for its flexibility and the growing interest that the industries have shown toward this platform. OpenFOAM® is the leading free, open source software for computational fluid dynamics (CFD), owned by the OpenFOAM Foundation and distributed exclusively under the General Public Licence (GPL). It is a C++ toolbox for the development of customized numerical solvers, and pre-/post-processing utilities for the solution of continuum mechanics problems, including computational fluid dynamics (CFD). OpenFOAM (originally, FOAM) was created by Henry Weller from the late 1980s at Imperial College, London, to develop a more powerful and flexible general simulation platform than the de facto standard at the time, FORTRAN. This led to the choice of C++ as programming language, due to its modularity and object oriented features. The basic directory structure for a OpenFOAM case, that contains the minimum set of files required to run an application, is shown in Figure 12 and described as follows:

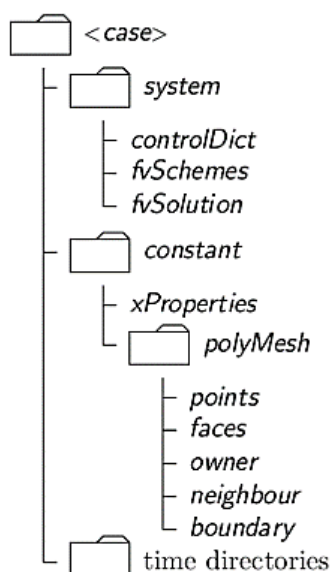


Figure 12 OpenFoam structure

**A constant directory** : that contains a full description of the case mesh in a subdirectory polyMesh and files specifying physical properties for the application concerned, e.g. transportProperties.

**A system directory** : for setting parameters associated with the solution procedure itself. It contains at least the following 3 files: controlDict where run control parameters are set including start/end time, time step and parameters for data output; fvSchemes where discretisation schemes used in the solution may be selected at run-time; and, fvSolution where the equation solvers, tolerances and other algorithm controls are set for the run.

**The 'time' directories** : containing individual files of data for particular fields. The data can be: either, initial values and boundary conditions that the user must specify to define the problem; or, results written to file by OpenFOAM. Note that the OpenFOAM fields must always be initialised, even when the solution does not strictly require it, as in steady-state problems. The name of each time directory is based on the simulated time at which the data is written. If the simulations are initialized at time  $t = 0$ , the initial conditions are usually stored in a directory named 0 or 0.000000e+00, depending on the name format specified.

## Chapter 3

---

# Materials & Methods

### 3.1 Introduction

In the present thesis different software have been used in order to create the numerical models, the geometry and the mesh and to post-process the numerical results. For this reason in this chapter all the software settings are presented in detail. In the first part information on the geometry and the grid independence are provided while in the second part details on solver, turbulence model, initial conditions and the numerical schemes for the 2D and 3D model are listed and explained.

### 3.2 Geometry and Mesh

In a numerical model the first step is building the geometry and the mesh. This is a crucial step that will affect the results of the simulations and/or the convergence of the solution. The present work is divided in two parts. In the first part a 2D Multi-phase model will be realized and in the second part a 3D Single-phase model is discussed. The software used is Salome 7.5.1, which is an open-source software that provides a generic platform for Pre- and Post-Processing for numerical simulation. It is based on an open and flexible architecture made of reusable components. Salome can be used for different aims :

- Create/modify, import/export (IGES, STEP, BREP), repair/clean CAD models
- Mesh CAD models, edit mesh, check mesh quality, import/export mesh (MED, UNV, DAT, STL)
- Handle physical properties and quantities attached to geometrical items
- Perform computation using one or more external solvers (coupling)
- Display computation results (scalar, vectorial)
- Manage studies (create, save, reload)

### 3.2.1 2D Geometry

The 2D model is a simple pipe with baffles to reproduce the ideal structure of a static mixer. Indeed the principle of a static mixer is to force the fluid to change direction improving the mixing. The pipe is long 20 cm and has a diameter of 12.6 cm , with an internal channel for the oil injection which has a diameter of 1.6mm. There are 4 baffles of 6.3 mm length and 2mm wide, at same distance, in the central part of the pipe. The geometry is realized with Salome 7.5.1 with simple steps:

- Create the points
- Create the lines linking the points
- Create a close contour (Wire)
- Create the groups (inlet, outlet, wall)

The 2D geometry is shown in figure 13.

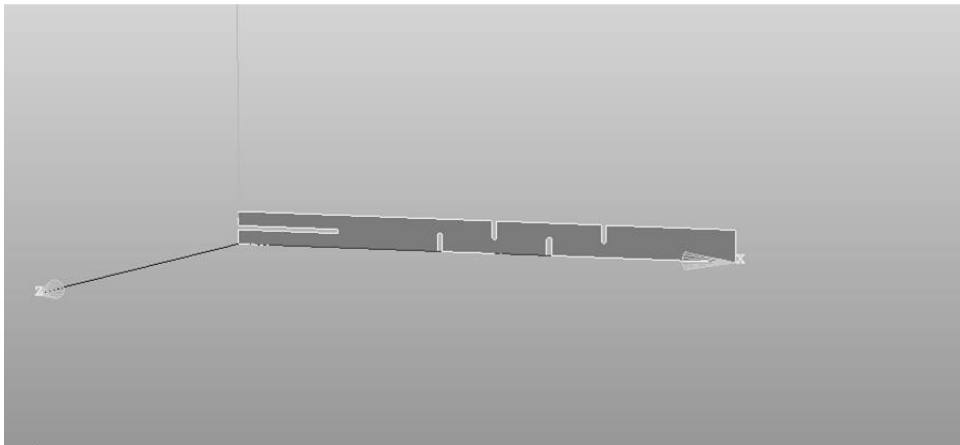


**Figure 13** 2D Geometry

After the geometry's construction the next step is the mesh generation, using the same software. The mesh is structured and the elements are triangles. Near the walls the grid is refined to obtain better numerical results and the dimension of the single cell is chosen by comparing to the minimum size necessary to capture the flow local effects. OpenFoam works also in the 2D cases with 3D geometries where in the third dimension there is just one cell. Therefore in order to not have problems during the process when exporting the Mesh from Salome to OpenFoam, it will be realized a 2D mesh and then by using an extrusion the mesh will become 3D. The figure 14 shows the 2D mesh.

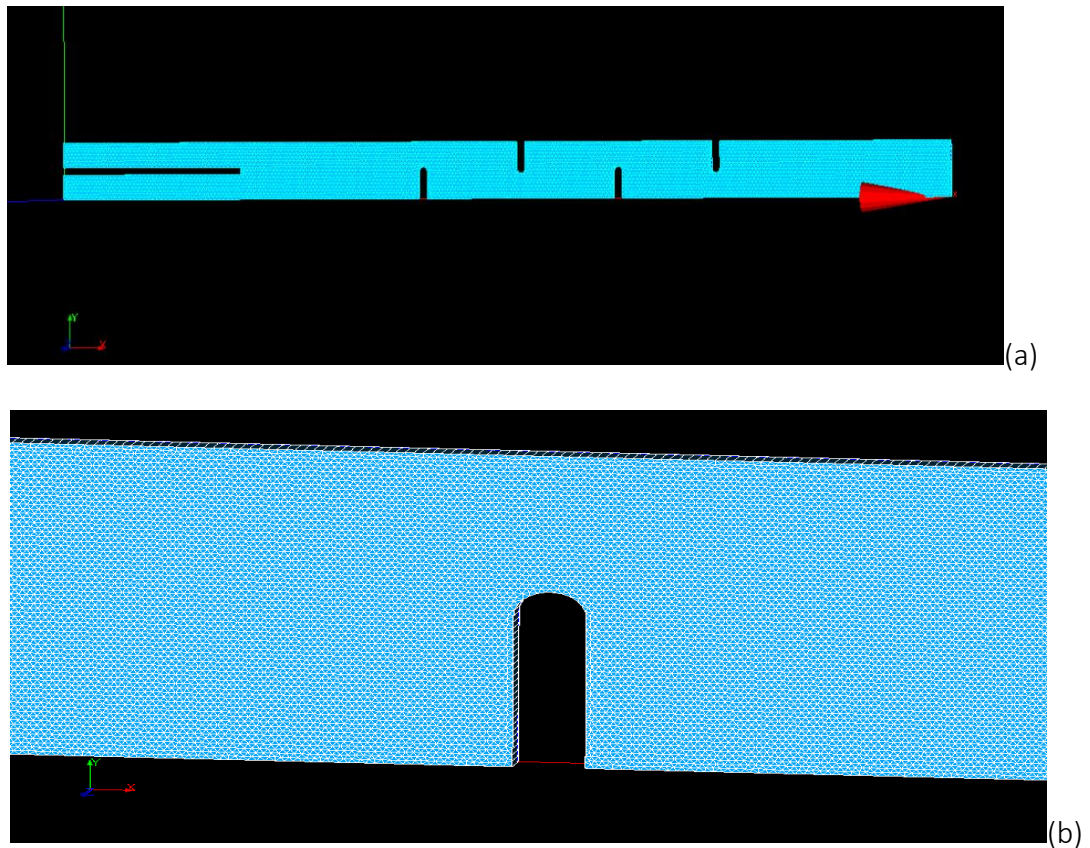


**Figure 14** 2D Mesh (a) , (b)

For the 2D case, different grids have been created, with different refine grade but further details will be given in the next section where the grid's independence will be discussed.

### 3.2.2 3D Geometry

The 3D model is a cylindrical pipe, which contains 6 Kenics static mixer elements. The pipe has the same length as for the 2D case 20 cm and has a diameter of 12.6 cm. Each static mixer element has a length of 18.9 mm, so all together the module takes 113.4 mm, this is because the ratio of  $L/D$  is equal to 1.5. The geometry is realized with Salome 7.5.1 in three main phases:

- In the first phase a cylindrical pipe is realized by extrusion a disk of diameter 12.6mm.
- In the second phase the static mixer element is drawn, starting with a rectangle. The idea is to discretize the element using a finite number of rectangles which are rotated around their axis from  $0^\circ$  to  $180^\circ$ . The helpful commands are "TRANSLATE" , "MIRROR" and "ROTATION". Then finally in order to obtain the static mixer shape , it is necessary to link all the points of these rectangles together. Once the first element is ready, the

second one is realized using the function copy and then to obtain a solid by using the “FUSION” function.

- In the third phase is necessary cut the cylindrical pipe with the 6 static mixers to obtain the final geometry and create all the groups which are fundamental to set the boundary conditions once the geometry will be exported to OpenFoam.

The 6 Kenics static mixer and the cylindrical pipe which contain the static mixers are shown in figures 15 and 16.

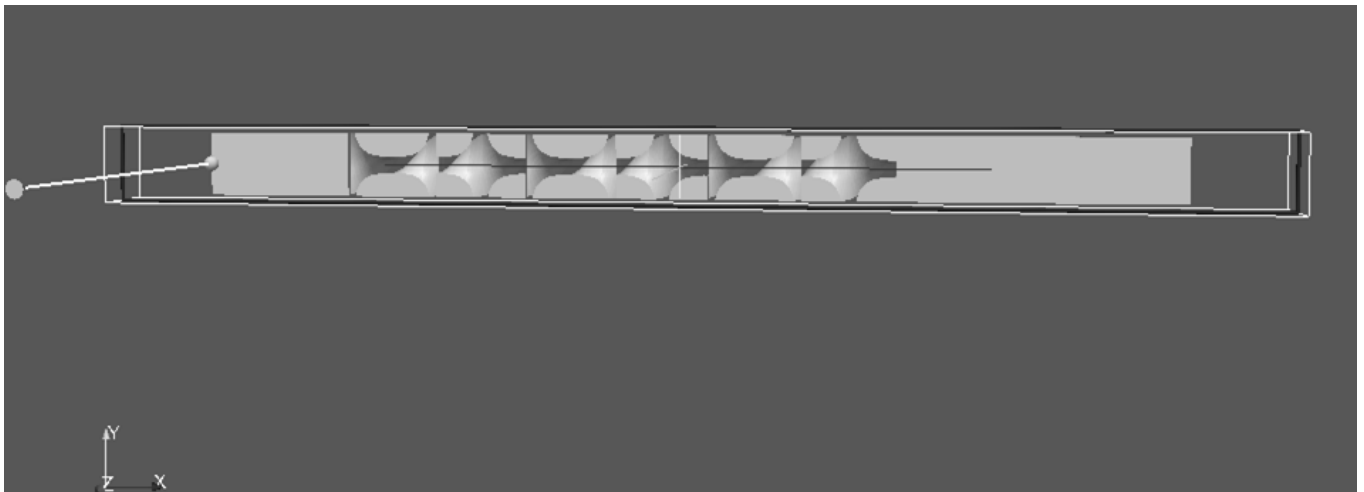


**Figure 15** Section pipe + static mixer

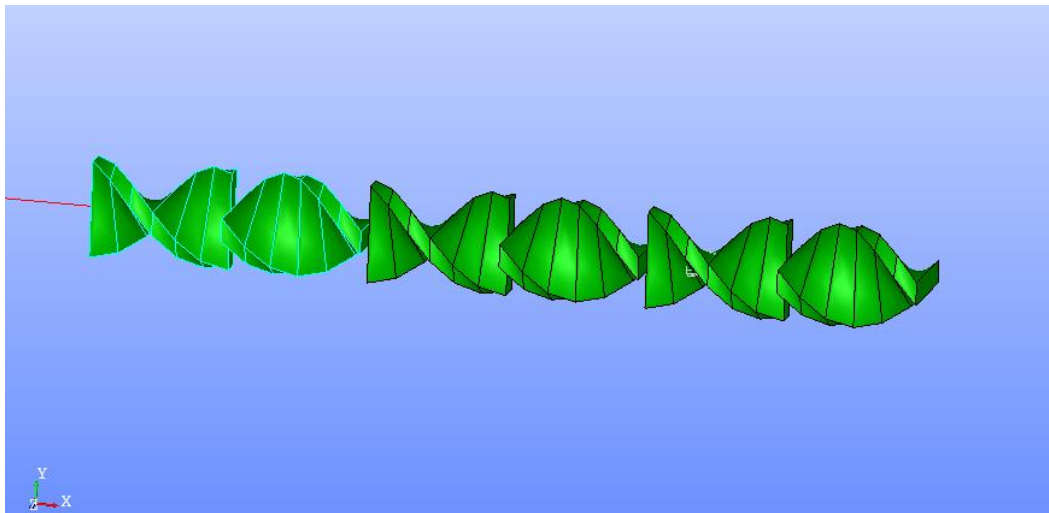


**Figure 16** Kenics static mixer

As for the 2D geometry, the mesh was realized using Salome, employing triangles for the 2D faces and tetrahedrons for the 3D volumes. The total number of cells is 2,091,246 cells , which is equivalent to 4 cells per millimetre. This number of cells allows a good accuracy of the results

to be obtained and at same time not too long computational times. The figure 17 shows an example of 3D mesh by using triangles and tetrahedrons for a Kenics static mixer element.

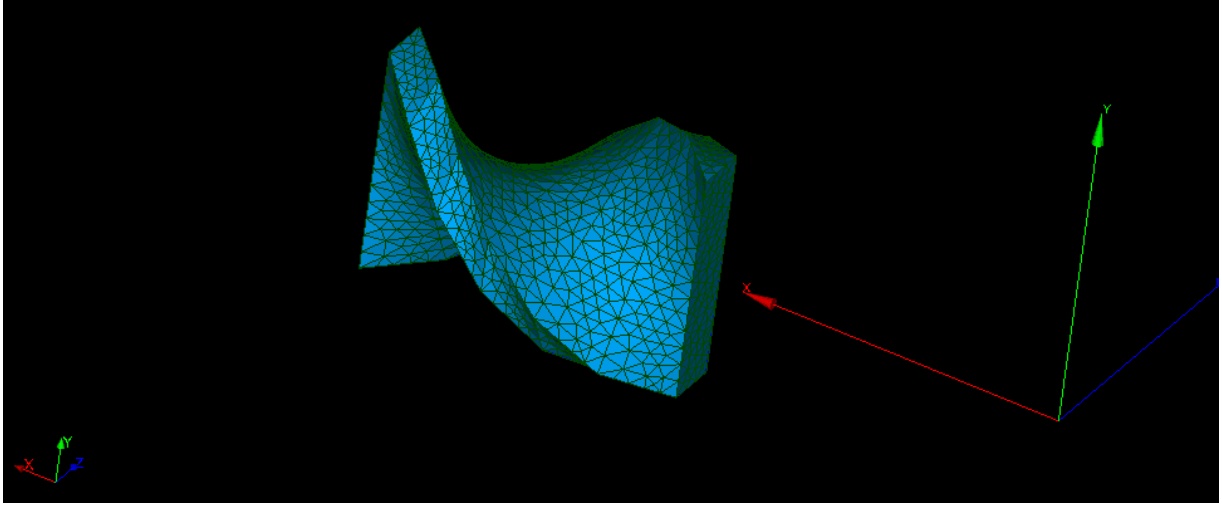


**Figure 17** Kenics static mixer mesh

### 3.3 Grid Independence

The Grid independence is a very important issue in numerical simulations, currently there is little literature concerned with this matter. Grid-independent means results change so little along with a denser or looser grid that the truncation error can be ignored in numerical simulations. Whether the grid is independent directly influences the truncation error or even the rationality of numerical results. The previous research reveals that the grid resolution and time step have a very large effect on the results of unsteady numerical simulation in a certain range. When considering grid-independent issue, in principle a very dense grid can avoid this problem but the calculational resource may be wasted unnecessarily. In practice, we usually increase the grid resolution according to a certain ratio, for example 1/3, and then compare the results of two neighbouring grids. If the results tend towards identical, the grid can be considered as grid-independent. Such strategy can utilize computational resource most efficiently as well as obtain reasonable results. The truncation error caused by grid resolution is defined as the difference between the grid independent result  $\phi_{grid\ indep.}$  and current numerical result  $\phi$  :

$$\varepsilon = \phi_{grid\ indep.} - \phi \quad (31)$$

The aims of the 2D multi-phase model are to resolve the flow field but at same time to simulate the drop's path. The point is that these two phenomena have different scales therefore for this reason the grid independence will be divided into two steps. Before the flow field independence will be guaranteed and then precautions toward the numerical diffusion will be discussed.

### 3.3.1 Flow field Independence

To guarantee the flow field independence three grids will be built increasing the grid resolution. The purpose is to match different solutions and attempt to utilize computational resource in an efficient way. Then comparing the solutions it will be searched a balance between accuracy and computational costs. In the table 6 are reported the characteristics of the grids.

	GRID 1	GRID 2	GRID 3
N° cells	26,052.0	98,922.0	387,954.0
Cells/ mm	1	2	4
Type of elements	Triangular	Triangular	Triangular
Max skewness	0.4325	0.4088	0.3522

**Table 6** Grid characteristics

The Skewness error is another numerical diffusion-type error. It effectively reduces the accuracy of face integrals to first order. Figure 18 shows a typical situation causing the skewness error.

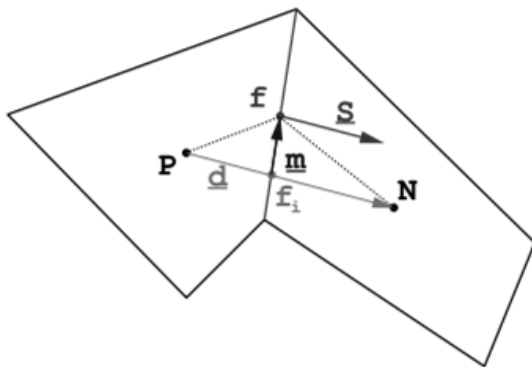


**Figure 18** Skewness error on the face.

The calculation of face integrals requires the value of the variable in the middle of the face (point f in Fig. 18) :

$$\oint_f \phi dS = \phi_f S \tag{32}$$

The value  $\phi_f$  is obtained by linear interpolation from the points P and N around the face. This interpolation actually gives the value of  $\phi$  in the point  $f_i$ , which is not necessarily in the middle of the face. It follows that the face integral reduces to first order accuracy.

Now to compare in a concrete way the three grids, three points within the 2D geometry will be chosen and their average velocity in the x direction and the statistical dispersion of the velocity vector evaluated.

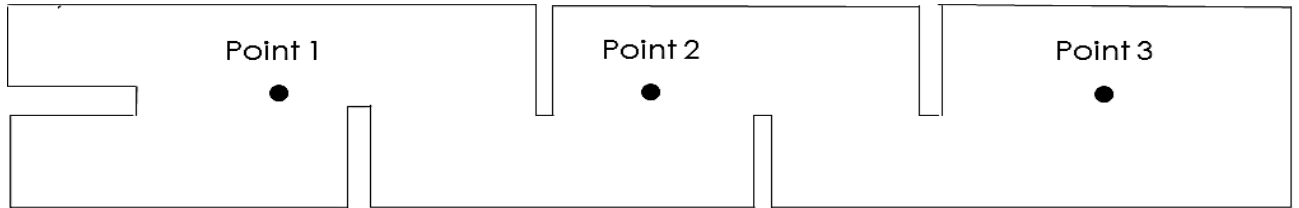
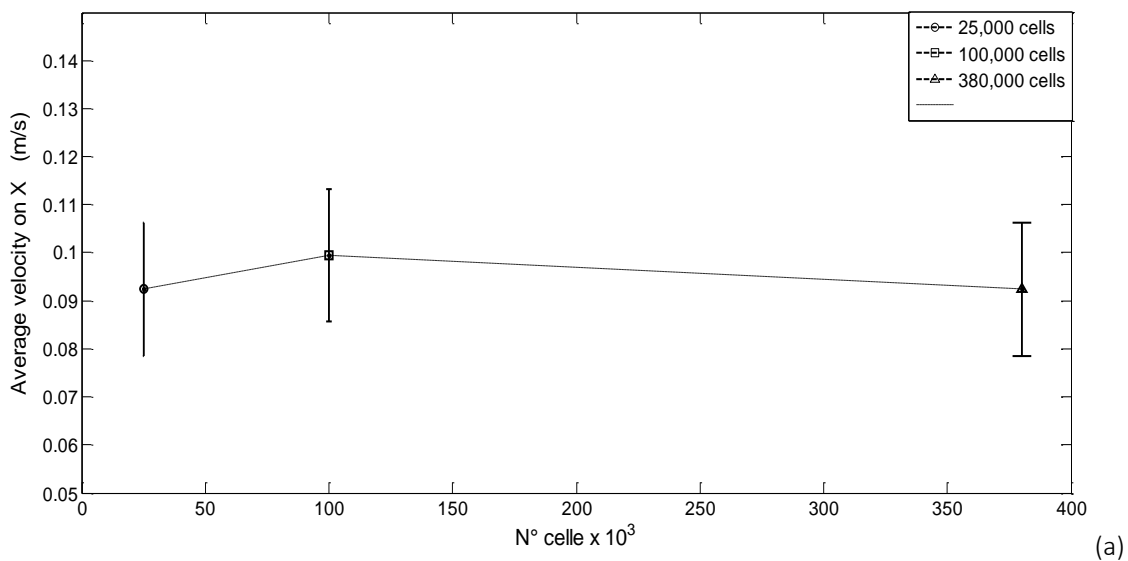


**Figure 19** Points for the grid independence

The coordinates of the three points are (figure 19):

- Points 1 :  $x=0.07\text{m}$  ,  $y=0.0063\text{m}$  ,  $z=0.001\text{m}$
- Points 2 :  $x=0.115\text{m}$  ,  $y=0.0063\text{m}$  ,  $z=0.001\text{m}$
- Points 3 :  $x=0.17\text{m}$  ,  $y=0.0063\text{m}$  ,  $z=0.001\text{m}$

This analysis has been done just for the continuous phase velocity of 0.1m/s but could also be done for the other velocities of 0.5m/s and 0.9m/s obtaining the same results. For the continuous phase with a velocity of 0.1m/s the results are presented in figure 20.



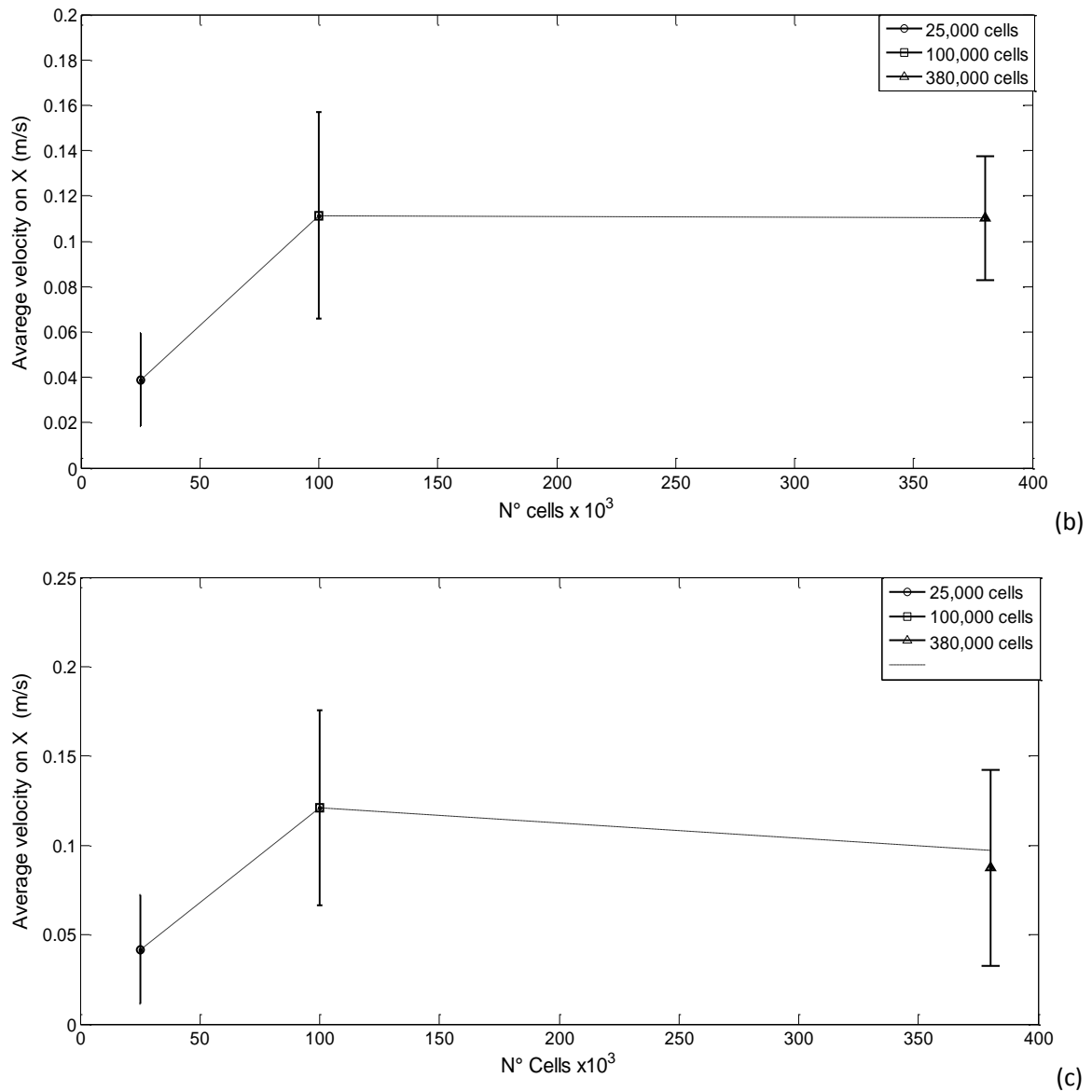


**Figure 20** Grid Independence : (a) Point 1 , (b) Point 2 , (c) Point 3 for velocity of 0.1m/s

These figures show that by increasing the refining grade the average velocity tends to stabilize on a value which is very similar for the grid 2 and 3, while the value on the grid 1 is every time significantly different from the other grids, it can be also 3 times greater than grid 2 and 3. Hence, it can be concluded that the choice of the grid should interest only the grid 2 and 3 which have 98,922 and 387,954 cells respectively. Whereas the solution does not vary between the two grids, the better choice could be the grid 2 because it allows computational resources to be saved.

### 3.3.2 Numerical diffusion

The 2D case is a multi-phase model using the VOF (volume of fluid method). The volume of fluid method is a numerical technique for tracking and locating the free surface (or fluid-fluid interface). It belongs to the class of Eulerian methods which are characterized by a mesh that is either stationary or is moving in a certain prescribed manner to accommodate the evolving shape of the interface.

The method is based on the idea of a so-called fraction function  $C$ . It is a scalar function, defined as the integral of a fluid's characteristic function in the control volume, namely the volume of a computational grid cell. The volume fraction of each fluid is tracked through every cell in the computational grid, while all fluids share a single set of momentum equations. When a cell is empty with no traced fluid inside, the value of  $C$  is zero; when the cell is full,  $C = 1$ ; and when there is a fluid interface in the cell,  $0 < C < 1$ .  $C$  is a discontinuous function, its value jumps from 0 to 1 when the argument moves into interior of traced phase. The normal direction of the fluid interface is found where the value of  $C$  changes most rapidly. With this method, the free-surface is not defined sharply, instead it is distributed over the height of a cell. Thus, in order to attain accurate results, local grid refinements have to be done. The refinement criterion is simple, cells with  $0 < C < 1$  have to be refined. A method for this, known as the marker and micro-cell method, has been developed by Raad and his colleagues in 1997.

The evolution of the  $m$ -th fluid in a system on  $n$  fluids is governed by the transport equation  $\phi$ :

$$\frac{\partial C_m}{\partial t} + \mathbf{v} \cdot \nabla C_m = 0 \quad (33)$$

with the following constraint

$$\sum_{n=1}^m C_m = 1 \quad (34)$$

For each cell, properties such as density  $\rho$  are calculated by a volume fraction average of all fluids in the cell:

$$\rho = \sum \rho_m \phi_m \quad (35)$$

These properties are then used to solve a single momentum equation through the domain, and the attained velocity field is shared among the fluids. The VOF method is computationally friendly, as it introduces only one additional equation and thus requires minimal storage.

So it is important to guarantee a good mesh refining to avoid problems in the cells where  $0 < C < 1$ , to limiting the numerical diffusion. The effect of the numerical diffusion on the drop interface is shown in figure 21.

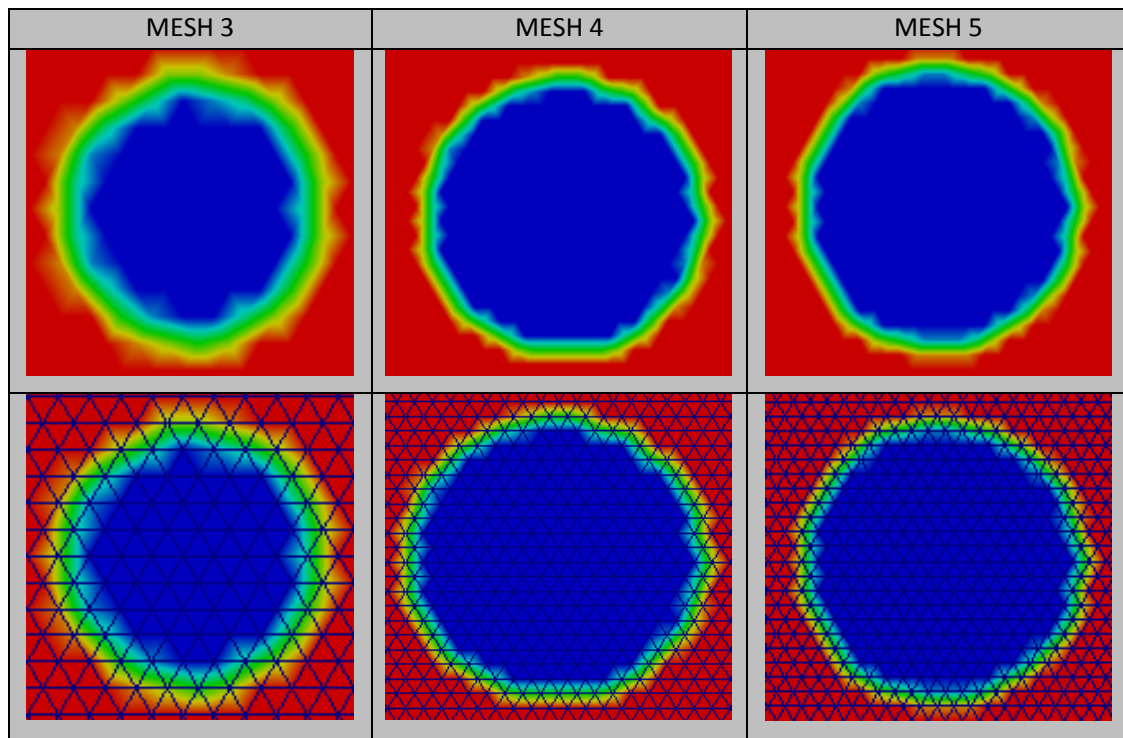


**Figure 21** Numerical diffusion for cells with  $0 < C < 1$

Basically after the flow field independence has been checked, other two grids are built (the grids 4 and 5). The characteristics of these grids are reported in table 7.

	GRID 4	GRID 5
N° cells	1,529,333.0	1,768,952.0
Cells/ mm	5	7
Type of elements	Triangular	Triangular
Max skewness	0.5113	0.7920

**Table 7** New Grid to avoid the numerical diffusion

It is clear that refining the grid is possible to obtain better results, because in realty the interface region should be very thin and not so thick. For this reason, all the following

calculations have been obtained using the finest grid, namely grid 5, in order to capture all the local flow effects.

## 3.4 Settings 2D Multi-phase Model

In this paragraph, all the settings necessary for the simulations will be listed and explained, to understand the reasons of each choice. It will be clarified which physical parameters have been used as input into the numerical model and what boundary conditions were set.

### 3.4.1 Choice of the Solver

The solver for the 2D multi-phase model has been chosen into the OpenFoam platform between several solvers available (it is reported the link to the web site <http://www.openfoam.org/features/standard-solvers.php> ). According to the characteristics of these simulations the more suitable solver has been “InterFoam” , which belongs to the Multiphase section and it is a Solver for 2 incompressible, isothermal immiscible fluids using a VOF (volume of fluid) phase-fraction based interface capturing approach. Indeed the aim of this work is to study a single oil drop to further understand the mixing processes. To easily reach the stationary time a modified version of this solver was performed “LTInterFOAM”, which is a local time stepping (LTS, steady-state) solver for 2 incompressible, isothermal immiscible fluids using a VOF (volume of fluid) phase-fraction based interface capturing approach.

### 3.4.2 Choice of the turbulence Model

The simulations have been performed with a Reynolds number ranging from 3,000 to more than 10,000 so a turbulence model is necessary. OpenFOAM offers a large range of methods and models to simulate turbulence as :

- Reynolds-average simulation (RAS), also known as Reynolds-averaged Navier-Stokes (RANS).
- Large eddy simulation (LES)
- Direct Numerical Simulation (DNS)

The turbulence model chosen is the Reynolds-average simulation (RAS) , because also if it has some limits and disadvantages, it is the most helpful for the industrial scopes. On the other hand, LES and DNS simulations are computationally expensive and currently prohibitive for practical problems. Between the RANS models available, two different turbulence model have been tested :

- **kEpsilon Model** : is the most common model used in Computational Fluid Dynamics (CFD) to simulate mean flow characteristics for turbulent flow conditions. It is a two equation model which gives a general description of turbulence by means of two transport equations . It has been performed at the beginning without obtaining convergence of the solution. The reason can be found in the specific geometry of the problem which is characterised for the presence of baffles which make the flow as a wave. Indeed the k-ε model also performs poorly in a variety of important cases such as unconfined flows, curved boundary layers, rotating flows and flows in non-circular ducts.
- **kOmegaSST Model:** The SST k-ω turbulence model [Menter 1993] is a two-equation eddy-viscosity model which has become very popular. The shear stress transport (SST) formulation combines the best of two worlds. The SST formulation also switches to a k-ε behaviour in the free-stream and thereby avoids the common k-ω problem that the model is too sensitive to the inlet free-stream turbulence properties. Authors who use the SST k-ω model often merit it for its good behaviour in adverse pressure gradients and separating flow and for rapidly changing flows. Indeed by using this model the convergence of the solution can be reached very quickly.

The Reynolds number for the 2D simulations are reported in table 8, using the properties of the continuous phase (water)  $\rho = 1000 \text{ kg/m}^3$  and  $\mu = 0.001 \text{ Pa s}$  and a pipe diameter of 12.7mm.

Velocity (m/s)	0.1	0.5	0.9
Re	1300	6400	11400

**Table 8** Reynolds number

In reality, the velocities of the continuous phase and consequently the Reynolds numbers are larger than the values presented in table 8, because of the baffles presence.

### 3.4.3 Set-up of the Initial Conditions & Physical properties in input

Before running every simulation the initial conditions set onto the BoundaryField are :

- the velocity of the continuous phase
- the fraction function  $C$ , which characterize the VOF
- the pressure
- $k$  (kinetic energy) &  $\omega$  from the turbulence model

Additionally, the physical properties in input into the model are :

- Density, viscosity for both the continuous phase and the disperse phase
- The surface tension

The values of these properties are reported in the table 8.

	CONTINUOS PHASE (Water)	DISPERSE PHASE (Oil)
$\rho$ (kg/m <sup>3</sup> )	1000	800
$\mu/\rho$ (m <sup>2</sup> /s)	1e-06	4e-06
$\sigma$ (N/m)	/	0.02267

**Table 9** Physical Properties

### 3.4.4 Utility SetFields

This utility has been performed in order to create a specific region occupied by the oil drop. Indeed with SetFields, it is possible to set values on a selected set of cells/patch faces through a dictionary. In a simple file the user defines two regions, giving the spatial coordinates, where the fluids are present. The aim of the 2D Multi-phase model is to create an oil drop, therefore the centre and radius of a sphere should be given. The drop used for the simulations has a diameter of 2mm. The SetFields file can be found in the final appendix.

### 3.5 Settings 3D Single-phase Model

The aim of the 3D single-phase model is to produce a real flow field when the continuous phase which is water is mixed in a pipe with 6 Kenics static mixer. Basically, information on the velocity field and the shear stress field are desired to assess how much changes in velocity of the continuous phase affects the mixing performance.

#### 3.5.1 Choice of the Solver

The solver “ *pisoFoam* ” has been used for this single-phase model because it is a transient solver for incompressible flow. Additionally, if in this case the geometry is much more complex compared to the 2D case, the solver needs less computational resources.

#### 3.5.2 Choice of the turbulence Model

In the 3D case has been performed the same turbulence model used for the 2D simulation, namely the *k-Omega SST* model.

The Reynolds numbers for the 3D simulations are reported in table 9. To compute the Reynolds numbers the properties of the water  $\rho = 1000 \text{ kg/m}^3$  and  $\mu = 0.001 \text{ Pas}$  and a pipe diameter of 12.7mm are used. The velocity used for the calculations takes account the space occupied by the static mixer, which reduces the section available for the flow.

Superficial velocity (m/s)	0.1	0.5	0.9
Velocity (m/s) /vacuum degree	0.16	0.76	1.4
Re	2200	9700	17700

### 3.5.3 Set-up of the Initial Conditions & Physical properties in input

As for the 2D model, before to run every simulation the initial conditions set onto the BoundaryField are :

- the velocity of the continuous phase
- the pressure
- k (kinetic energy) & omega from the turbulence model. To help the convergence of the solution an appropriate initialization of the turbulence parameters k and  $\Omega$  has been done by using formula taken from the literature review.

Furthermore, the only physical property as an input is the viscosity of the continuous phase (water).

## 3.6 Cluster BlueBear

The Birmingham Environment for Academic Research (BEAR) is a collection of complimentary IT resources managed by IT Services that are designed to help research, all of which are free at the point of use. The procurement for the current suite of services resulted in a framework agreement with OCF, IBM, Adaptive Computing, Mechdyne and IOCOM who bring different areas of expertise to the overall research environment. One of the components of BEAR is BlueBEAR, a Linux-based batch processing High Performance Computing (HPC) cluster. The additional modelling power will enable researchers to process larger, more detailed, more accurate simulations and test cases in less time than was possible on the previous service. Within the School of Chemistry Professor Roy Johnston and his team, one of the service's major users, are using the Linux HPC service for research into many areas including computational nanoscience. Professor Johnson's team is trying to understand how to create more cost effective and more environmentally friendly catalysts for fuel cells and hydrogen cars, for example.

The centrally-funded BlueBEAR cluster is based on IBM's iDataPlex servers and consists of:

- dual-processor 8-core (16 cores/node) 64-bit 2.2 GHz Intel Sandy Bridge E5-2660 login nodes with 64 GB of memory logon nodes in a round-robin configuration for resiliency

- 1 dual-processor 8-core (16 cores/node) 64-bit 2.2 GHz Intel Sandy Bridge E5-2660 login node with 64 GB of memory for applications that make use of a Graphical user Interface (GUI)
- 72 dual-processor 8-core (16 cores/node) 64-bit 2.2 GHz Intel Sandy Bridge E5-2660 worker nodes with 32 GB of memory giving a total of 1152 cores
- dual-processor 8-core (16 cores/node) 64-bit 2.2 GHz Intel Sandy Bridge E5-2660 worker nodes with 256 GB of memory forming a large memory (SMP) service
- 2 GPU-assisted compute nodes with 2 two 8 core 64-bit 2.2 GHz Intel Sandy Bridge E5-2660 processors, 32 GB of memory and an nVIDIA Kepler-based Tesla K20 GPU forming a GPGPU service
- over 150 TB (raw) disk space primarily allocated to BlueBEAR users using IBM's GPFS cluster file system

The theoretical peak performance of the centrally-funded compute nodes is  $1216 \text{ (cores)} * 2.2 \text{ (GHz)} * 8 \text{ (floating point operations/cycle)} = 21.4 \text{ TFlop/s}$ .

Thanks to this powerful cluster, it has been possible to easily run complex simulations with grids really fine. To do this it has been necessary to learn how to handle the cluster interface. The main steps needed to run a simulation are reported below:

- Register to the BluBEAR cluster and create an user folder
- Transfer the data for the simulation (solver, turbulence model, geometry) into the user folder
- Add into the simulation settings a file that decomposes the computational domain in function of the number of cores used
- Create and run a script where the user defined all the commands necessary to perform the simulation
- Transfer to your own laptop the numerical results

To conclude a job submitted for BluBEAR is attached in the final appendix.

# Chapter 4

---

## Results

### 4.1 Introduction

In this chapter the post- processing of the numerical solution of the simulations by using Matlab will be discussed. In the first part of this section the results from the 2D Multi-phase model will be presented and a study of the drop surface in order to observe the changes of two important properties such as the shear stress and the energy turbulence dissipation will be done. After this, a streamlines analysis will be shown, to link the break up phenomenon with the local flow characteristics. In the second part of this section the results from the 3D Single-phase model will be also presented, by using an image flow characterization.

### 4.2 2D Multi-phase Results

The 2D Multi-phase simulations have been performed changing the continuous phase (water) velocity, to investigate the effect on the mixing performance, attempting to observe changes for the droplet break up. The same geometry has been run for three times with different values of the velocity: 0.1m/s , 0.5m/s and 0.9m/s with the aim to discover why the experimental data from a previous work (Forte Giuseppe (2015)) have shown a better mixing performance around 0.5m/s and not 0.9m/s, which is the highest velocity. Consequently, two ideas have been developed during post-processing:

- Comparing the local analysis on the oil drop surface with a global analysis
- A streamlines analysis

Before to present in details the post- processing analysis, the flow field for the continuous phase velocity of 0.1m/s is reported in figure 22. For the velocities of 0.5m/s and 0.9m/s similar considerations can be done, so their flow fields are not presented.

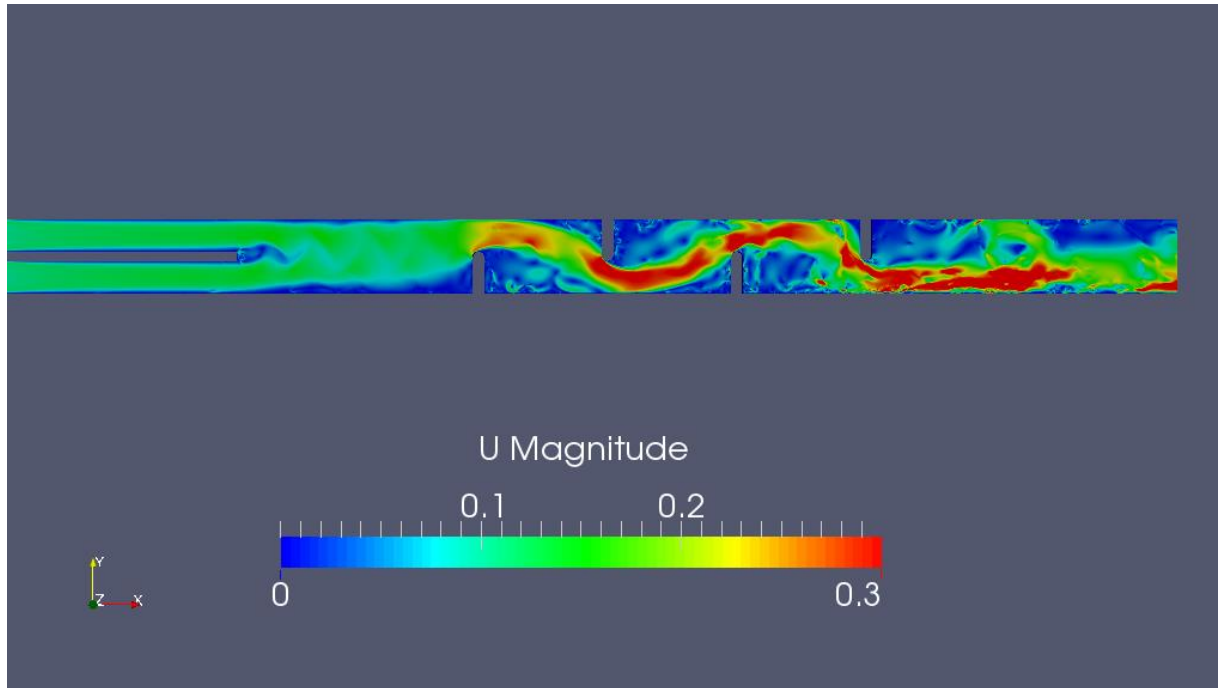


**Figure 22** Flow field for 0.1m/s

The magnitude of the velocity is presented in figure 22. It is very similar to the X-velocity because in this system the Y-velocity is a small component. The flow field shows that there are two regions:

- The inlet for the water, where the flow is uniform and the velocity value of about 0.1m/s is reached
- The region which contains the baffles, where there are recirculation areas behind the baffles and regions at high velocity near the centre of the pipe

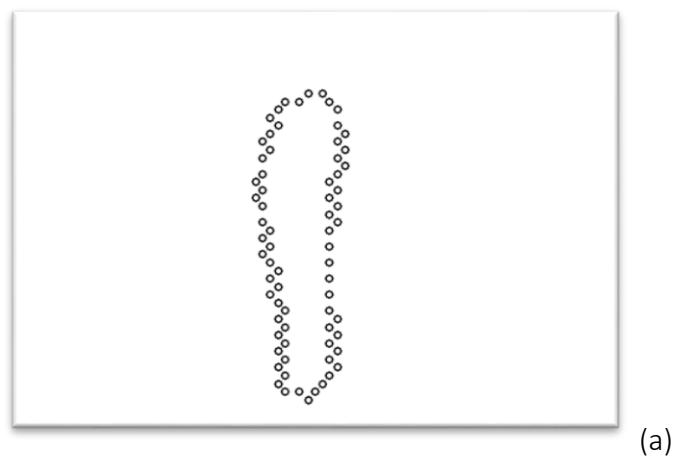
### 4.2.1 Analysis of the oil drop surface

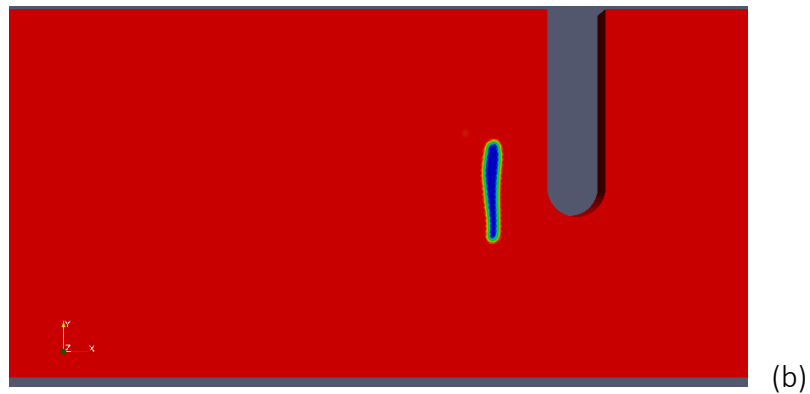
The drop break up is a local phenomenon which rises from the balance between an external disturbing force, induced by the flow field, which tries to deform the droplet and an internal restoring force which tries to keep the droplet in its original shape. The developed idea is to observe and study the drop surface and in particular take account of changes of two important parameters:

- The shear stress
- The energy turbulence dissipation

This is because both the parameters can be linked with the external disturbing force causing the drop break up. It is also possible to follow the shape changes of the drop and study the deformation in the x and y directions.

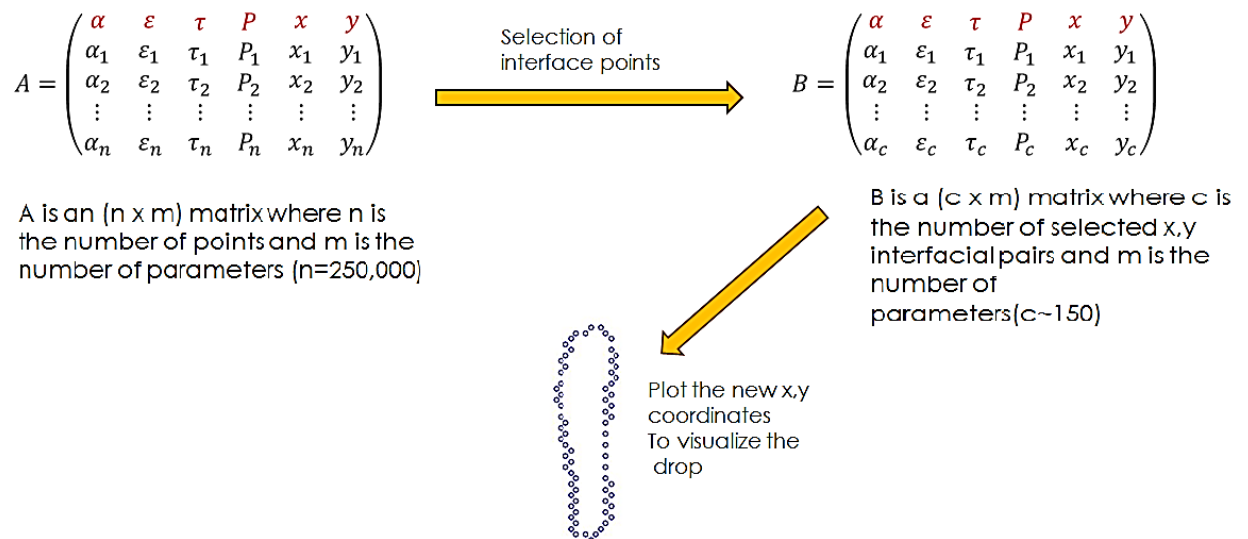
Basically, in order to study the drop surface, it is necessary to import the raw data of the simulations from OpenFoam to Matlab in a matrix form. The imported matrix contains all the numerical variables defined in each cell of the numerical grid. So to re-build the drop surface and keep only the variables defined onto it, a Matlab script has been created (which is attached in the final appendix). This code, by using the value of the mass fraction, is able to find the cells where the C function or mass fraction has values between 0 and 1, namely it finds the interface cells. An example of drop re-built with Matlab compared with a drop image took from the OpenFoam viewer is shown in figure 22.





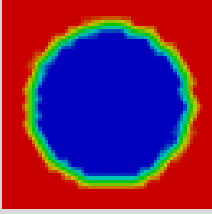
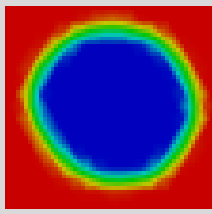
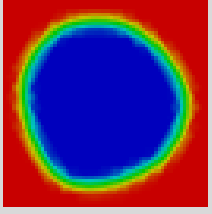
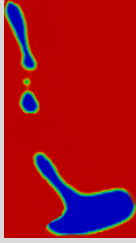
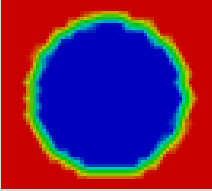
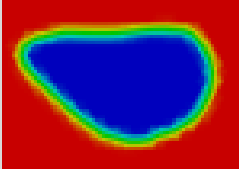
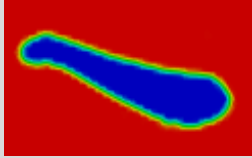
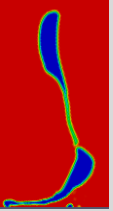
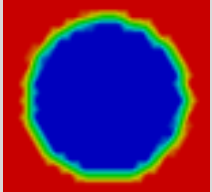
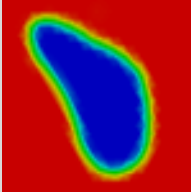
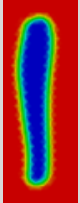
**Figure 23** Drop re-built with Matlab (a) , Drop image from simulation (b)

In all the points which make up the drop contour, it is known the velocity in x, y directions , the shear stress , the energy dissipation and other variables, so a complete analysis can be done. In order to explain how the Matlab script works to convert the initial matrix in a new matrix a simple scheme is presented in figure 23.

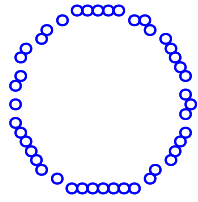
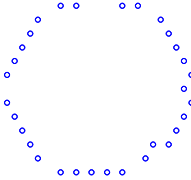
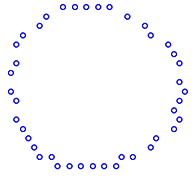
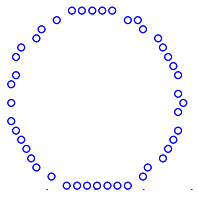
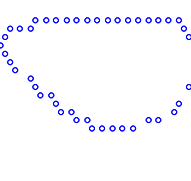
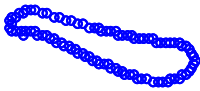
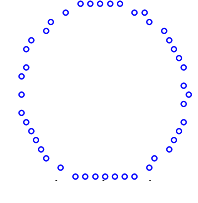
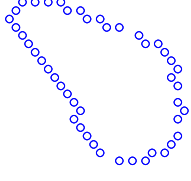
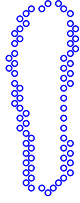


**Figure 24** Steps of the Matlab Script

In the next step the number of droplets to analyse it has been decided. In each simulation, which lasts for two seconds, and for different continuous phase velocities, the time at which the first droplet breakage occurs was obtained. The break up time was then divided in three equal intervals, to focus the analysis only on 4 drops. This time division is done because by increasing the velocity of the continuous phase in theory the time when the first rupture happens is expected to decrease, so with an equal division it is possible to then compare drops at different velocities. All the drops observed at different time and different continuous phase velocities are reported in table 10 with the Matlab reconstructions.

v(m/s)	$t_1=0$	$t_2$	$t_3$	$t_4$ (first breakage)
0.1				
0.5				
0.9				

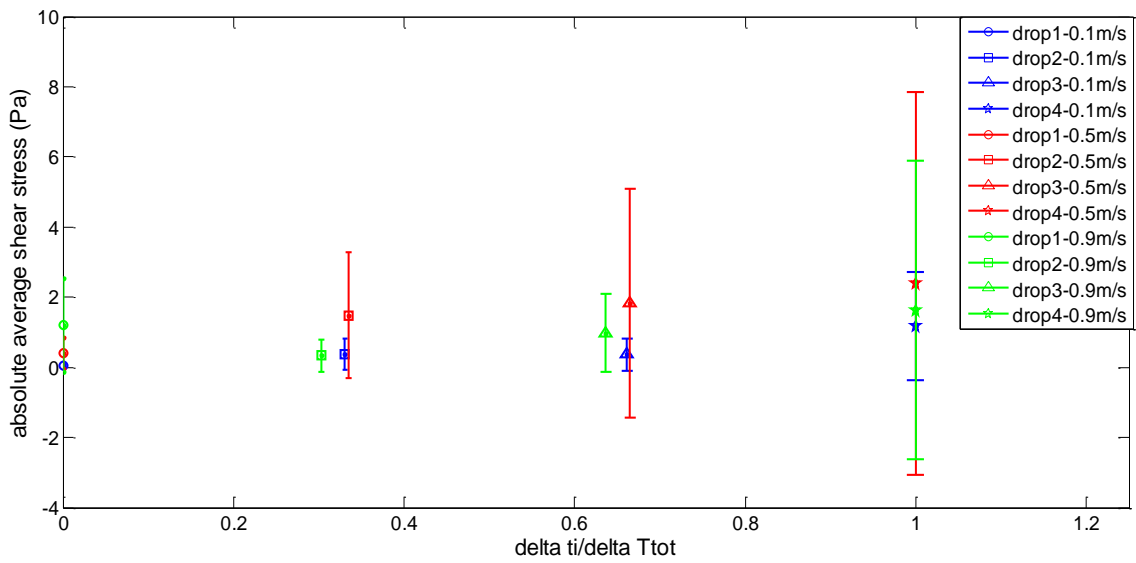
**Table 10** Study of the drop break up

v(m/s)	$t_1=0$	$t_2$	$t_3$	$t_4$
0.1				
0.5				
0.9				

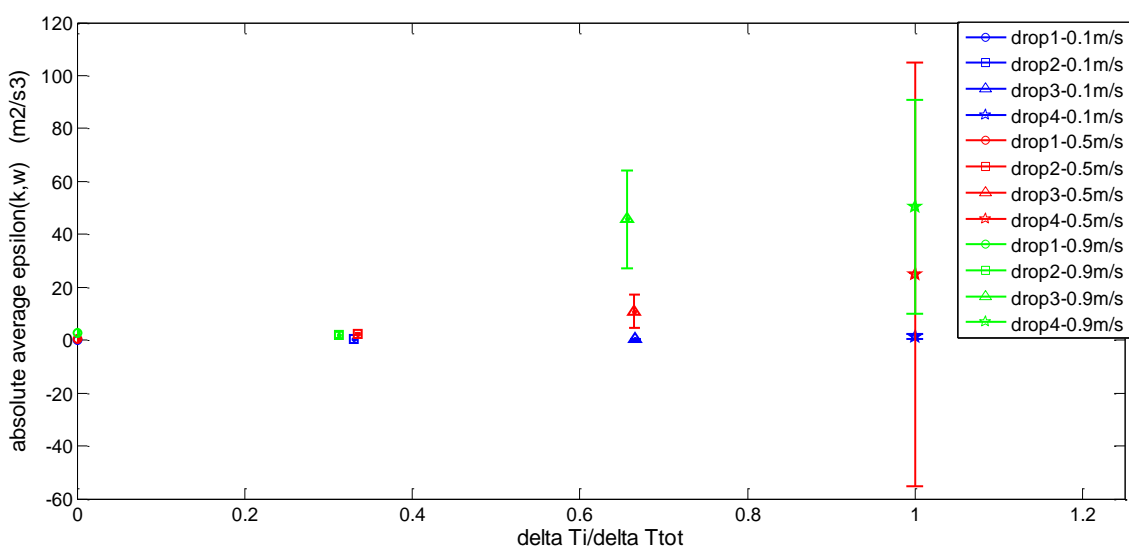
**Table 11** Drop re-building with Matlab

Therefore, from the figures above, it can be seen that there is a good agreement between the images of the droplets and the Matlab reconstructions. Now the next step is the analysis of the shear stress and energy turbulence dissipation. The aim of this is to understand how these parameters change for different drops at different velocities. Then these variables will be linked to the drop deformation along the two principle directions.

For each continuous phase velocity (0.1m/s , 0.5m/s and 0.9m/s) 4 drops are analysed. The absolute average shear stress is reported on the y axis with the dispersion of the shear on the drop surface while on the x axis the dimensionless time is plotted. The same study is repeated for the energy turbulence dissipation. The figures 24 report the shear stress and energy dissipation trends.



(a)



(b)

Figure 25 Shear stress (a) and energy dissipation (b) on the oil drop surface

According to this legend, a different colour is assigned for each continuous phase velocity:

- Blue for 0.1m/s (drop 1 , 2 , 3 , 4)
- Red for 0.5m/s (drop 1 , 2 , 3 , 4)
- Green for 0.9m/s (drop 1 , 2 , 3 , 4)

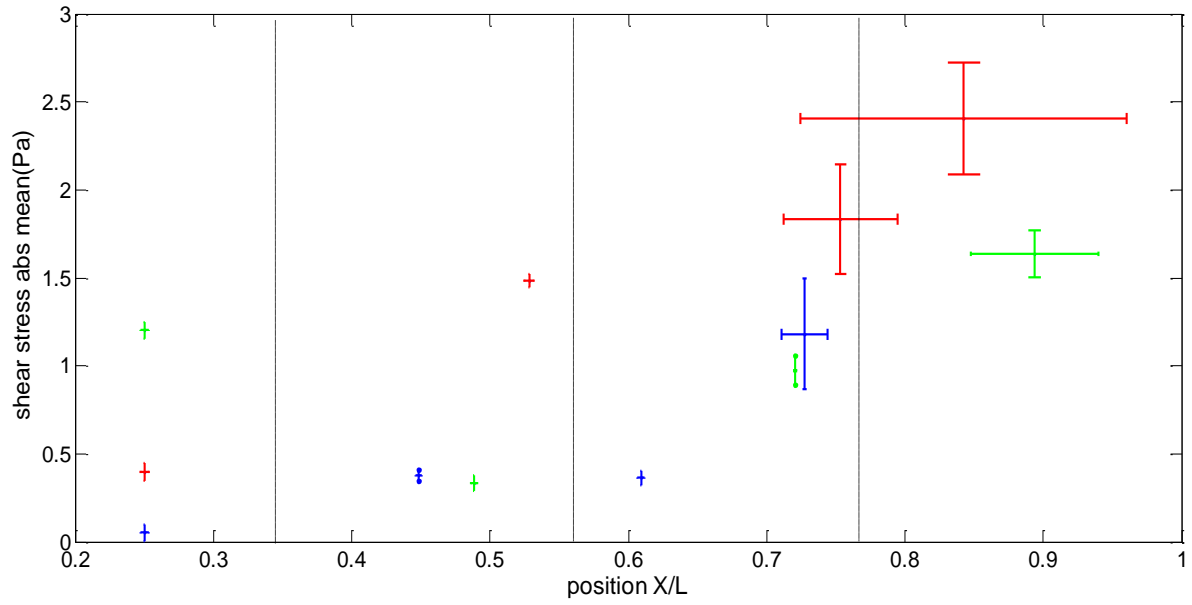
For a specific velocity (figure 24 (a) ), the shear stress plot shows that from the drop 1 to the drop 4, which have different deformations, the absolute average shear stress is enhancing and reaches a maximum value at drop 4 which represents the break up condition. The reason of this behaviour can be found in the link between the extent of the deformation and the shear stress. It is important to highlight that, also the shear stress dispersion on the drop surface increases in an objective way with the deformation for a specific velocity, as expected.

If a comparison between different velocities but on similar drop is done, it is shown that from 0.1m/s to 0.5m/s both the absolute average shear stress and the shear dispersion are enhancing with the velocity magnitude and that the behaviour changes from 0.5m/s to 0.9m/s. Indeed, it is observed that for every drop the best conditions of shear stress are reached at 0.5m/s and not 0.9m/s. This was not obvious.

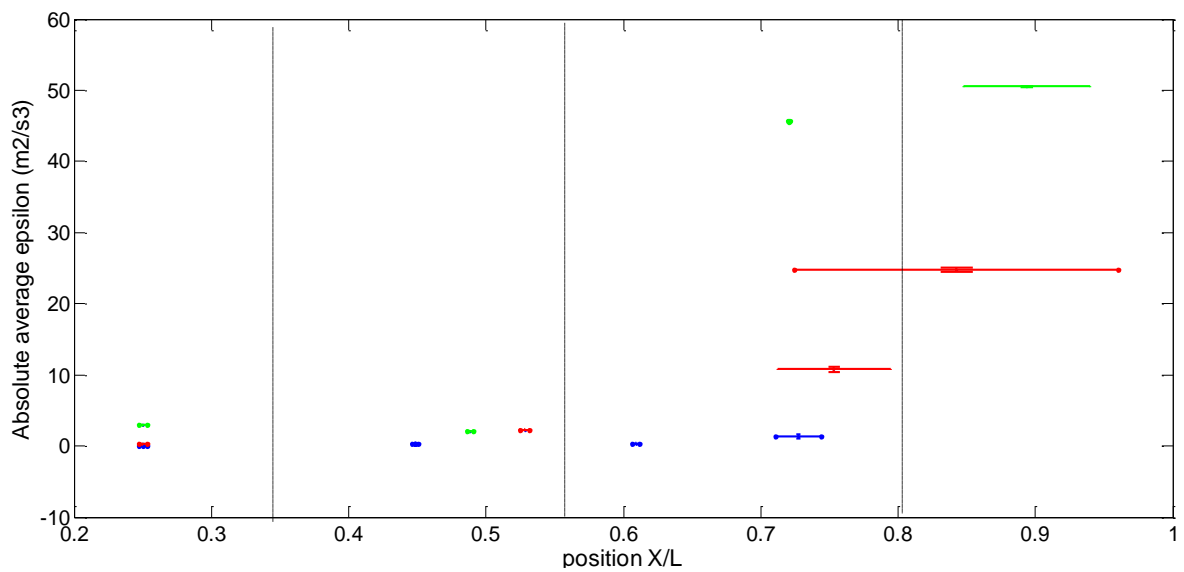
So it is possible conclude that the velocity and the shear stress are not correlated by a linear relation. This result was not expected, because in theory by increasing the continuous phase velocity, the shear stress should also increases. Furthermore, the dispersion of the shear stress is also particularly important because it is a measure of the necessary conditions for the break up. Indeed a large value of the shear dispersion on the drop surface means that the drop experiences regions with high shear stress and regions with low shear stress, a condition that is favourable to the rupture.

In addition, by observing the energy turbulence dissipation (figure 24 (b) ), it is shown that the behaviour of the energy at constant velocity and when increasing the velocity is the same. Basically the energy increases with the deformation and reaches the maximum value with the drop 4 ( break up condition) at constant velocity. Also, when increasing the magnitude of the velocity, the same trend is maintained. In the opposite way of the shear stress, the energy dissipation is related with the magnitude of the velocity in a linear way. This seems sensible because in the turbulence break up, increasing the turbulence intensity is expected to also cause a gain in energy.

To link both the shear stress and the energy dissipation trends to the deformation of the drops, a study to value the deformation on x and y directions is done, by using the dispersion of the x and y drop coordinates. In the figure below an extent of the drop deformation is given for all the drops, for different velocities.



(a)



(b)

**Figure 26** Link between shear stress , energy dissipation and deformation

As for the plots above, a different colour is assigned for each continuous phase velocity, according to this legend:

- Blue for 0.1m/s (drop 1 , 2 , 3 , 4)

- Red for 0.5m/s (drop 1 , 2 , 3 , 4)
- Green for 0.9m/s (drop 1 , 2 , 3 , 4)

In this plot the vertical bar is the dispersion of the y coordinate and the horizontal bar is the dispersion of the x coordinate. In other words, the error bars are a measure of the drop deformation. Then there are lines, to attempt to divide similar drops but at a different velocity, to make easier the comparisons.

Basically, it is possible to notice that at a constant velocity, the deformation is very small for the first two drops, which tend to preserve their shape and it increases for the drops 3 and 4 which are respectively more deformed and broken. These plots have confirmed that the higher values of shear stress observed at 0.5m/s instead at 0.9m/s can be explained with the maximum drop deformation on x and y registered for the drop 3 and 4 at 0.5m/s. On the other hand, there is no correlation between the energy turbulence dissipation trend and the extent of the deformation. Indeed although at 0.5m/s it was found the maximum drop deformation, the highest values of the energy correspond to the velocity of 0.9m/s.

Additionally, a strange behaviour of the shear stress with the velocity by means a local study of the drop surface was discovered. It is now interesting to compare these results with a global study done on the whole geometry, considering both the shear stress and the energy dissipation, as done previously. First of all, using the statistical tool of Matlab a distribution fitting an histogram for the shear stress is presented in figure 26.

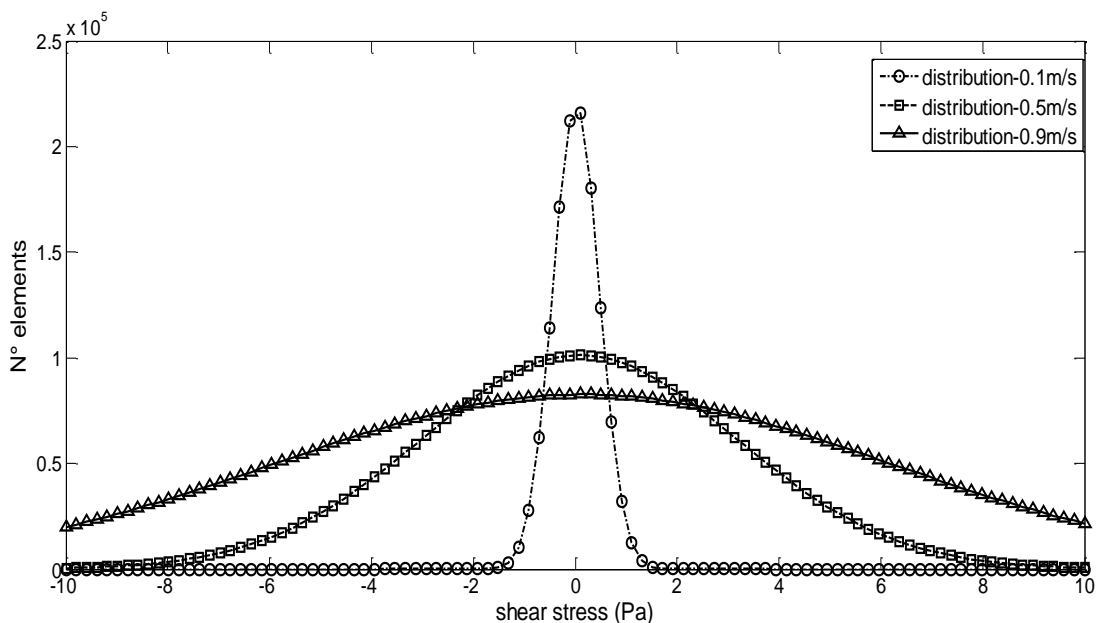
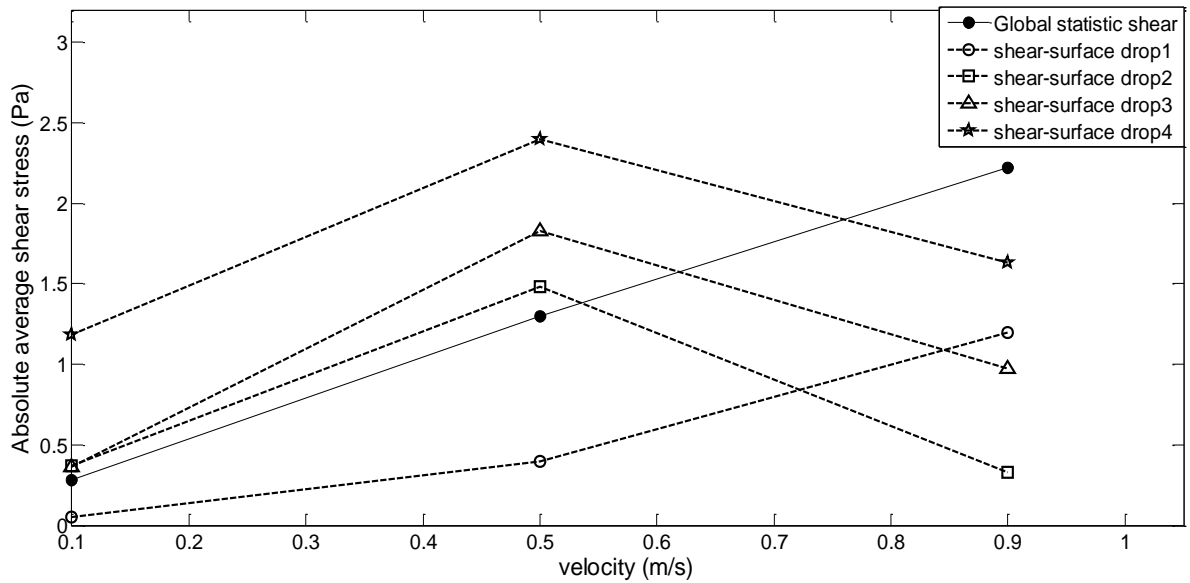


**Figure 27** Global analysis on the shear stress

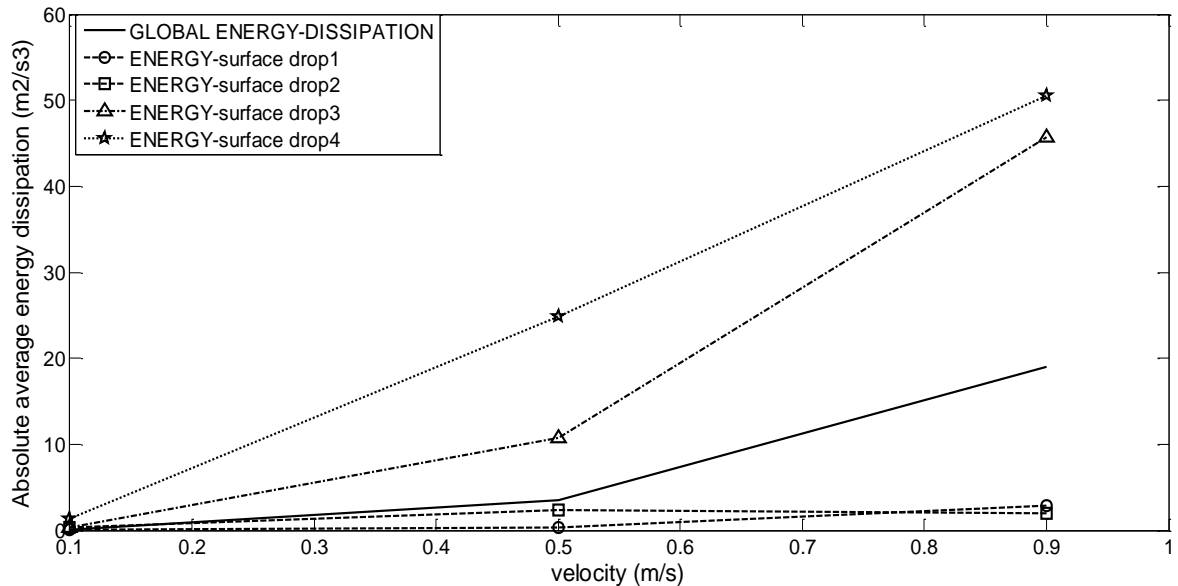
On the y axis the number of cells which has a specific value of the variable is reported and on the x axis the shear stress (variable) is reported. This plot give us an obvious result, namely

increasing the continuous phase velocity the N° of cells which has an higher value of shear stress increase or in other words increasing the velocity the variance of these curve increases. This behaviour of the shear stress is different from the behaviour highlighted with the local analysis of the drop surface.

Hence to clarify this discrepancy, the shear stress on the drop surface for each drop will be compared with the global shear stress just presented, changing the continuous phase velocity. The same analysis will be done also for the energy dissipation.



(a)



(b)

Figure 28 Local approach vs Global approach

Figure 27 (a) reports the average shear stress on y axis and different continuous phase velocity on the x axis. The black line is the global shear stress, namely it is another way to represent the previous distributions, while the other lines feature the absolute average shear stress evaluated on the drop surface for each drop, at different velocity.

Two important aspects should be noticed :

- The global and the local shear stress trend are different. The first one takes into account the whole fluid flow field and the other it is focused on the drop surface where changes of the shape take place. It is also shown how for all the drops, except the drop 1 , the absolute average shear stress decreases from 0.5m/s to 0.9m/s.
- Only the drop 1 , drop initialized at time  $t=0$ , does not follow the local trend but follow the global trend. This can be explained as a numerical effect of the initialization process.

On the other hand, the figure 27 (b) shows an agreement between the local approach and the global approach because in both the cases the energy grows with the velocity. The energy turbulence dissipation is a function of the turbulence intensity so it is no surprise that its module enhance increasing the continuous phase velocity.

### 4.2.2 Streamlines analysis

For a better understanding of the previous shear stress trend, a streamlines analysis has been performed to attempt to link the position of the drops with the velocity of the continuous phase. The streamlines utility is an OpenFoam filter which is available for the user during the post-processing of the solution with Paraview. This filter allows the creation of several streamlines with a specific length and with a specific distance from the centre of the pipe cross section. The user specifies also the number of points necessary to build the streamline, called “seed points”. In the figure below, the streamlines for the 2D geometry are shown. In figure 28 the streamline colour changes with the module of the velocity.

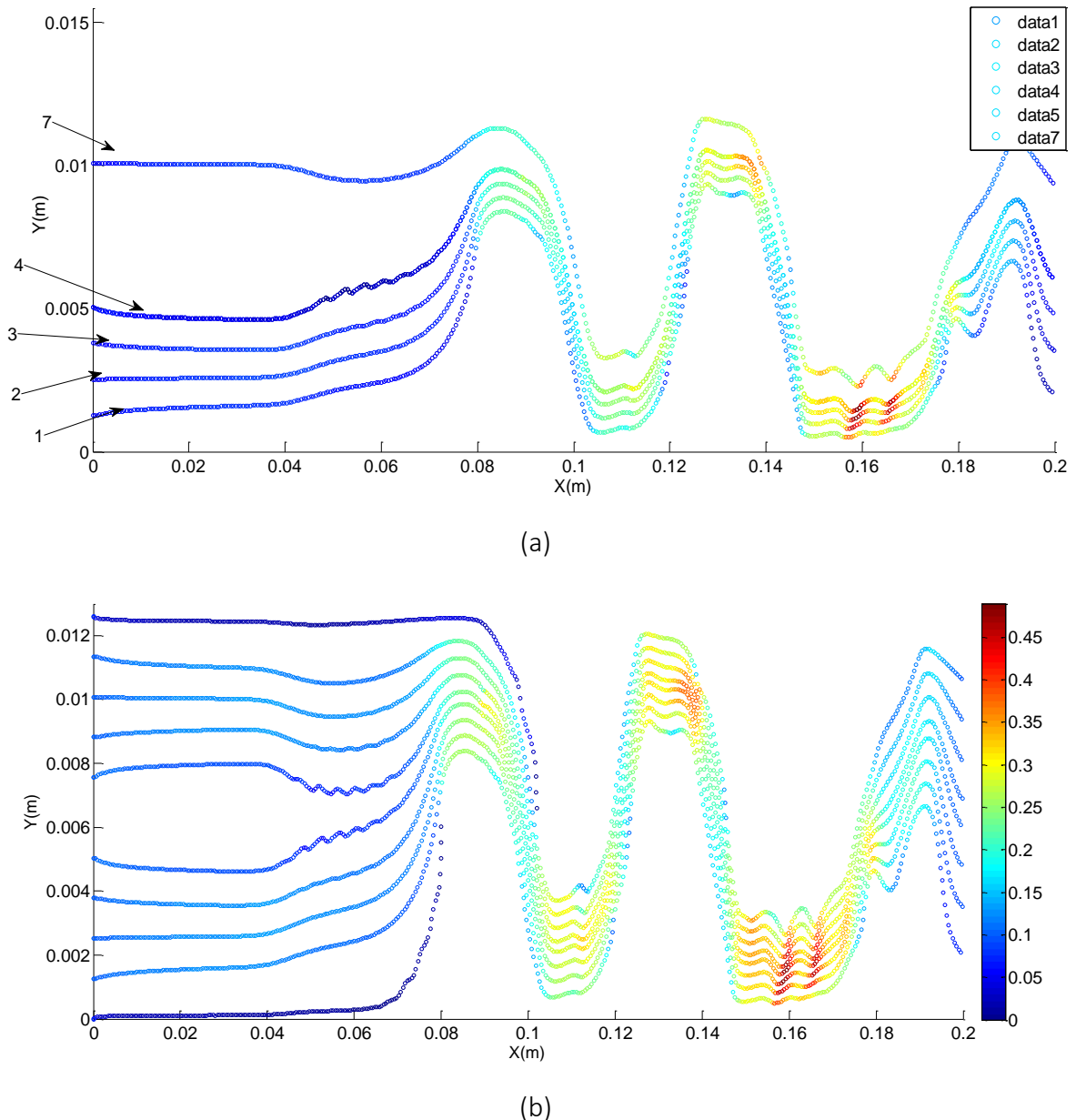
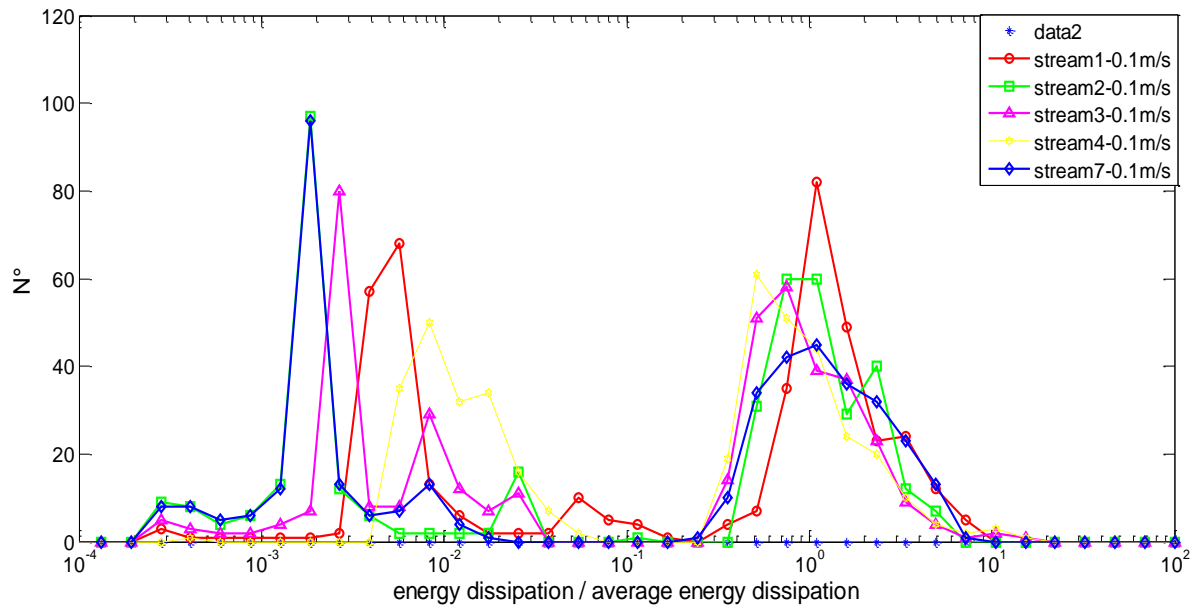


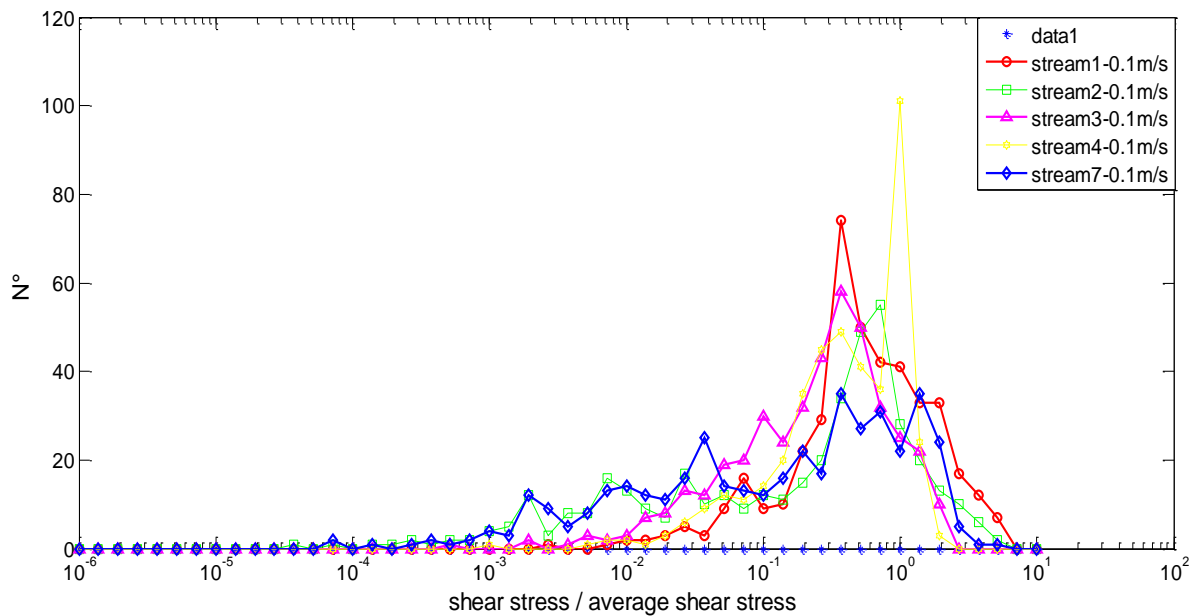
**Figure 29** streamlines studied (a) , all the streamlines (b)

The purpose of this analysis is to find a relation between the drop position in the flow field and the behaviour of the shear stress. To do this, it is necessary make a difference between streamlines near the wall, called for simplicity external streamlines and streamline near the centre of the pipe, called internal streamlines. This division is appropriate because in these two regions different shear stress gradients are expected.

Basically, both distributions of the shear stress and the energy turbulence dissipation will be done for different streamline at constant velocity and changing the continuous phase velocity. The variables reported for the distributions (shear stress and energy turbulence dissipation) are made dimensionless by using average values referred to the whole geometry.



(a)



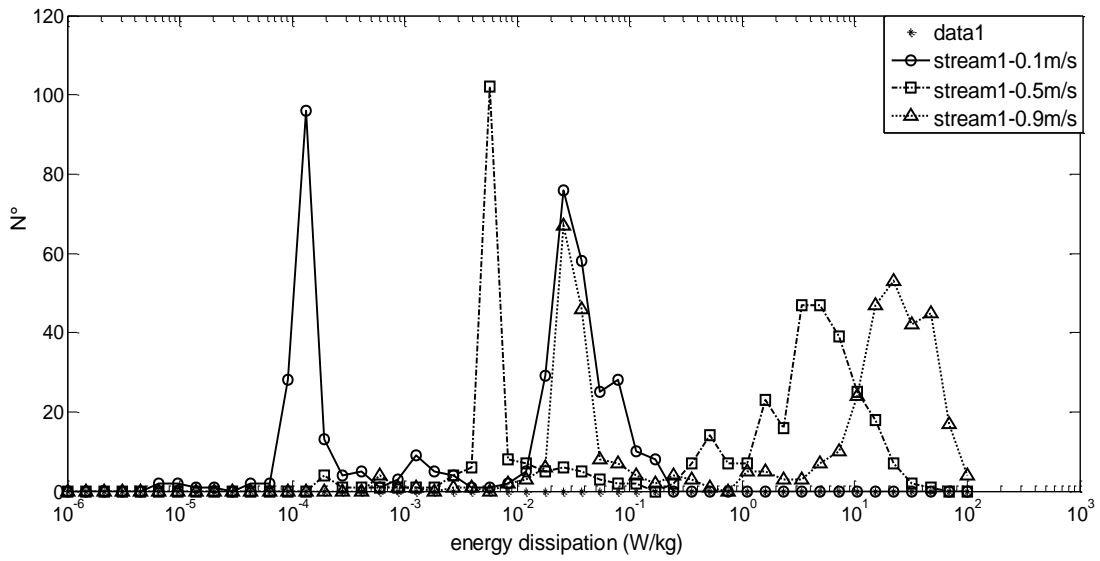
(b)

**Figure 30** Distributions of shear stress (a) and energy turbulence dissipation (b)

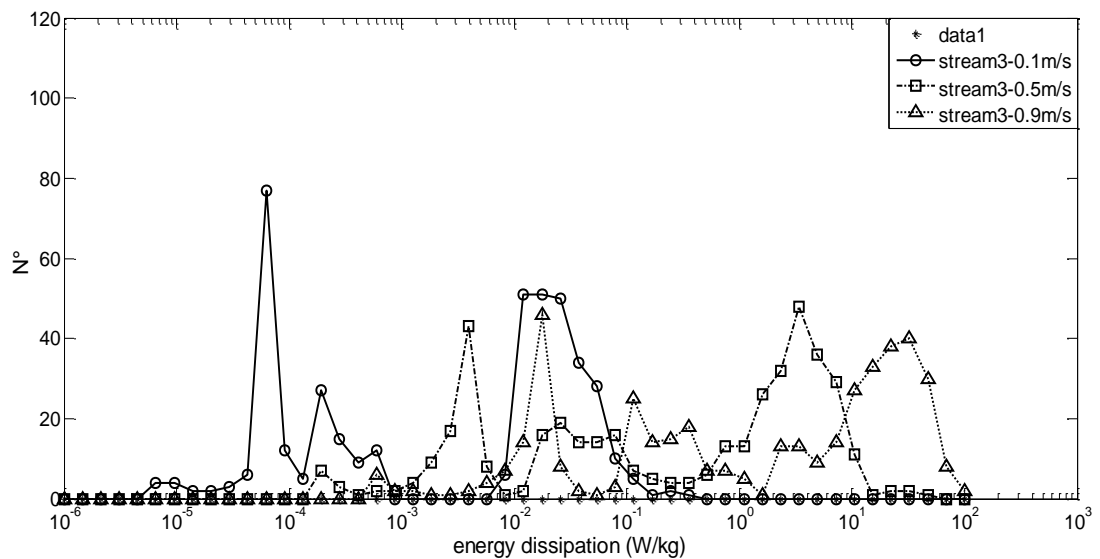
The charts reported consider 7 streamlines for a constant velocity of 0.1 m/s. The charts for the same streamlines but for the other velocities (0.5m/s and 0.9m/s) have given the same trends hence they are not presented.

The figure 29 (a) and (b) shows that moving from the external streamlines (stream 1) to the internal streamlines ( stream 4 or 7) the distributions of shear stress and energy turbulence dissipation are moving to the left, toward smaller values of the variables. From another point of view, this means that on the internal streamlines, the variations of the properties tend to be smaller compare with the external streamlines. To clarify this behaviour, the same streamlines

for different continuous phase velocities will be analysed and this will be repeated only for two streamlines.



(a)

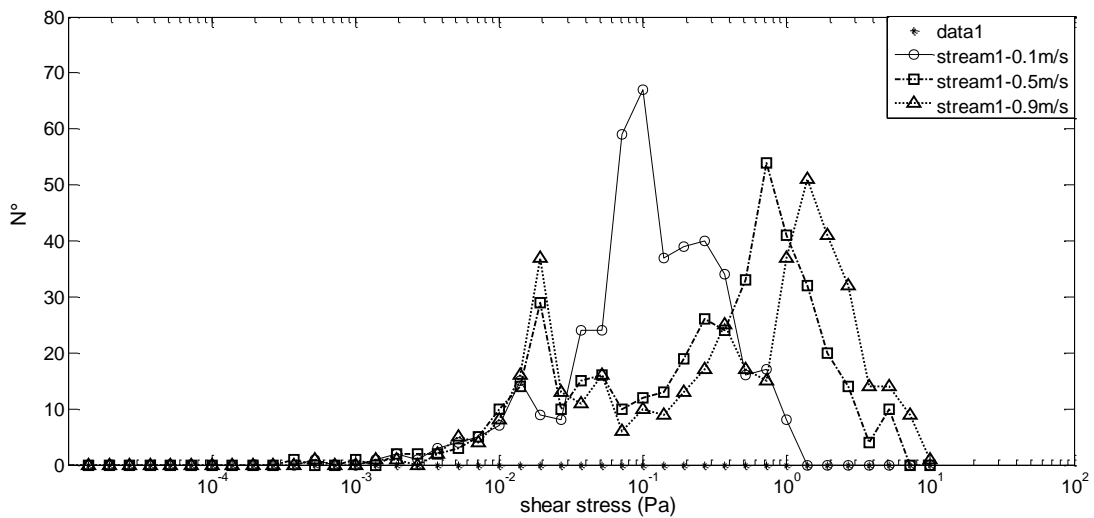


(b)

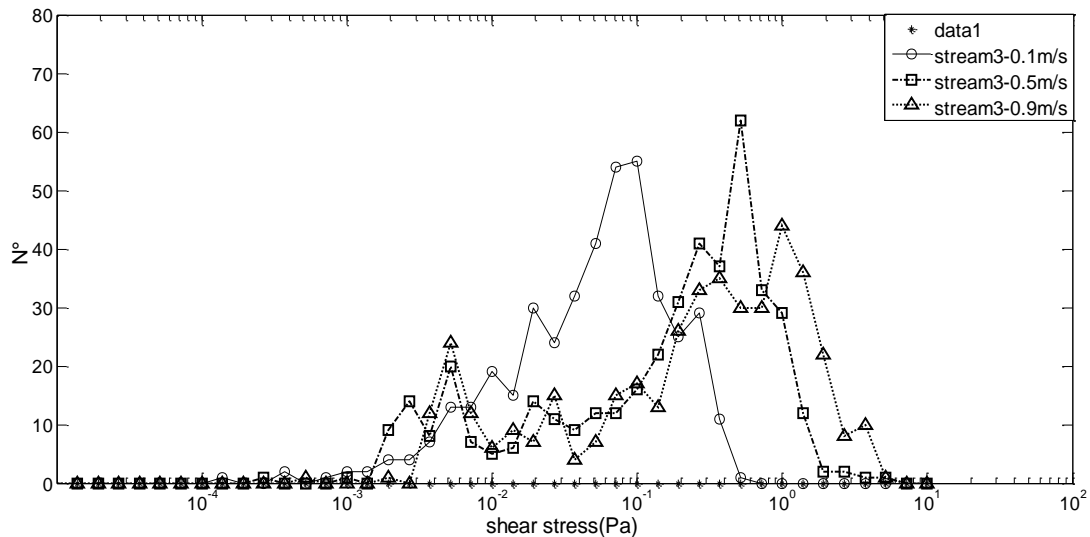
**Figure 31** Energy turbulence dissipation distribution at different velocity for the stream 1 (a) and the stream 3 (b)

Figure 30 (a) and (b) shows clearly that increasing the velocity, the energy distributions move to right, toward higher values in energy and this trend is respected also changing the streamlines considered. This result was expected and it is in agreement with the global approach seen in figure 26.

The same charts have been realized for the shear stress, in the figure below:



(a)



(b)

**Figure 32** Shear stress distribution at different velocity for the stream 1 (a) and the stream 3 (b)

The shear stress distributions in figure 31 are referred on a specific streamline for different continuous phase velocity. The charts show how increasing the velocity the shear stress distributions are moving to right, toward higher values of the shear. This result was expected and in agreement with the global approach which has shown that a linear relationship occurs between shear stress and velocity.

All the data, which came from the streamline analysis presented until now, have shown that both the shear stress and the energy turbulence dissipation enhance increasing the velocity, according to the global approach (figure 26). Hence, in order to explain the weird values of the shear stress measured on the drops surface (figure 26) another aspect should be investigated. Indeed by using images came from the post-processing of the numerical simulations and

Matlab reconstructions, it will be shown how the drop path changes increasing the continuous phase velocity.

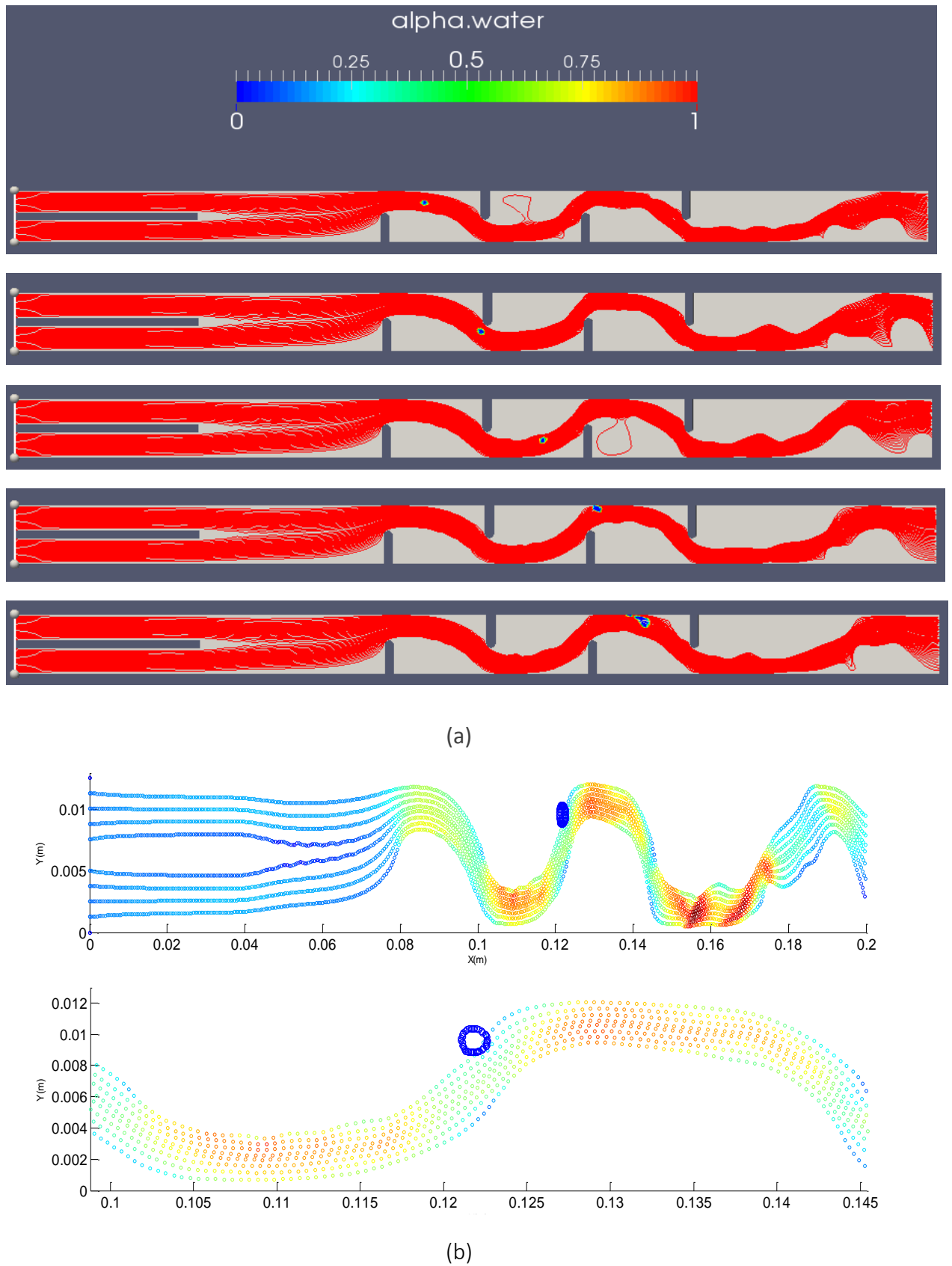
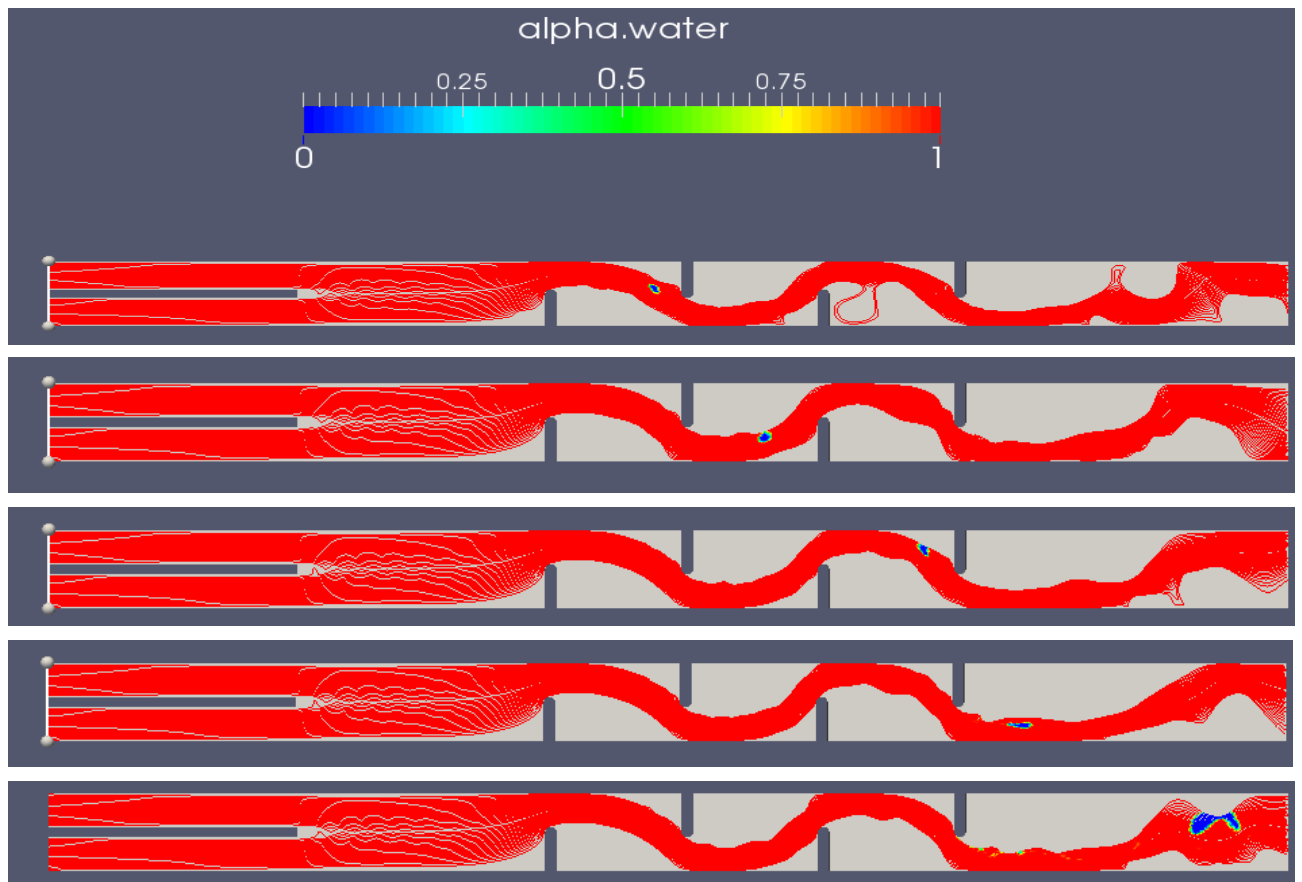
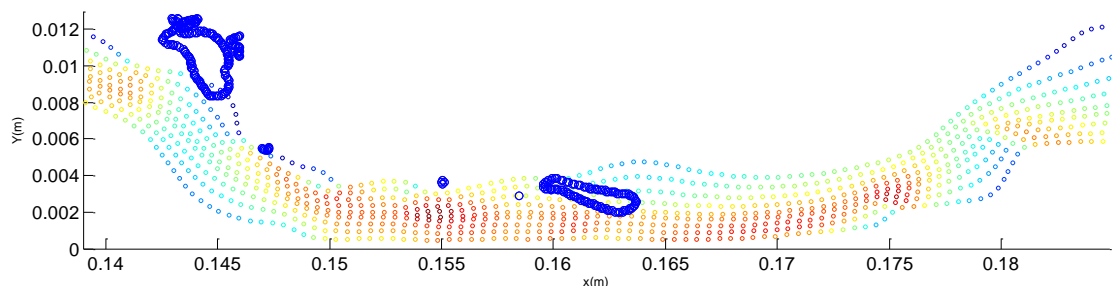
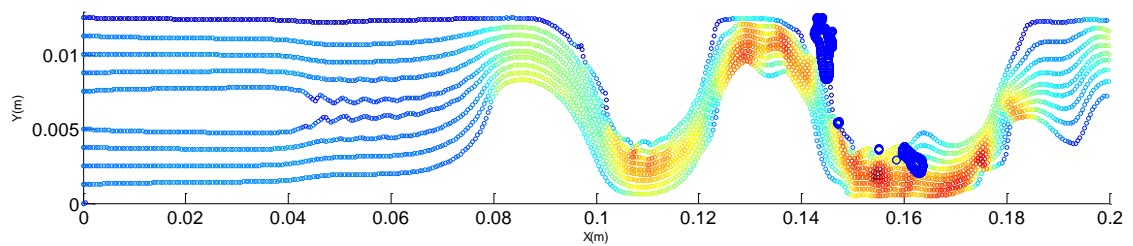


**Figure 33** Drop path (a) , Matlab reconstruction for a specific time (b) at velocity of 0.1m/s

The figure 32 shows how at low velocity the drop tends to pass in external regions, near the walls of the pipe, between regions characterized with high shear stress and regions with low shear stress.



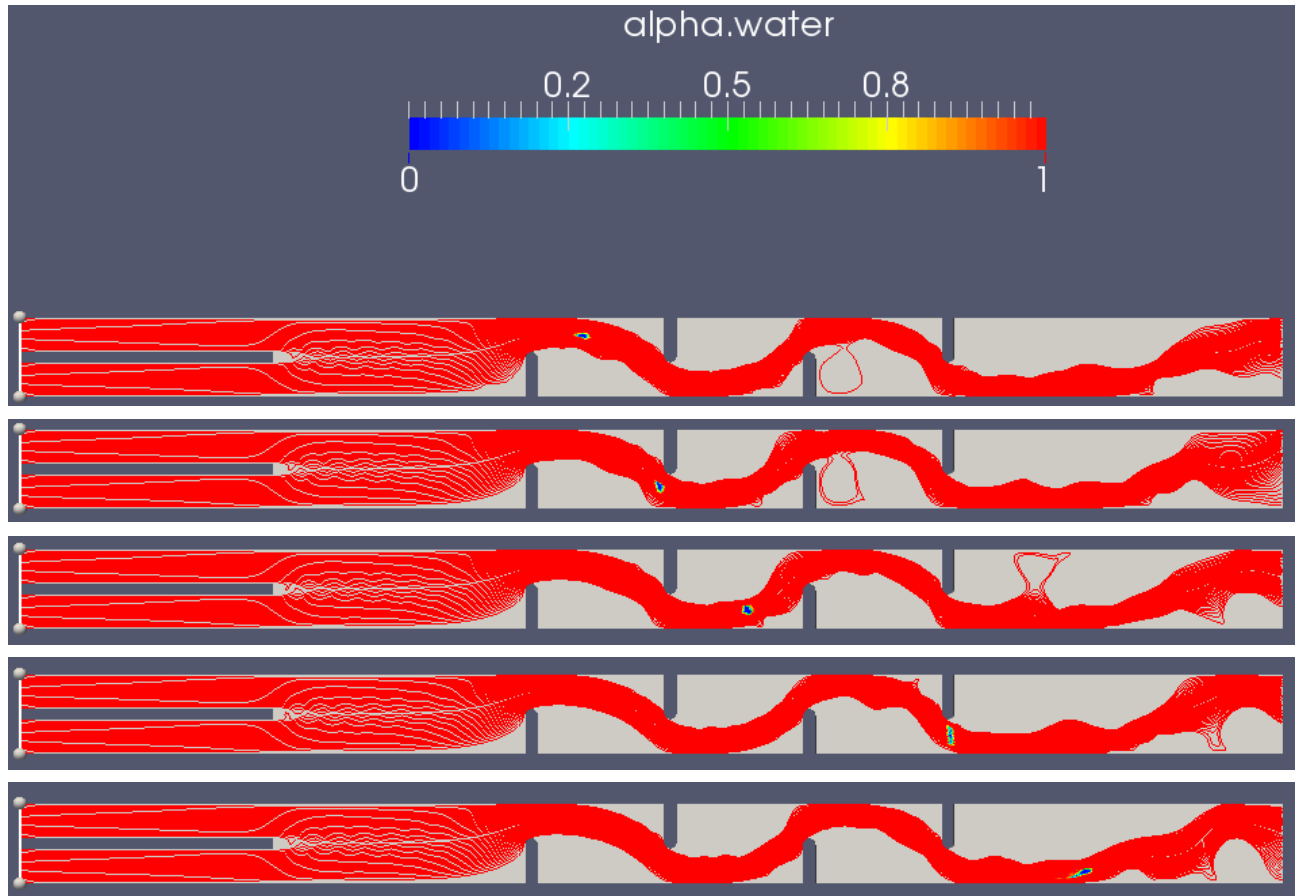
(a)



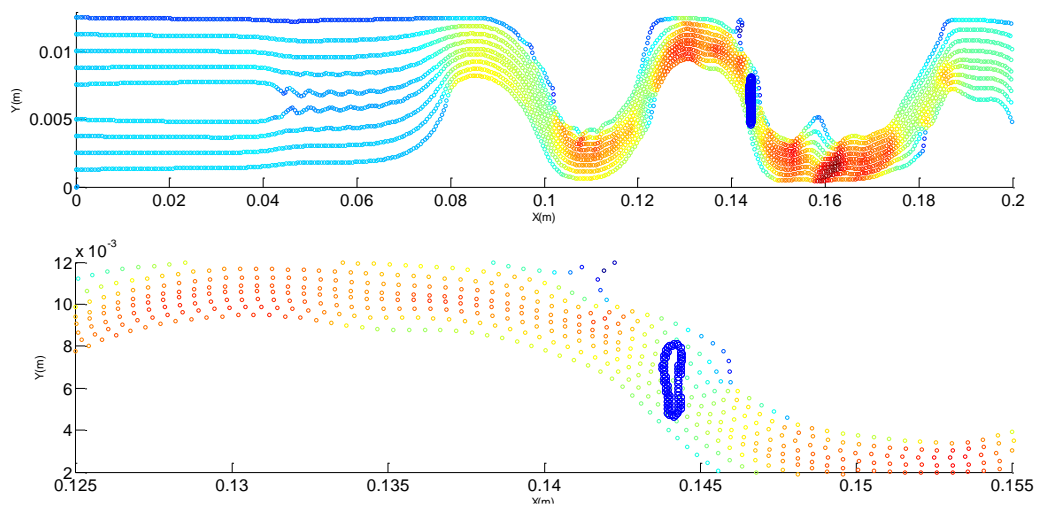
(b)

Figure 34 Drop path (a) , Matlab reconstruction for a specific time (b) at velocity of 0.5m/s

The figure 33 shows how at medium velocity the drop still tends to pass in external regions, between regions characterized with high shear stress and regions with low shear stress. This is because the momentum transferred to the drop is not enough to keep it along the main flow lines.



(a)



(b)

**Figure 35** Drop path (a) , Matlab reconstruction for a specific time (b) at velocity of 0.9m/s

The figure 34 shows how at higher velocity the drop tends to pass in the centre of the pipe, moving to the main flow lines. This condition is not ideal for the break up because the gradients of velocity are not very large and consequently the shear stress field around the drop will be uniform.

According to these charts, it is possible conclude that also if for the velocity of 0.9m/s the shear stress both in the external streamlines and the internal streamlines is higher than the shear stress at 0.5m/s, maybe for the latter velocity the drop crossed regions with larger values of the velocity gradients so it has experienced better condition for the rupture. The different drop path could be the explanation for the unusual shear stress measured on the drop surface for the two velocity.

Now to conclude the streamlines analysis both the energy profile for different streamlines and the residence time study will be presented.

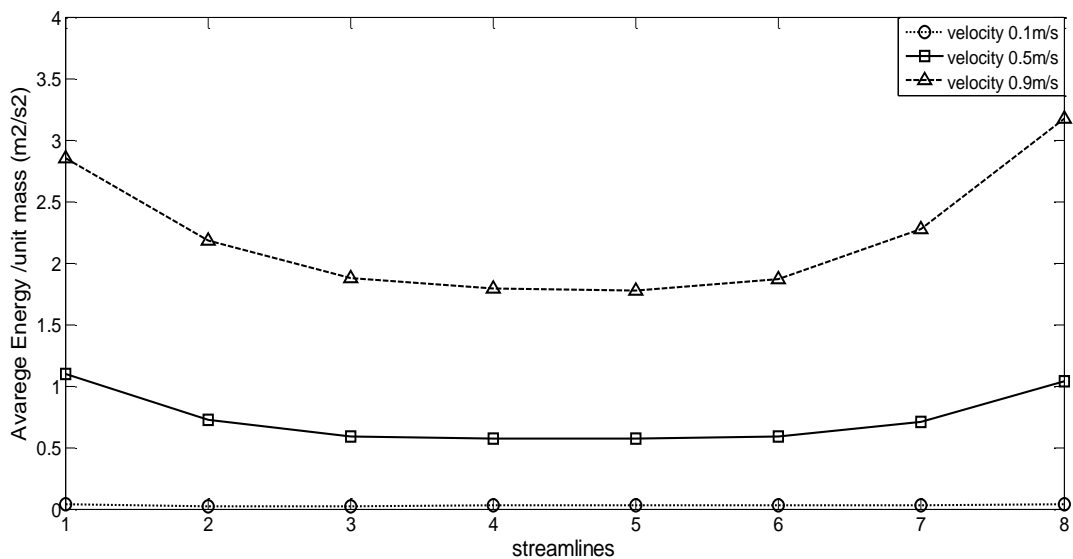


**Figure 36** Energy profile for the streamlines, changing the continuous phase velocity

The figure 35 shows an expected result, namely for the lowest velocity of 0.1m/s the average energy /unit of mass is minimum while for the highest velocity of 0.9m/s the average energy /unit of mass is maximum. Additionally, at constant velocity can be noticed that the external streamlines (near the walls pipe) are characterized with higher values of the energy while the internal streamlines (in the centre of the pipe) are characterized with lower values of the energy. The first evidence depends on the fact that, the energy is a function of the owned flow velocity. The second evidence can be explained by using the concept that within the external regions larger values of the velocity gradients are expected because more changes in flow

happen while within the internal regions, the velocity field is almost uniform so small velocity gradients are present.

It is interesting to analyse the residence time profile, presented in the figure below.

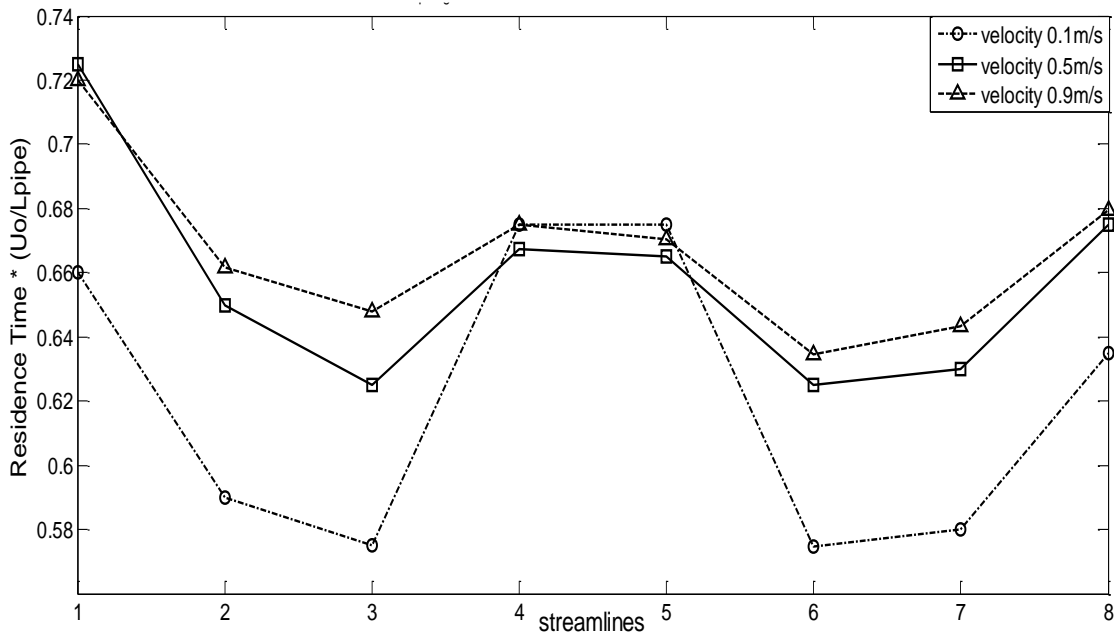


**Figure 37** Residence time profile changing the continuous phase velocity

The chart reports the dimensionless residence time profile changing the continuous phase velocity from 0.1m/s to 0.9m/s. The dimensionless has been done by using the average velocity for each simulation and the pipe length (20cm) equal for every case. It should be noticed that both the external streamlines and the streamlines in the pipe centre are characterized by the highest residence time while the streamlines between these regions have the shortest residence time. It is important to highlight this point because if we consider a group of streamlines, some within the external region and some within the internal region, a hypothetical drop will be experienced for the same residence time different shear stress at constant velocity. It is more difficult to anticipate what will happen when the same streamlines but at different velocities are considered.

The last figure in this chapter will show that for different streamlines and when increasing the velocity, the reduction of the residence time is not equal. On the y axis it is reported the residence time and on the x axis is reported the continuous phase velocity, then different streamlines are considered.

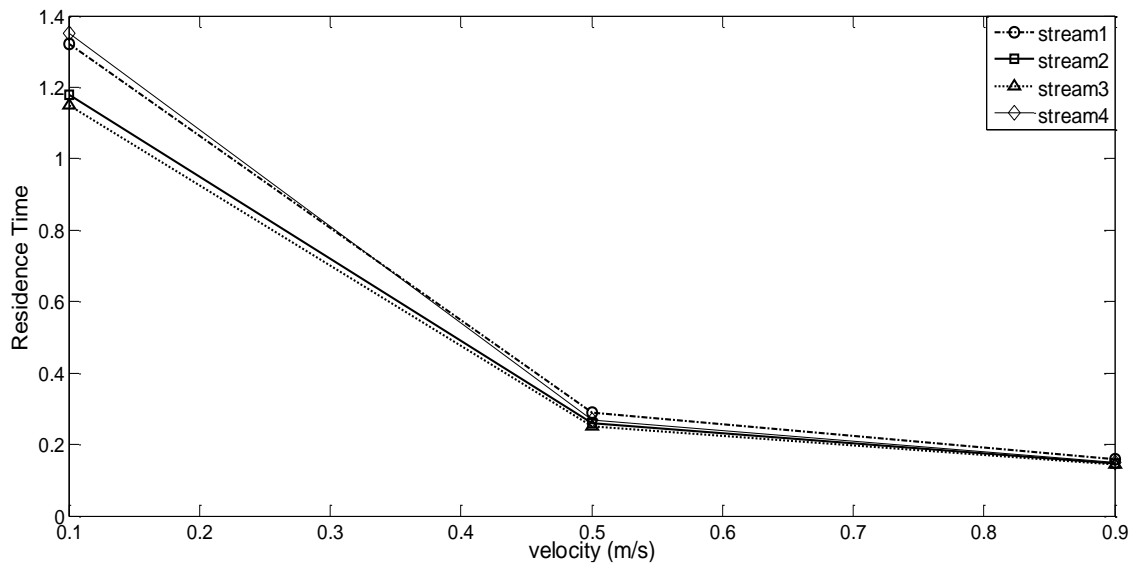


**Figure 38** Residence time profile for different velocity, changing the streamlines

It is possible to observe that at low velocity (0.1m/s) there is a larger difference in residence time changing the streamline considered than the difference that exists for higher velocities (0.5m/s and 0.9m/s).

### 4.3 3D Single-phase Results

The aim in this last phase of the work is both to link and to attempt extend the results obtained for the 2D case to the 3D case. Indeed it has been repeated the streamlines analysis to focus on :

- The energy profile for each velocity
- The residence time profile for each velocity
- The shear stress trends changing streamlines
- The energy turbulence dissipation changing streamlines

The objective will be to match the experimental results obtained in a previous study by using 6 Kenics static mixer elements with the numerical results obtained with the same geometry. In the experimental work a bi-modal distribution of the drop diameter has been found increasing the velocity from 0.5m/s to 0.9m/s and a better mixing performance it has found for the 0.5m/s. That was not an obvious result.

#### 4.3.1 3D Streamlines analysis

The streamlines analysis is repeated but in the 3D case to mark the external streamlines from the internal streamlines it is necessary a new parameter that measure the distance between the initial point of the stream and the centre of the pipe. This parameter marked with  $r$ , is made dimensionless by using the radius of the pipe  $R$ . In this way, it will be easier to highlight a potential different behaviour between the regions near the wall and the regions near the pipe centre. The figures 39, 40 show the pipe section ZY that reports the initial points for some streamlines at the inlet and the streamlines paths increasing the velocity of the fluid (water), for a better understanding of the advantages of this analysis.

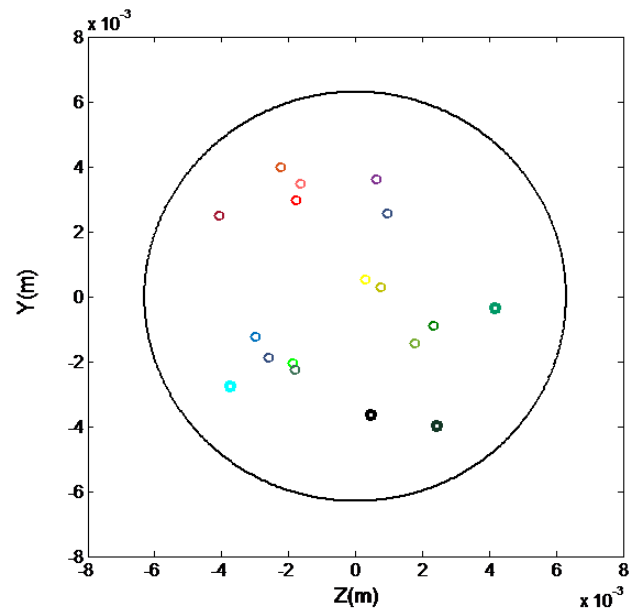
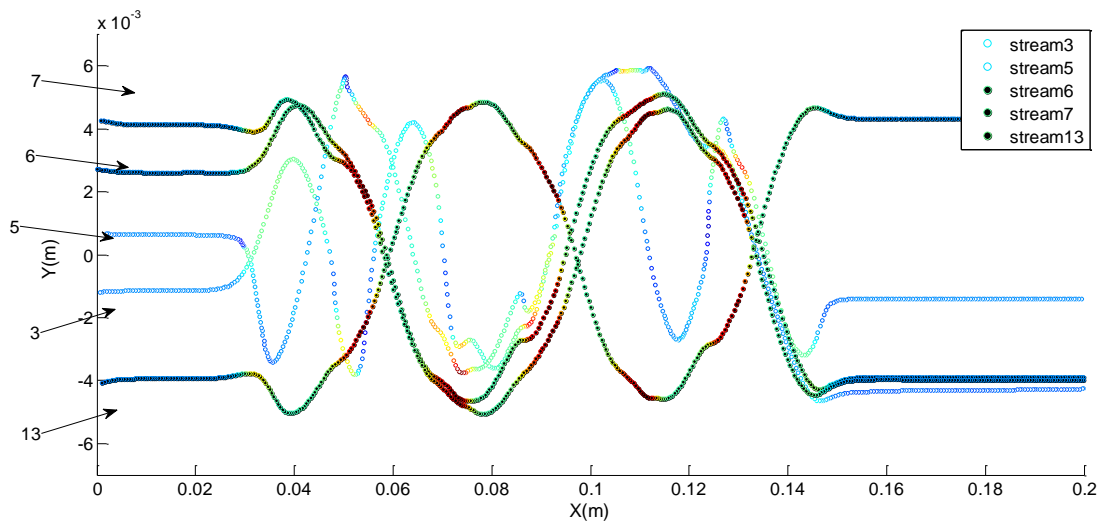
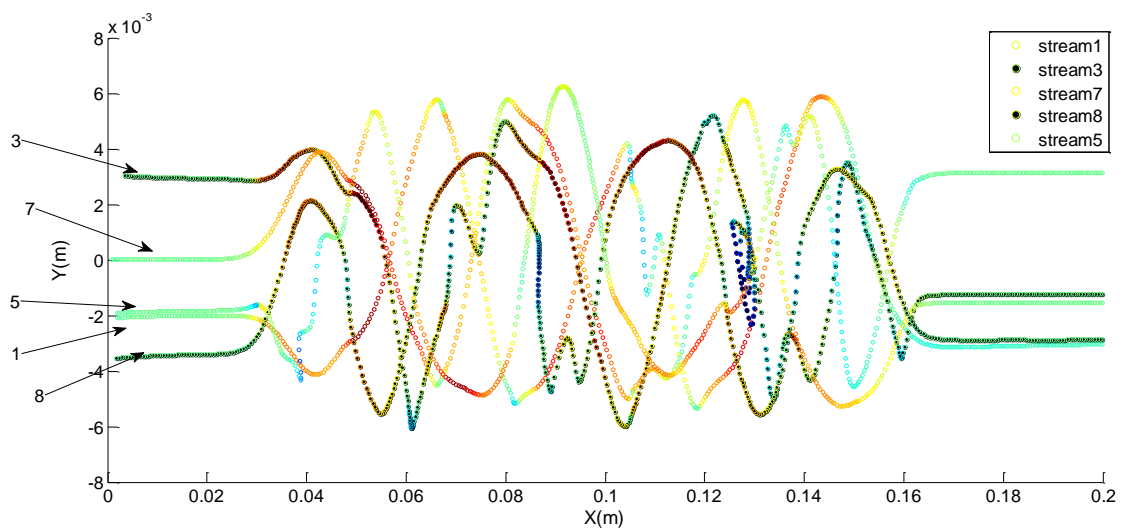


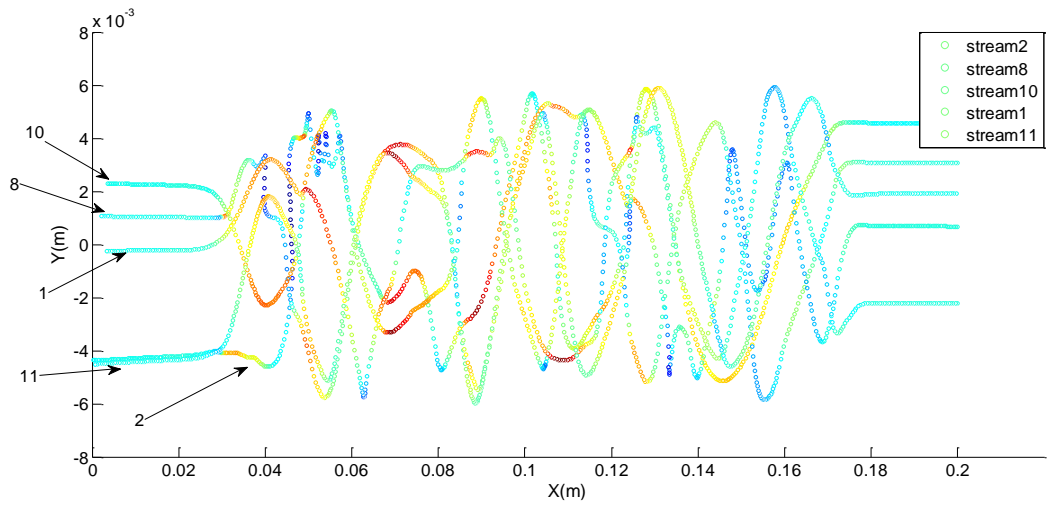
Figure 39 ZY pipe section, seeding points to create the streamlines



(a)



(b)

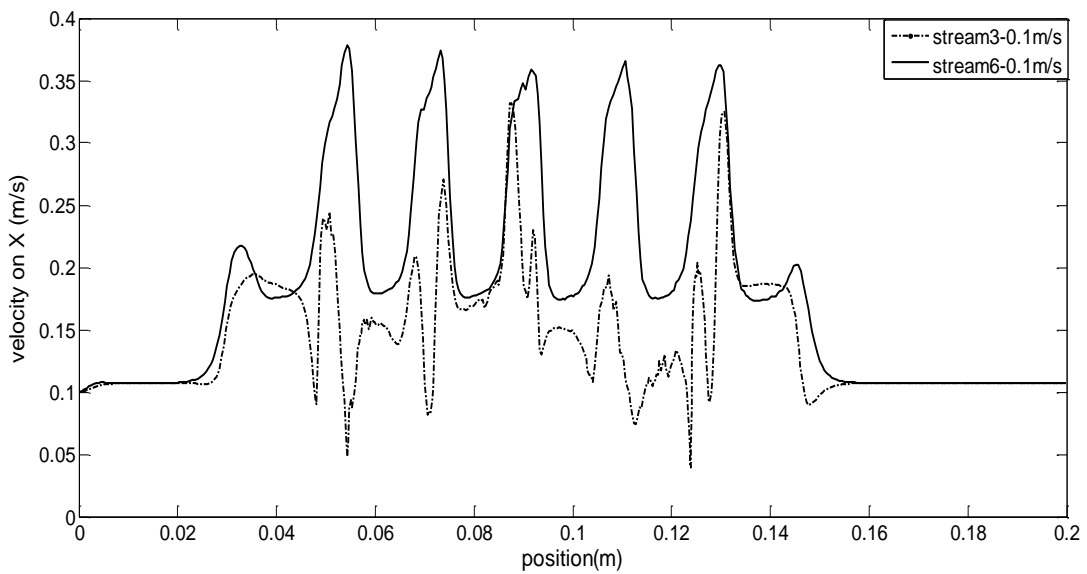


(c)

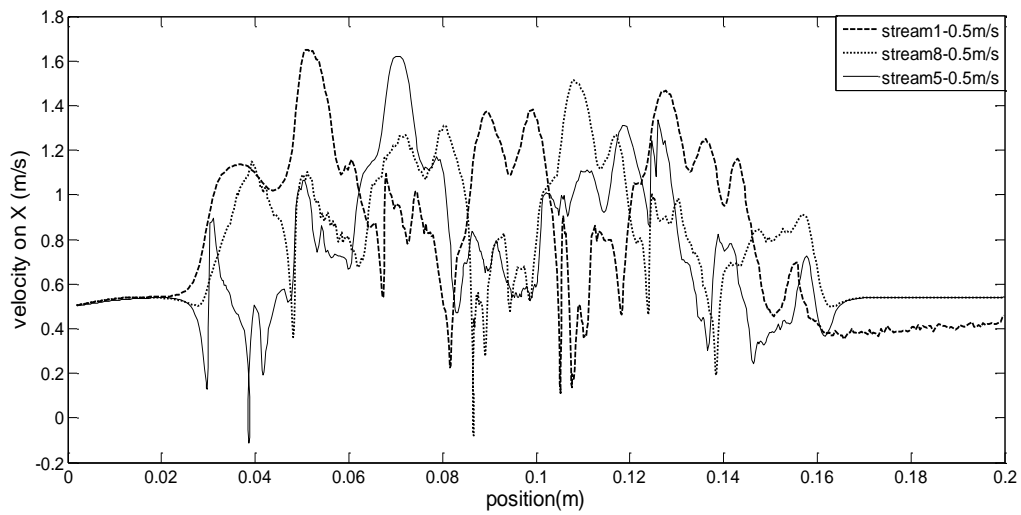
**Figure 40** Streamlines paths for 0.1m/s (a) , for 0.5m/s (b) and for 0.9m/s (c)

The figure 39 shows clearly that increasing the velocity, the flow path changes so it is expected that also other properties such as the shear stress, the residence time and the energy turbulence dissipation will be different.

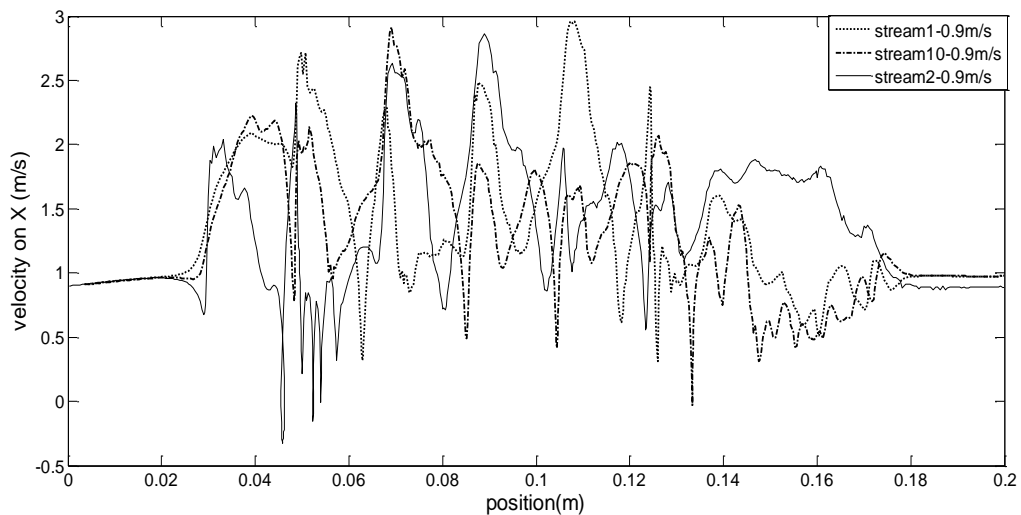
On the other hand, the streamlines path can give us only qualitative information while to obtain quantitative information it is necessary to match the different velocity profiles, reported in the figure below.



(a)



(b)



(c)

**Figure 41** Velocity on X direction for 0.1m/s (a) , for 0.5m/s (b) , for 0.9m/s (c)

The figure 40 shows the velocity on X direction along the pipe length for some streamlines and changing the velocity from 0.1m/s to 0.9m/s. Two observations should be done:

- For the velocity of 0.1m/s, it was found that all the streamlines considered follow two different paths and one of this has a residence time considerably inferior. Furthermore, the two velocity paths are enough regular.
- Increasing the velocity from 0.5m/s to 0.9m/s, also increases the number of possible paths for the streamlines and the velocity profiles become more irregular.

So it can be concluded for this first part that, the velocity of 0.1m/s is very different from the other velocities, namely 0.5m/s and 0.9m/s, for this reason also a large difference in flow properties is expected.

The first property analysed is the energy, reported in the figure below for different velocity. The energy of each streamline is evaluated as the product between the average energy turbulence dissipation which is a power/unit of mass (W/kg) and the residence time (s). On the axes of this chart are reported: the energy on the y axis and the dimensionless parameter  $r/R$  on the x axis.

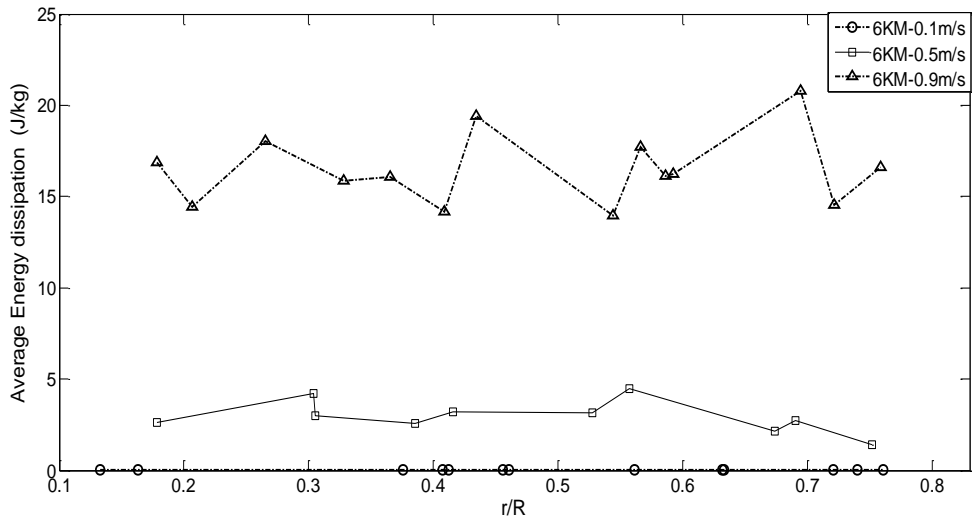


**Figure 42** 3D Energy profile for different velocity with 6 Kenics static mixer

The figure 41 shows that the highest value of energy is related to the highest velocity and the minimum value of the energy is related to the lowest velocity. Hence, this result was absolutely expected. Instead, it is more difficult to try to find a difference between internal streamlines (with low value of  $r/R$ ) and external streamlines (with high value of  $r/R$ ). It seems there is not a clear correlation between the energy of the streamline and its position.

The second chart proposed is the average shear stress for different streamlines changing the velocity.

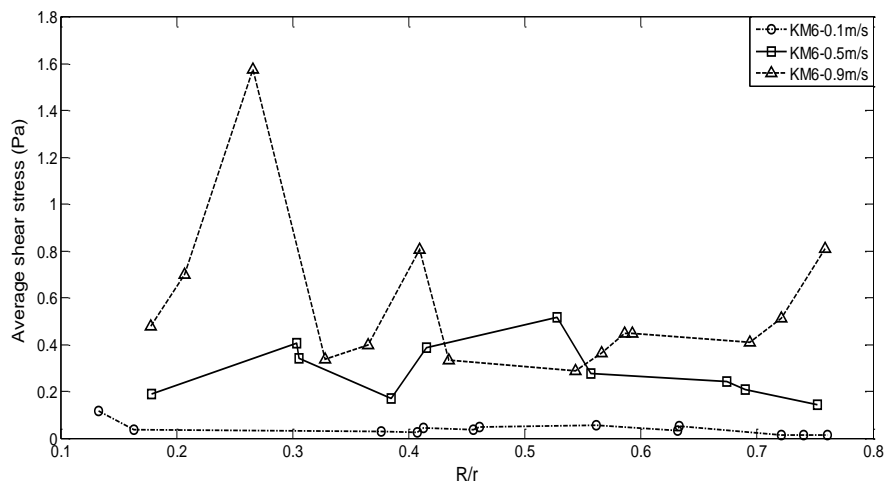


**Figure 43** 3D shear stress trend for different velocity with 6 Kenics static mixer

Again it is not clear the difference in behaviour between the internal and the external streams while the maximum average shear stress is for the maximum velocity of 0.9m/s and in the same way the minimum value of the shear is for 0.1m/s, the minimum velocity.

Finally, to close this paragraph the residence time profile will be discussed, in the figure below.

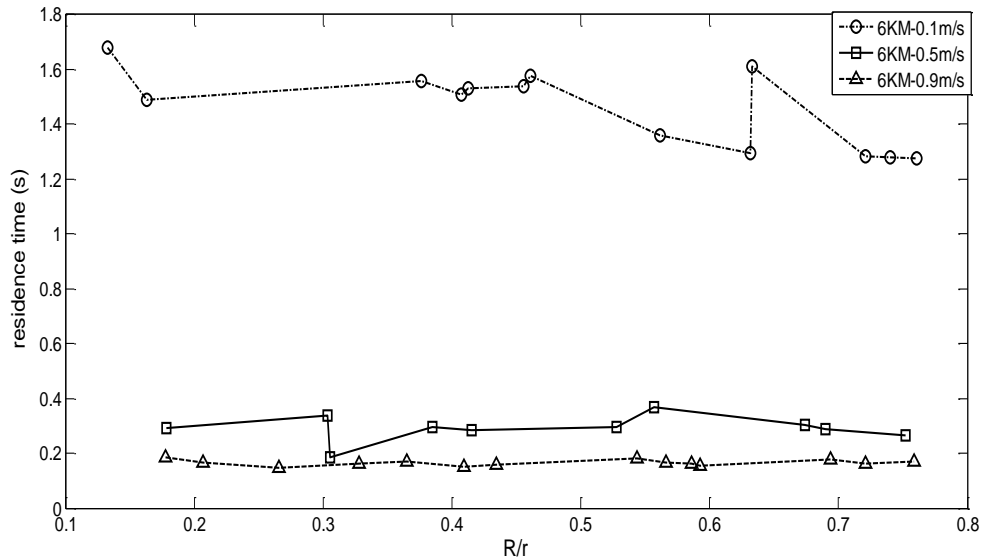


**Figure 44** 3D residence time profile with 6 Kenics static mixer

It is obvious to note that there is an inverse relation between the velocity and the residence time so the highest velocity corresponds to the shortest time. Therefore, it may be interesting to try to compare the residence times at different velocities. For the lowest velocity of 0.1m/s it is noticed that when increasing the r/R parameter the time tends to decrease. For the medium velocity of 0.5m/s there are some fluctuations of the residence time while for the highest velocity of 0.9m/s the profile is rather constant without large variations.

At low velocity, it is reasonable that there are preferential paths (function of the static mixer geometry) which can be characterized with residence time very different while increasing the velocity this effect should become smoother. Indeed, for the velocity of 0.9m/s the residence time profile is quite flat, with small differences in time between the streamlines.

This study of the residence time has been done by using 40 streamlines, but to have a more general statistical result the number of the streamlines considered has been increased until 2000, distributed on the pipe section ZY. Then the 2000 streamlines have been processed with Matlab as before, by means of histogram to reproduce the residence time profile.

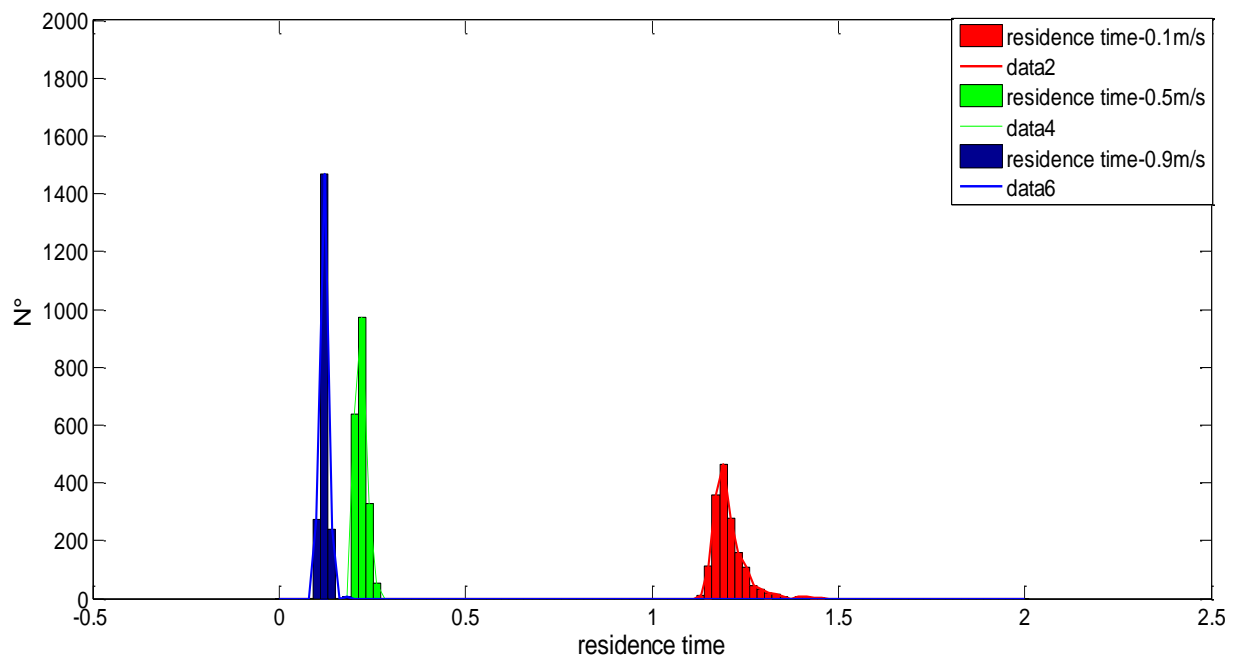


**Figure 45** Residence Time profile for all the velocity, by using 2000 streamlines

The figure 44 reports on the y axis the number of the streamlines which have a specific value of the residence time and on the x axis the residence time. It can be observed that there is good agreement between the average residence times shown in the previous plot (figure 43) and that shown in this figure. It is also evident that the lowest velocity of 0.1m/s has a distribution with a larger variance compared with the other distributions. This was absolutely expected because at low velocity there are preferential paths which determine different residence time, as shown in the figures 39 and 40 which report respectively the streamlines path and the velocity profile on the x axis, changing the superficial velocity.

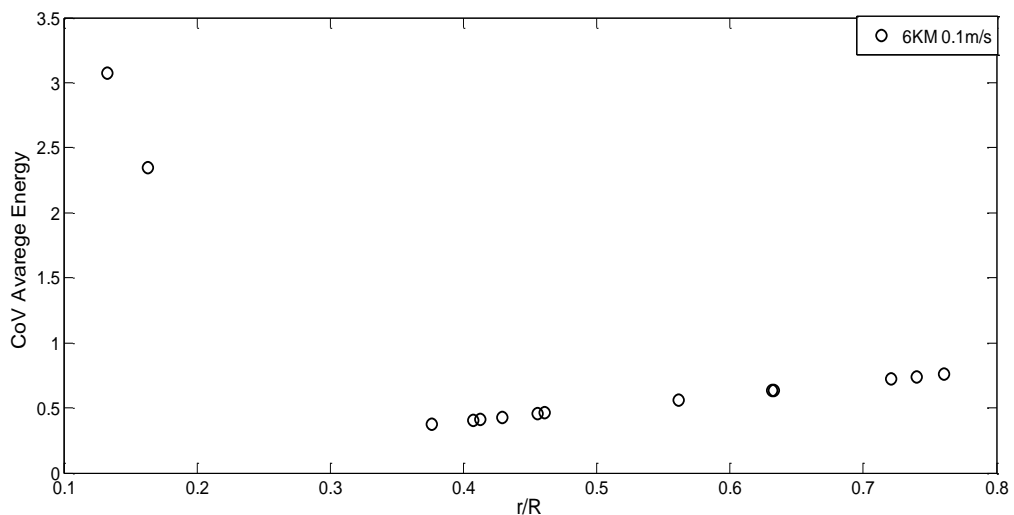
This residence time analysis did not show the potential presence of a by-pass as hypothesized in the previous experimental study (Forte Giuseppe (2015)), to explain the behaviour of the droplet diameter distributions increasing the velocity of the continuous phase.

### 4.3.2 Analysis of the coefficient of variation (CoV)

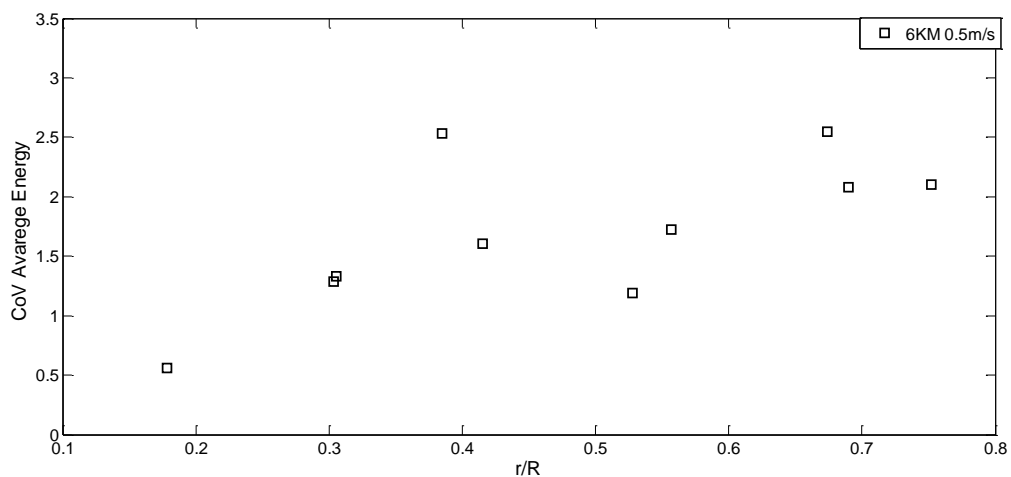
The previous charts about the shear stress, the energy turbulence dissipation and the residence time do not show in a clear way the effect of a change in velocity on the mixing performance. Hence, for this reason an analysis on the coefficient of variation will be conducted.

In probability theory and statistics, the coefficient of variation (CoV), also known as relative standard deviation (RSD), is a standardized measure of dispersion of a probability distribution or frequency distribution. It is often expressed as a percentage, and is defined as the ratio of the standard deviation  $\sigma$  to the mean  $\mu$  (or its absolute value,  $|\mu|$ ). It shows the extent of variability in relation to the mean of the population. The variables analysed by using the coefficient of variation are: the velocity, the shear stress, the energy turbulence dissipation.

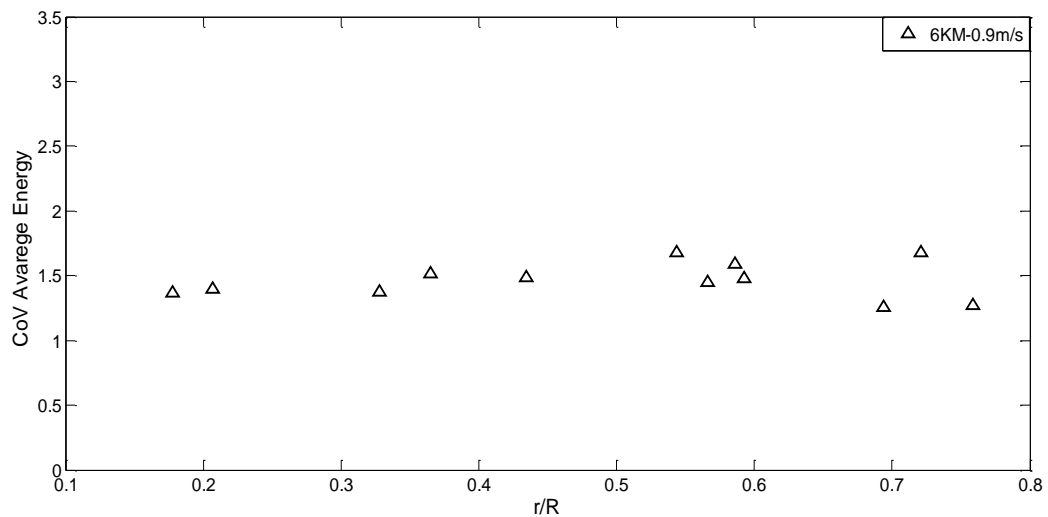
First, the energy turbulence dissipation CoV will be presented in the figure below.



(a)



(b)



(c)

**Figure 46** Energy CoV for 0.1m/s (a) , for 0.5m/s (b) , for 0.9m/s (c) by using 6 Kenics static mixer

The charts above report on the y axis the CoV of the specific property and on the x axis the parameter  $r/R$ . The absolute mean on the streamline is used to compute the CoV for each property studied. Figure 45 (a), (b) and (c) show that for a fixed velocity, the external streamlines (with large values of  $r/R$ ) have a higher variation of the property compared to the mean property value. It is interesting to notice that for the lowest velocity of 0.1m/s the maximum value of the CoV is registered for a low values of  $r/R$  parameter but the trend inverts for the other velocities (0.5m/s and 0.9m/s). A higher value of the energy CoV on the external streams can be explained with a higher velocity of these streamlines.

Basically, these new charts give us more information compared to the previous plots of the average energy ( Figure41 ). Indeed, it can be observed that for the velocity of 0.1m/s the CoV of the energy turbulence increases with the  $r/R$  parameter. For the velocity of 0.5m/s the CoV has a larger variation with the parameter  $r/R$  and this can be justified with a different flow field. A large value of the CoV means that the series of values of the velocity on the stream are different from the average value of the velocity on the same stream.

Finally, for the velocity of 0.9m/s the CoV of the velocity show small variations, this means that the local values of the velocity on the streamlines are not so different from the average value of the velocity on the single stream and this was expected.

The shear stress CoV is reported in the figure below.

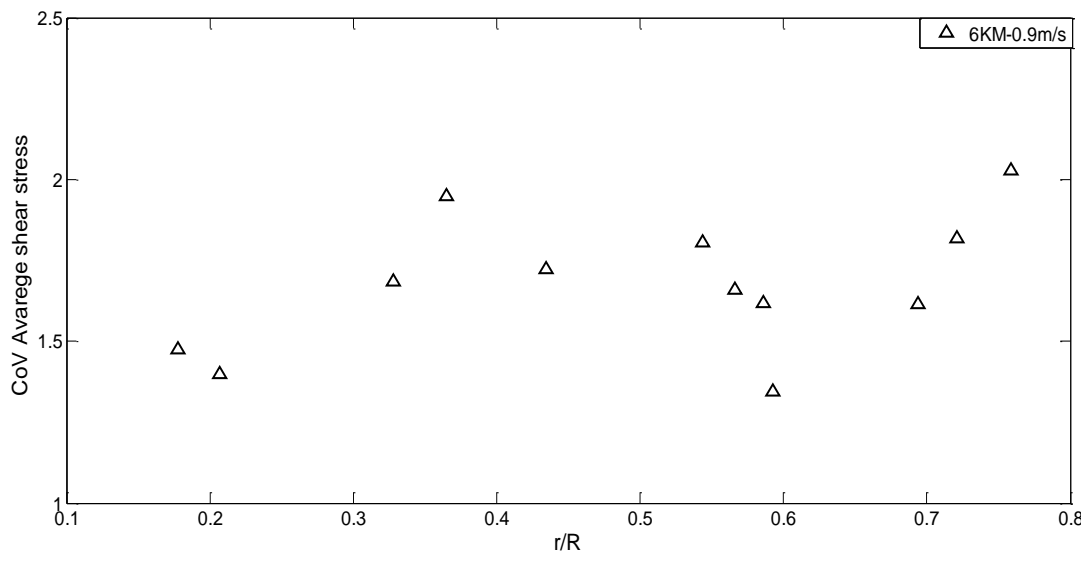
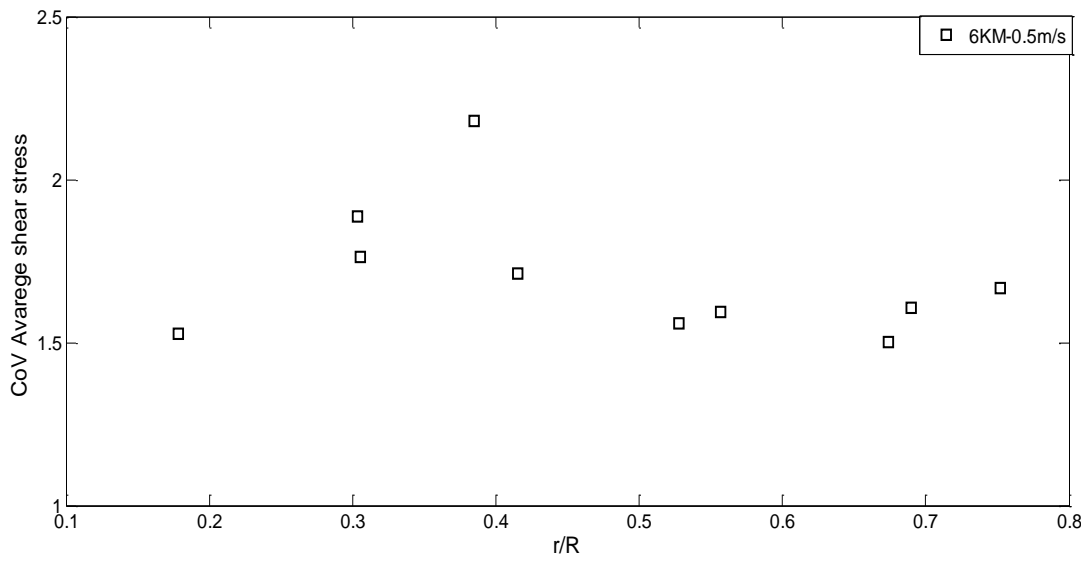
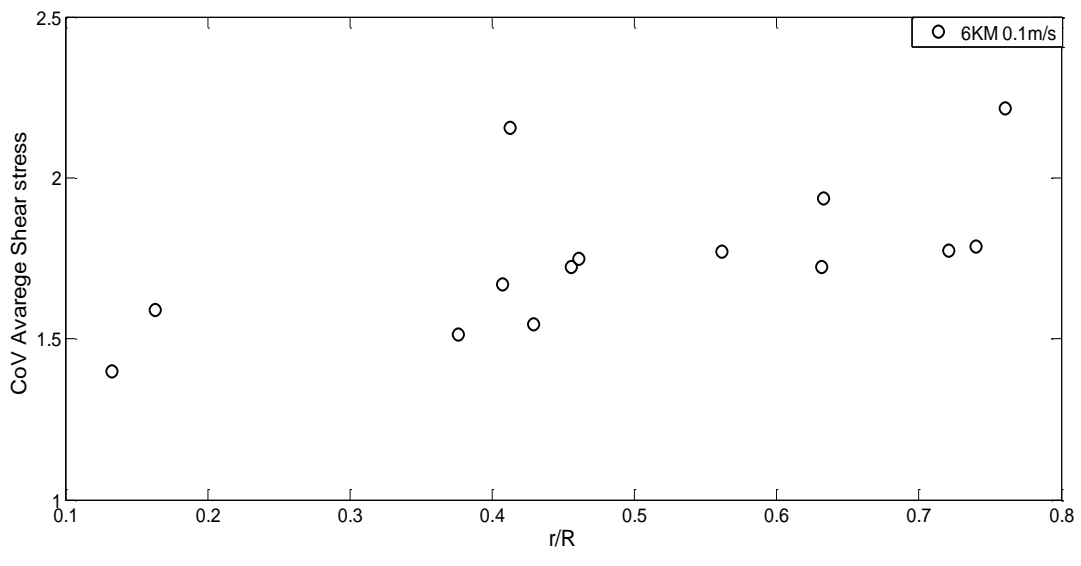
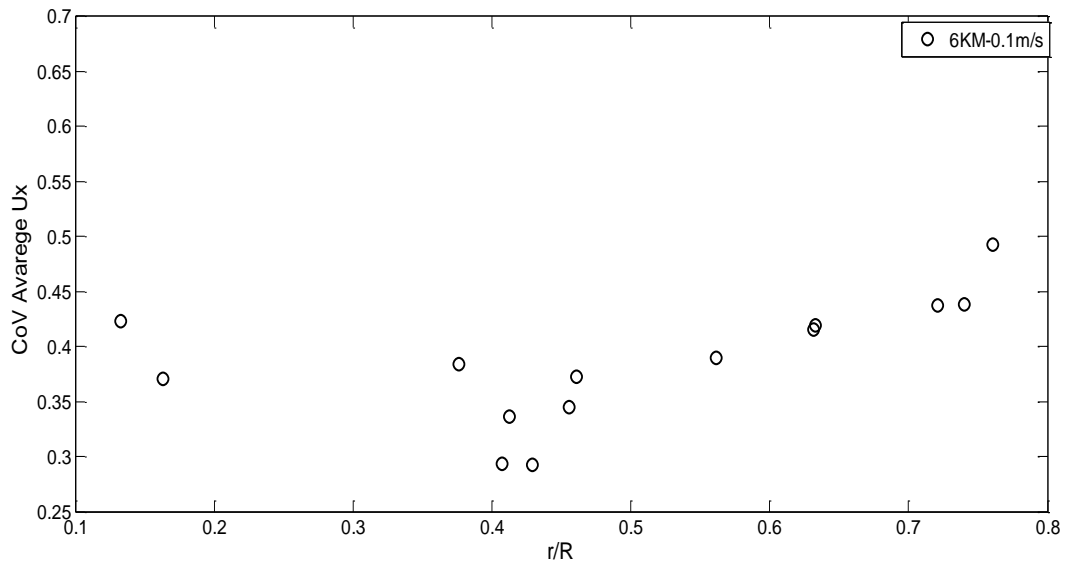


Figure 47 Shear stress CoV for 0.1m/s (a) , for 0.5m/s (b) , for 0.9m/s (c)

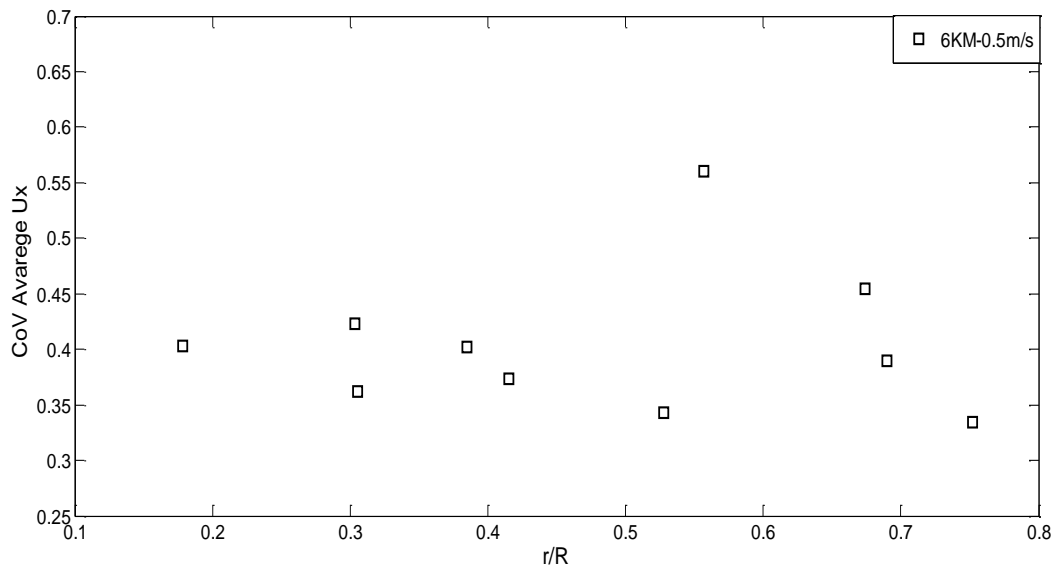
Figure 46 shows that for 0.1m/s and 0.9m/s the CoV of the shear stress increases with the  $r/R$  parameter while a different behaviour is shown for the 0.5m/s where there is not a clear trend.

Comparing all the velocities together it can be seen that the higher values of the CoV belong to the lowest velocity, namely 0.1m/s. This can be explained with a lower uniformity of the velocity field compare with the other velocities where the velocity field tends to be more uniform, with a central region at high velocity and an external region at low velocity.

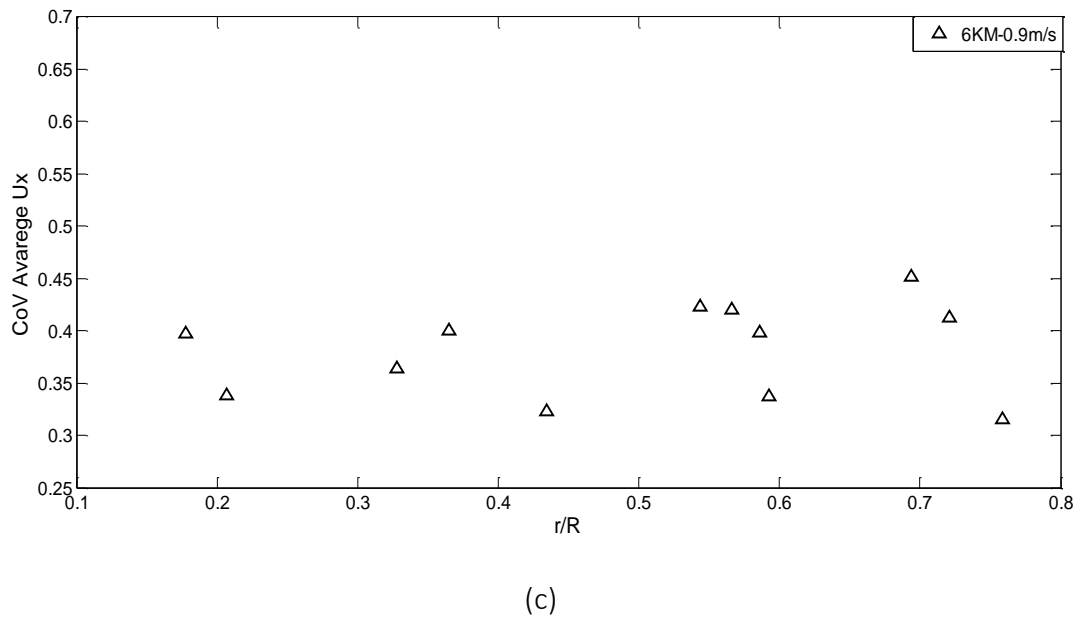
Finally, the velocity CoV is reported in the figure below.



(a)



(b)



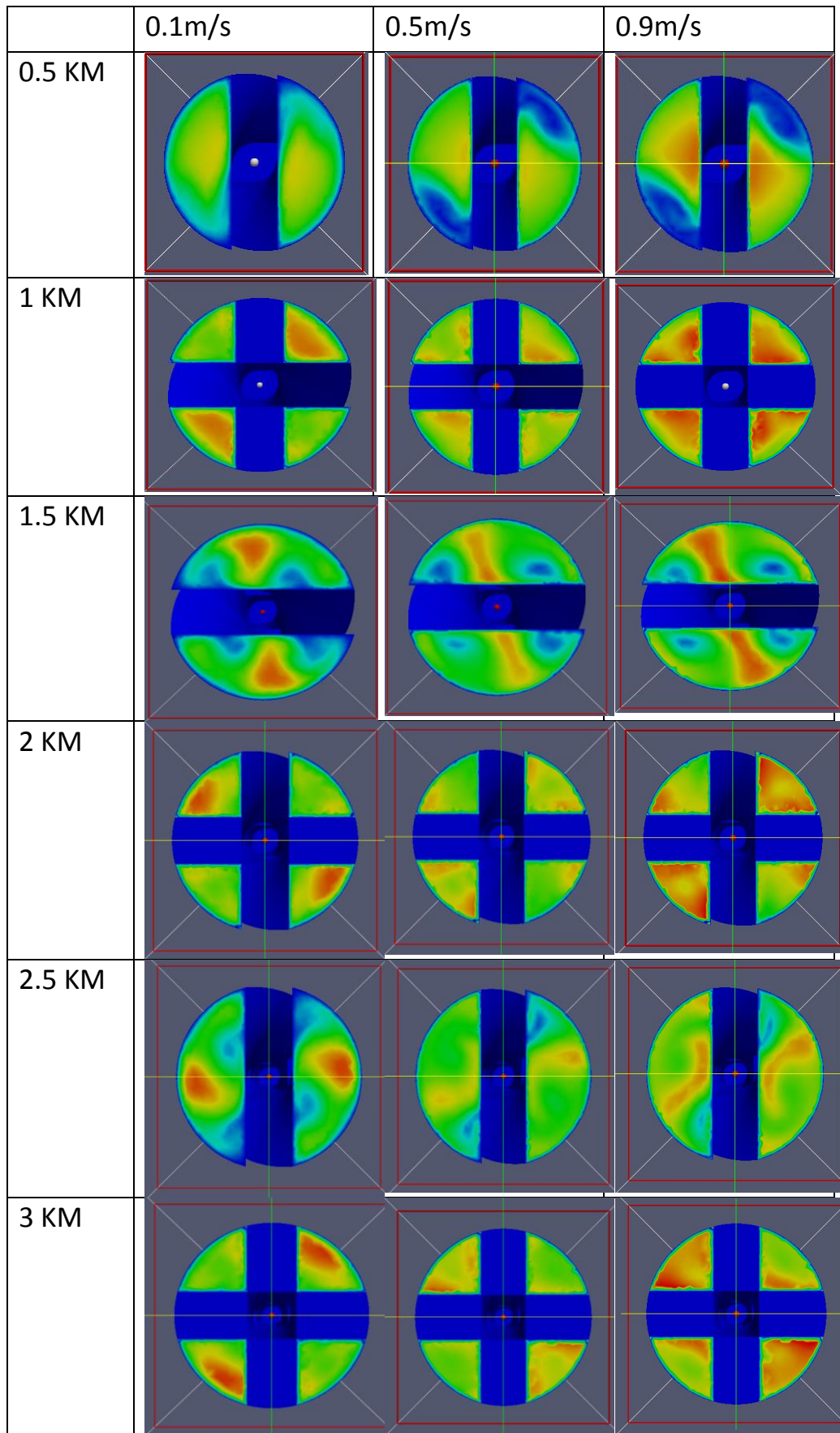
**Figure 48** The velocity CoV for 0.1m/s (a), for the 0.5m/s (b) , for the 0.9m/s (c) , by using 6 Kenics static mixer

Figure 47 shows for the velocities of 0.1m/s and 0.5m/s that, the CoV is higher for the external streamlines than the internal streams while this trend is not evident for the velocity of 0.9m/s. This can be explained thinking that the velocity gradients are not too large at 0.9m/s because the flow field is relatively uniform.

The analysis of the coefficient of variation can be concluded observing that there were higher values of the CoV of the properties for the external streamlines compared to the internal streams. This is not surprising because the external regions take account of the wall effects.

### 4.3.3 3D flow field

To conclude the chapter of the results, images of the 3D flow field will be show to highlight the difference existing increasing the velocity, then finally, the stream path will be observed by using the section pipe ZY to attempt to understand the effect of the velocity on a hypothetical mixing.



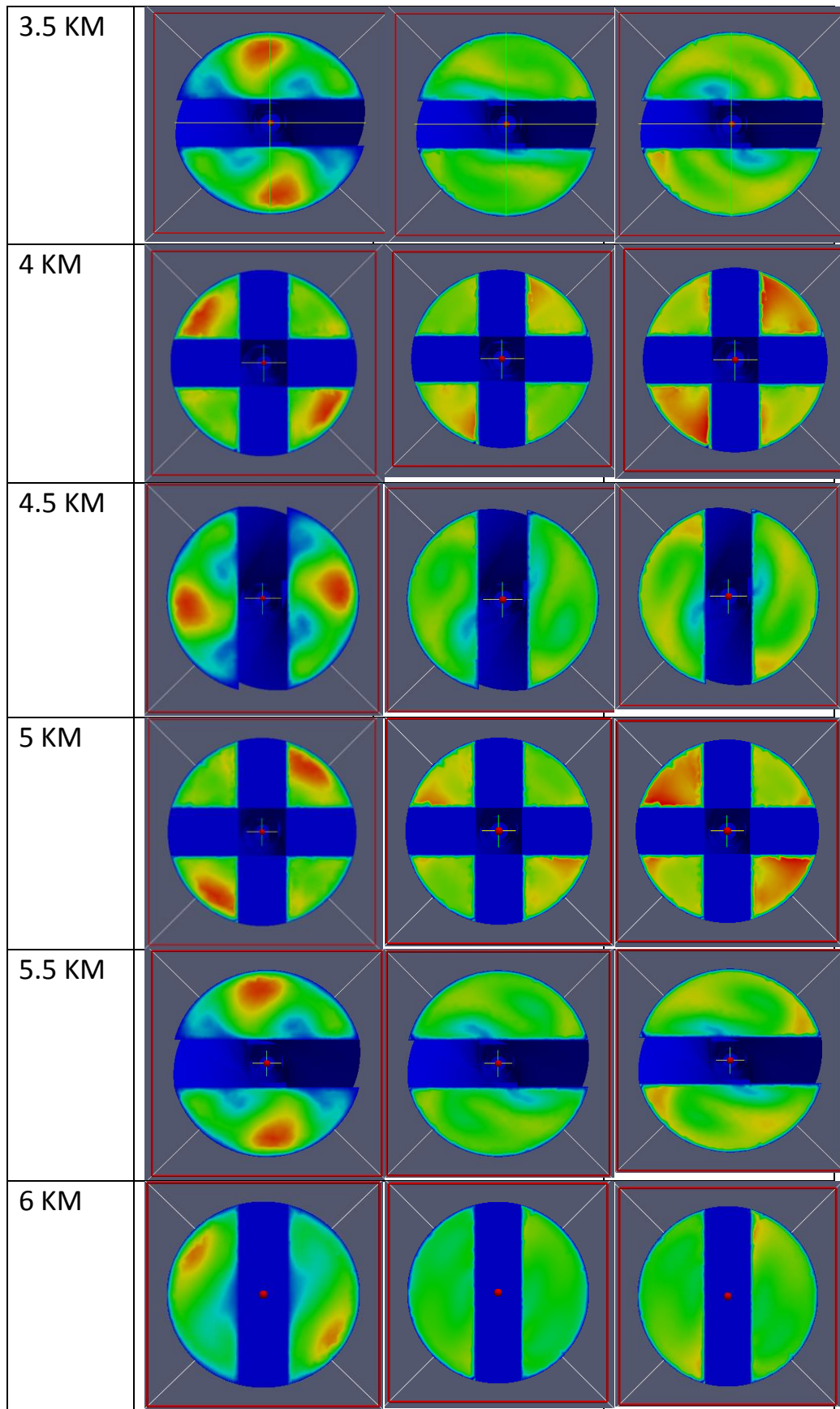
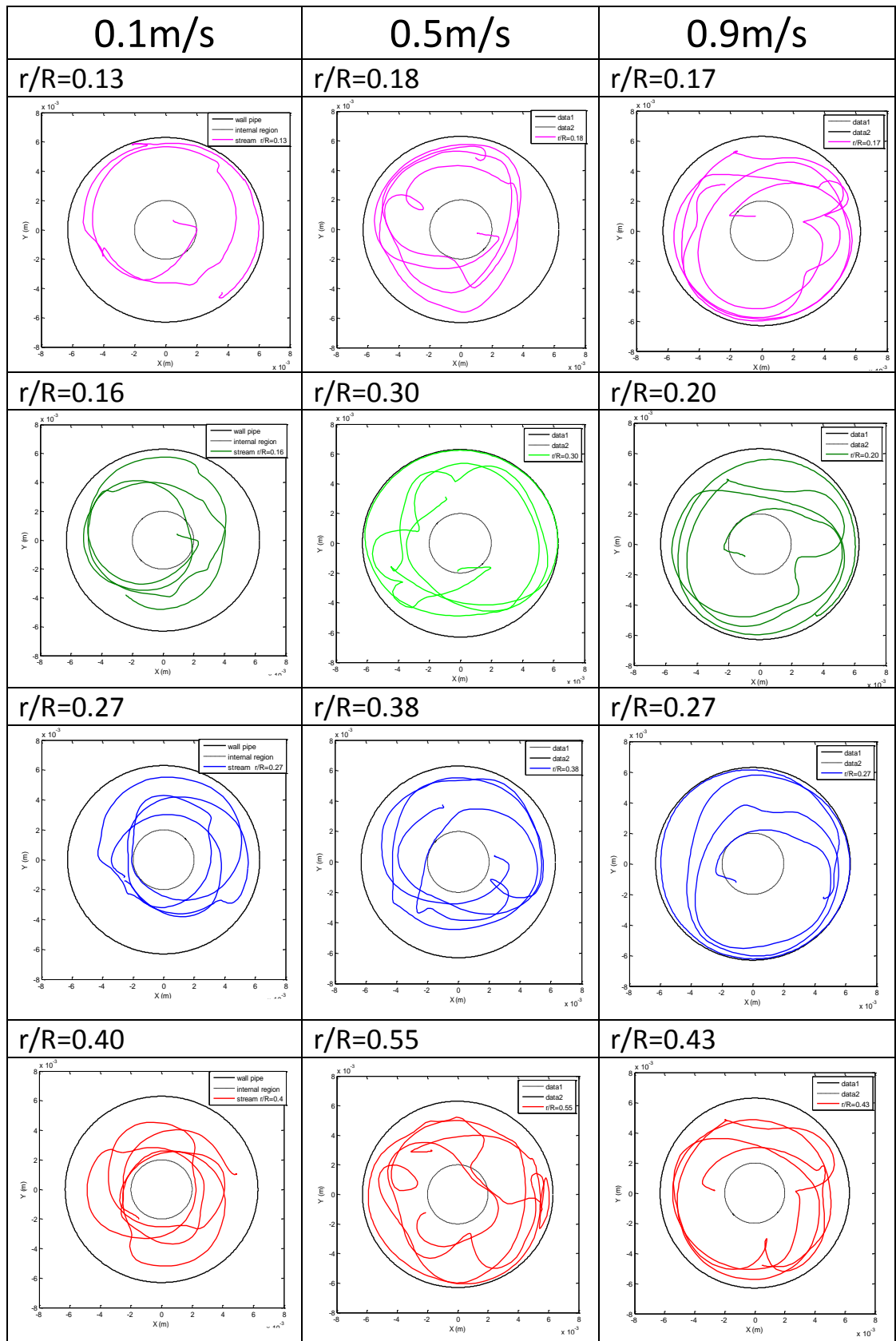


**Figure 49** 3D velocity field with 6 Kenics static mixer (Magnitude of the velocity)

In the images reported above, for each half of the static mixer a section pipe is reported to analyse the flow field and its development. The figure 48 shows that there is an evident difference between the structure of the velocity field at 0.1m/s and those at 0.5m/s and 0.9m/s. Indeed, a flow transition can be observed between these range of velocity. It should be noticed that:

- The static mixer configuration makes the structure of the flow repeatable, indeed for the section of the element 1,3,5 or 2,4 or 0.5, 2.5, 4.5 the flow is exactly the same.
- Increasing the velocity from 0.5m/s to 0.9m/s the flow quality is the same. The flow structure does not change but what changes is the magnitude of the velocity.

The last data collection will show the streamline path across the pipe section ZY, for a better understanding of how the mixing can develop from the pipe centre to the pipe walls. Indeed, in the following images streamlines with similar values of the parameter  $r/R$  will be compared, for different velocities.



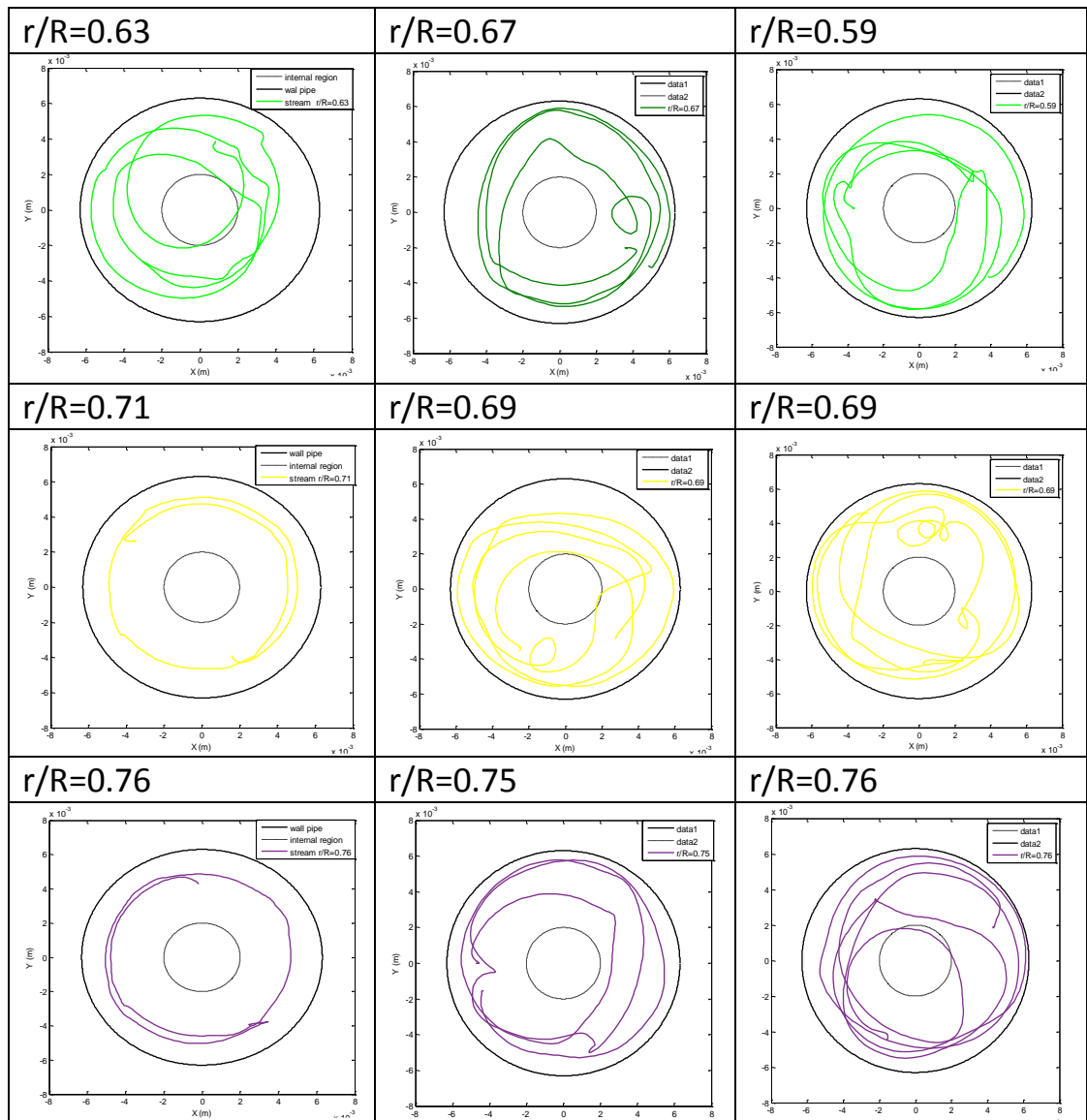


**Figure 50** Streamlines on the ZY pipe section for all the velocities (with 6 Kenics static mixer)

In the figure 49 two circles are represented, the bigger is the pipe wall, with a diameter of 0.5 inch while the smaller represents an internal region and has a diameter of 4mm. These images show that:

- For low values of the  $r/R$  (parameter which define the streamline position), the mixing capacity seems to increase with the velocity. Indeed, at the velocity of 0.1m/s the mixing is not efficient because the streamlines start around the pipe centre and then do not cover the external regions near the wall. But this difference in mixing between the velocities is not so large and tends to decrease enhancing the  $r/R$  parameter.

- For high values of the  $r/R$ , for the velocity of 0.1m/s the streamlines have a regular path which does not allow a penetration of the layers of the fluid, indeed the streamline turns around the external region, while for the velocity of 0.5m/s or 0.9m/s , a larger portion of the section is interested by the mixing.

Finally, to conclude this work a comparison of the  $K_T$  parameter in turbulence flow between the theoretical value, the numerical value and the experimental value is done. The  $K_T$  parameter is obtained as the ratio of the pressure drop through the mixer to the pressure drop through the same diameter and length of open pipe. The values of  $K_T$  are reported in table 12.

	Theoretical value	Numerical values	Experimental values
$K_T$	150	65-71	38-45

**Table 12** Comparison between the  $K_T$  parameters

The values of  $K_T$  parameter obtained from the simulations are larger than the experimental values, this leads to two possible conclusions:

- The  $K_T$  values obtained from the simulations are larger than the experimental values so a possible by pass was present during the experimental measurements
- The numerical values of  $K_T$  are affected by the turbulence model, so changing the turbulence model the values of the  $K_T$  change. In this case a comparison with the experimental values is not reasonable

## Chapter 5

---

### Conclusions

In this work, static mixer performance in mixing of immiscible fluids has been investigated by using a numerical approach. Several simulations have been performed during this research work, by means of the open source platform OpenFoam. Simulations have investigated the mixing performance, exploring the effect of the continuous phase velocity on the disperse phase. Indeed, the velocity was ranging from 0.1m/s to 0.9m/s. The static mixer geometry tested has been the Kenics (KM) 6 elements, realized with the open source software Salome 7.5.1 . Basically, for a better understand of the mixing of immiscible fluids two properties have been studied: the energy turbulence dissipation and the shear stress, because both the properties can be linked with the break up mechanisms.

In the paragraph 4.2.1 the 2D results are presented, starting with the study of the drop surface, in order to observe the shear stress and the energy turbulence dissipation, by using a Matlab reconstruction of the drop. Basically, this local approach has found that the shear stress as the energy turbulence dissipation increases with the drop deformation and with the velocity of the continuous phase in a different way. Indeed for the shear stress, it was found that it increases with the drop deformation and it is not linear with the velocity, because the better shear stress conditions are at 0.5m/s and not 0.9m/s which is the highest velocity. This result can be linked with the experimental results obtained in a previous study, but need further explanation. For the energy turbulence dissipation, a linear relation with the velocity was found, while a linear relation with the drop deformation does not exist. This result is not surprising because basically the energy is a function of the turbulence intensity which increases with the velocity. To clarify the result obtained for the shear stress valuated on the drop surfaces, a global approach is used, by means of a histogram of the shear stress computed in all the points of the geometry. This different approach leads to the conclusion that the shear stress should increase in a linear way with the velocity, but this was expected because the break up of the drop is a local phenomenon which can be lost with a global statistical approach.

In the paragraph 4.2.2 a streamlines analysis is conducted with the aim to confirm the shear stress trend found when analysing the drop surface and at the same time to attempt to link the drop position in the velocity field with the break up conditions. The analysis of single streamlines for different velocity has shown that:

- Increasing the continuous phase velocity, properties such as the shear stress and the energy turbulence dissipation increase, confirming the previous results obtained from the global approach
- By using enough streamlines along the pipe length, it was shown that the drop path changes increasing the velocity. Indeed, at low velocity the drop crosses external regions, with large velocity gradients and so a higher shear stress. While at the high velocity, the drop tends to move to the centre pipe, where the gradients are smaller because the velocity fields is quite uniform.

Furthermore, by means the residence time, it has found that the streamlines near the wall have longer time compared to the streams near the centre pipe. This means that also if the shear stress conditions could be permit the rupture of the drop, a mechanical equilibrium should be taken into account.

In the paragraph 4.3 the 3D results are presented and the streamlines analysis is repeated, in order to attempt to confirm or extend the 2D results. The streamlines results do not show for the properties such as the shear stress and the energy turbulence dissipation a clear behaviour increasing the  $r/R$  parameter (which define the stream position). Hence, a further analysis of the coefficient of variation is done. This analysis leads to the conclusion that increasing the  $r/R$  parameter the shear stress and the energy turbulence dissipation tend to increase. So as for the 2D analysis, it was found that the external streams involve larger variation in the properties compared to the internal streams. Finally, the 3D velocity field is shown and additionally, the path of the streamlines across the ZY pipe section, give us a better idea of the mixing efficiency increasing the velocity. Indeed, it noticed that above certain values of  $r/R$  parameter ( $>0.65$ ) at low velocity the stream follows a regular path and does not cross from the external region to the centre of pipe. Furthermore, by increasing the velocity, better mixing is obtained, with streams which interest a large part of the pipe section. Instead, for low values of  $r/R$  parameter, by increasing the velocity an improvement in the mixing can be observed, but it is not possible to quantify how much the mixing at 0.9m/s is better than that at 0.5m/s or vice versa.

## 5.1 Future work

Further simulations could enhance the consistency of the numerical model and integrate it. It would be useful to repeat the simulations raising the number of elements or testing different static mixer geometry, as the Sulzer SMX plus. It could be very interesting to perform the same 3D geometry but by using a multi-phase model to trace the oil drop along the pipe and to attempt to extend the 2D multi-phase results obtained with this work. The principal obstacle is the computational costs required, which limit the possible applications and the difficulties to transfer large data for the post-processing of the numerical solution.

# Appendix A

## OpenFoam Turbulence Model ( 2D Multi-phase model)

```

/*-----*- C++ -*-----*/
| ===== |
| \\ / F i e l d | OpenFOAM: The Open Source CFD Toolbox |
| \\ / O p e r a t i o n | Version: 2.3.1 |
| \\ / A n d | Web: www.OpenFOAM.org |
| \\ / M a n i p u l a t i o n |
|-----*/
FoamFile
{
    version      2.0;
    format       ascii;
    class        dictionary;
    location     "constant";
    object       turbulenceProperties;
}
// * * * * *
* * * //

simulationType  RASModel;

//
*****
** //

```

## OpenFoam Turbulence Properties ( 2D Multi-phase model)

```

/*-----*- C++ -*-----*/
| ===== |
| \\ / F i e l d | OpenFOAM: The Open Source CFD Toolbox |
| \\ / O p e r a t i o n | Version: 2.3.1 |
| \\ / A n d | Web: www.OpenFOAM.org |
| \\ / M a n i p u l a t i o n |
|-----*/
FoamFile
{
    version      2.0;
    format       ascii;
    class        dictionary;
    location     "constant";
    object       transportProperties;
}
// * * * * *
* * * //

phases (water oil);

water
{

```

## Appendix A . OpenFoam file

---

```
transportModel Newtonian;
nu              nu [ 0 2 -1 0 0 0 0 ] 1e-06;
rho            rho [ 1 -3 0 0 0 0 0 ] 1000;
}

oil
{
    transportModel Newtonian;
    nu              nu [ 0 2 -1 0 0 0 0 ] 4e-06;
    rho            rho [ 1 -3 0 0 0 0 0 ] 800;
}

sigma          sigma [ 1 0 -2 0 0 0 0 ] 0.02267;

//
*****
** //
```

## OpenFoam RAS Properties ( 2D Multi-phase model)

```
/*-----*- C++ -*-----*\
| ===== |
| \\      / F ield      | OpenFOAM: The Open Source CFD Toolbox |
| \\      / O peration  | Version: 2.3.1 |
| \\      / A nd        | Web: www.OpenFOAM.org |
| \\      / M anipulation | |
\*-----*/
FoamFile
{
    version      2.0;
    format       ascii;
    class        dictionary;
    location     "constant";
    object       RASProperties;
}
// * * * * *
* * * //

RASModel        kOmegaSST;

turbulence      on;

printCoeffs     on;

//
*****
** //
```

## ControlDict file ( 2D Multi-phase model)

```

/*-----*-- C++ -*-----*\
| ===== |
| \\      /  F ield      | OpenFOAM: The Open Source CFD Toolbox |
| \\      /  O peration  | Version: 2.3.1 |
| \\      /  A nd        | Web:      www.OpenFOAM.org |
| \\      /  M anipulation | |
\*-----*--*/
FoamFile
{
    version      2.0;
    format       ascii;
    class        dictionary;
    location     "system";
    object       controlDict;
}
// * * * * *

application    LTSInterFoam;

startFrom      startTime;

startTime      10;

stopAt         endTime;

endTime        12; // il tempo di attraversamento è 0.4s con
Vw=0.5m/s

deltaT         1e-4;

writeControl   adjustableRunTime;

writeInterval  0.05; //modificato

purgeWrite     0;

writeFormat    ascii;

writePrecision 6;

writeCompression uncompressed;

timeFormat     general;

timePrecision  6;

runTimeModifiable yes; //se modifico il file dict vedo le modifiche in
tempo reale

adjustTimeStep on;

maxCo          0.5; //cambiato manualmente prima era 1
maxAlphaCo     0.5; //cambiato manualmente prima era 1

maxDeltaT      1;

//
*****
** //

```

## FvSchemes file ( 2D Multi-phase model)

```

/*-----*-- C++ --*-----*\
|=====|
|  \ \   /  F i e l d           | OpenFOAM: The Open Source CFD Toolbox |
|  \ \   /  O p e r a t i o n   | Version:  2.3.1                |
|  \ \   /  A n d                | Web:      www.OpenFOAM.org         |
|   \ \ /  M a n i p u l a t i o n |                               |
|-----*-----*\
FoamFile
{
    version      2.0;
    format       ascii;
    class        dictionary;
    location     "system";
    object       fvSchemes;
}
// * * * * *

ddtSchemes
{
    default      localEuler rDeltaT;
}

gradSchemes
{
    default      Gauss linear;
}

divSchemes
{
    div(rhoPhi,U) Gauss linearUpwind grad(U);
    div(phi,alpha) Gauss vanLeer;
    div(phirb,alpha) Gauss linear;
    div(phi,k)      Gauss upwind;
    div(phi,omega)  Gauss upwind;
    div((muEff*dev(T(grad(U)))) Gauss linear;
}

laplacianSchemes
{
    default      Gauss linear corrected;
}

interpolationSchemes
{
    default      linear;
}

snGradSchemes
{
    default      corrected;
}

fluxRequired
{
    default      no;
    p_rgh;
    pcorr;
    alpha.water;
}

```

## FvSolution file ( 2D Multi-phase model)

```

/*----- C++ -----*\
|=====|
|  \ \ /  F i e l d      | OpenFOAM: The Open Source CFD Toolbox |
|  \ \ /  O p e r a t i o n | Version: 2.3.1 |
|  \ \ /  A n d           | Web: www.OpenFOAM.org |
|  \ \ /  M a n i p u l a t i o n |
|-----*\
FoamFile
{
    version      2.0;
    format       ascii;
    class        dictionary;
    location     "system";
    object       fvSolution;
}
// ***** //

solvers
{
    alpha.water
    {
        nAlphaCorr      1;
        nAlphaSubCycles 3;
        cAlpha          1;
    }

    pcorr
    {
        solver          PCG;
        preconditioner
        {
            preconditioner  GAMG;
            tolerance       1e-05;
            relTol          0;
            smoother        DICGaussSeidel;
            nPreSweeps      0;
            nPostSweeps     2;
            nFinestSweeps   2;
            cacheAgglomeration true;
            nCellsInCoarsestLevel 10;
            agglomerator     faceAreaPair;
            mergeLevels     1;
        }
        tolerance       1e-05;
        relTol          0;
        maxIter         100;
    }

    p_rgh
    {
        $pcorr;
        tolerance       1e-6;
        relTol          0.01;
    };

    p_rghFinal
    {
        $p_rgh;
        tolerance       1e-6;
        relTol          0;
    }
}

```

```

    }

    "(U|k|omega).*"
    {
        solver            smoothSolver;

        smoother          GaussSeidel;
        nSweeps            1;

        tolerance         1e-7;
        relTol             0.1;
    };
}

PIMPLE
{
    momentumPredictor yes;
    nCorrectors          2;
    nNonOrthogonalCorrectors 0;

    maxCo                0.5;
    maxAlphaCo           0.2;
    nAlphaSweepIter      1;

    rDeltaTSmoothingCoeff 0.1;
    rDeltaTDampingCoeff  1;
    maxDeltaT            1;
}

relaxationFactors
{
    fields
    {
    }
    equations
    {
    }
}

//
*****
** //

```

## SetFields file ( 2D Multi-phase model)

```
/*-----*- C++ -*-----*\
| ===== |
| \\ / F i e l d | OpenFOAM: The Open Source CFD Toolbox |
| \\ / O p e r a t i o n | Version: 2.3.1 |
| \\ / A n d | Web: www.OpenFOAM.org |
| \\ / M a n i p u l a t i o n |
|-----*\
FoamFile
{
    version      2.0;
    format       ascii;
    class        dictionary;
    location     "system";
    object       setFieldsDict;
}
// ***** //

defaultFieldValues
(
    volScalarFieldValue alpha.water 1
);

regions
(
    sphereToCell
    {
        centre (0.05 0.0063 0);
        radius 0.001;
        fieldValues
        (
            volScalarFieldValue alpha.water 0
        );
    }
);
```



## DecomposeParDict file ( 3D Single-phase model)

```

/*-----*- C++ -*-----*\
| ===== |
| \\      /  F ield      | OpenFOAM: The Open Source CFD Toolbox |
| \\      /  O peration  | Version: 2.1.1 |
| \\      /  A nd        | Web:      www.OpenFOAM.org |
| \\      /  M anipulation | |
\*-----*\
FoamFile
{
    version      2.0;
    format       ascii;
    class        dictionary;
    location     "system";
    object       decomposeParDict;
}
// * * * * *
* * * //

numberOfSubdomains 16;

method          scotch;
//
*****
** //

```

## FvSchemes file ( 3D Single-phase model)

```

/*-----*-- C++ -*-----*\
| ===== |
| \\ / F i e l d | OpenFOAM: The Open Source CFD Toolbox |
| \\ / O p e r a t i o n | Version: 2.3.1 |
| \\ / A n d | Web: www.OpenFOAM.org |
| \\ / M a n i p u l a t i o n | |
\*-----*--\
FoamFile
{
    version      2.0;
    format       ascii;
    class        dictionary;
    location     "system";
    object       fvSchemes;
}
// * * * * *
* * * //

ddtSchemes
{
    default      Euler;
}

gradSchemes
{
    default      Gauss linear;
}

divSchemes
{
    default      none;
    div(phi,U)   Gauss limitedLinearV 1;
    div(phi,k)   Gauss limitedLinear 1;
    div(phi,omega) Gauss limitedLinear 1;
    div(phi,R)   Gauss limitedLinear 1;
    div(R)       Gauss linear;

    div((nuEff*dev(T(grad(U)))) Gauss linear;
}

laplacianSchemes
{
    default      Gauss linear corrected;
}

interpolationSchemes
{
    default      linear;
}

snGradSchemes
{
    default      corrected;
}

fluxRequired
{
    default      no;
    p            ;
}

```

## FvSchemes file ( 3D Single-phase model)

```

/*-----*-- C++ -*-----*\
| ===== |
| \\ / F i e l d | OpenFOAM: The Open Source CFD Toolbox |
| \\ / O p e r a t i o n | Version: 2.3.1 |
| \\ / A n d | Web: www.OpenFOAM.org |
| \\ / M a n i p u l a t i o n |
\*-----*/
FoamFile
{
    version      2.0;
    format       ascii;
    class        dictionary;
    location     "system";
    object       fvSolution;
}
// * * * * * //

solvers
{
    p
    {
        solver          GAMG;
        tolerance       1e-06;
        relTol          0.1;
        smoother        GaussSeidel;
        nPreSweeps      0;
        nPostSweeps     2;
        cacheAgglomeration on;
        agglomerator     faceAreaPair;
        nCellsInCoarsestLevel 100;
        mergeLevels     1;
    }

    pFinal
    {
        $p;
        tolerance       1e-06;
        relTol          0;
    }

    "(U|k|omega).*"
    {
        solver          smoothSolver;

        smoother        GaussSeidel;
        nSweeps          1;

        tolerance       1e-7;
        relTol          0.1;
    };
}
PISO
{
    nCorrectors      2;
    nNonOrthogonalCorrectors 3;
    pRefCell         0;
    pRefValue        0;
}

relaxationFactors

```

## Appendix A . OpenFoam file

---

```
{
  fields
  {
    p          0.3;
  }
  equations
  {
    U          0.7;
    k          0.7;
    omega      0.7;
  }
}

//
*****
** //
```

## Job submitted for BlueBear

CASE STUDY : Investigation on time break up using static mixer for an emulsion oil/water

### Challenge

The work is focussed on the computational understanding of the phenomena and the validation of experimental results obtained with PLIF.

### Background

The performance of Kenics (KM) and Sulzer (SMX+) designs of static mixer has been investigated for the mixing of immiscible fluids using situ optical measurements. The fluids used are water as the continuous phase and either silicone oil in the presence ODF surfactant (Sodium Lauryl Ether Sulfate), or Lytol mineral oil in the presence of a nonionic surfactant (Span 80). The dispersed phase volume fraction was between 0,0072% and 0,028% and the superficial velocities ranged from 0,16 to 0,9 m/s. The pipe diameter was 0,0127 m and 6 or 12 mixing elements were used for each mixer type. For this work we are using the CFD software OpenFoam 2.3.1 an open source. We want reproduce a turbulent flow in a pipe , with inside a static mixer module and two different phases. This case requires a numerical model which can consider :

- the turbulent flow
- the presence of two immiscible phases
- the interface changings between the two phases

Results and Geometry The first part of this work will focus on the setting of right parameters to find the right turbulent model and the right solver, in a 2D geometry. After that we will extend the same study on a 3D geometry.

### Client profile

Domenico Daraio  
School of Chemical Engineering  
The University of Birmingham  
Edgbaston  
Birmingham  
B15 2TT

### Contact detail

dxd429@bham.ac.uk

### Contributors

Federico Alberini  
Alessio Alexiadis

# REFERENCES

---

- Aveyard, R., et al. (2003). "Emulsions stabilised solely by colloidal particles." Advances in Colloid and Interface Science **100–102**: 503-546.
- Barnes, H. A. (1994). "A selection of papers presented at the First World Congress on Emulsions Rheology of emulsions — a review." Colloids and Surfaces A: physicochemical and Engineering Aspects **91**: 89-95.
- Briscoe, B. J., et al. (1999). "A review of immiscible fluid mixing." Advances in Colloid and Interface Science **81**(1): 1-17.
- Ceylan, S., et al. (2003). "Estimation of the maximum stable drop sizes, coalescence frequencies and the size distributions in isotropic turbulent dispersions." Colloids and Surfaces A: Physicochemical and Engineering Aspects **212**(2–3): 285-295.
- Chern, C.-S., et al. (1997). "Emulsion polymerization of styrene stabilized by mixed anionic and nonionic surfactants." Polymer **38**(8): 1977-1984.
- Clark, M. M. (1988). "Drop breakup in a turbulent flow—I. Conceptual and modeling considerations." Chemical Engineering Science **43**(3): 671-679.
- Das, P. K., et al. (2005). "Drop breakage model in static mixers at low and intermediate Reynolds number." Chemical Engineering Science **60**(1): 231-238.
- Daub, A., et al. (2013). "Measurement of maximum stable drop size in aerated dilute liquid–liquid dispersions in stirred tanks." Chemical Engineering Science **104**: 147-155.
- Eastwood, Craig Douglas, L. Armi, and J. C. Lasheras. "The breakup of immiscible fluids in turbulent flows." Journal of Fluid Mechanics **502** (2004): 309-333.
- Fernandez, P., et al. (2004). "Nano-emulsion formation by emulsion phase inversion." Colloids and Surfaces A: Physicochemical and Engineering Aspects **251**(1–3): 53-58.
- Forte Giuseppe (2015). "Use of PLIF to investigate mixing of immiscible liquids in static mixer." Thesis from University of Pisa
- Galinat, S., et al. (2005). "Drop break-up in turbulent pipe flow downstream of a restriction." Chemical Engineering Science **60**(23): 6511-6528.

## References

---

Ghanem, A., et al. (2014). "Static mixers: Mechanisms, applications, and characterization methods – A review." Chemical Engineering Research and Design **92**(2): 205-228.

Han, L., et al. (2011). "A theoretical model for droplet breakup in turbulent dispersions." Chemical Engineering Science **66**(4): 766-776.

Hausawa, F. and T. Mitsui (1975). "Stability of emulsions." Progress in Organic Coatings **3**(2): 177-190.

Hesketh, R. P., et al. (1991). "Bubble breakage in pipeline flow." Chemical Engineering Science **46**(1): 1-9.

Israelachvili, J. (1994). "The science and applications of emulsions — an overview." Colloids and Surfaces A: Physicochemical and Engineering Aspects **91**: 1-8.

Ivanov, I. B. and P. A. Kralchevsky (1997). "Stability of emulsions under equilibrium and dynamic conditions." Colloids and Surfaces A: Physicochemical and Engineering Aspects **128**(1–3): 155-175.

Jafari, S. M., et al. (2008). "Re-coalescence of emulsion droplets during high-energy emulsification." Food Hydrocolloids **22**(7): 1191-1202.

Kékesi, T., et al. "Drop deformation and breakup in flows with shear." Chemical Engineering Science.

Kumar, S., et al. (1991). "Alternative mechanisms of drop breakage in stirred vessels." Chemical Engineering Science **46**(10): 2483-2489.

Lazaridis, N., et al. (1999). "Steric stabilization in emulsion polymerization using oligomeric nonionic surfactants." Chemical Engineering Science **54**(15–16): 3251-3261.

Lee, C. H. and R. D. Reitz (2000). "An experimental study of the effect of gas density on the distortion and breakup mechanism of drops in high speed gas stream." International Journal of Multiphase Flow **26**(2): 229-244.

Lemenand, T., et al. (2003). "Droplets formation in turbulent mixing of two immiscible fluids in a new type of static mixer." International Journal of Multiphase Flow **29**(5): 813-840.

Lemenand, T., et al. (2003). "Droplets formation in turbulent mixing of two immiscible fluids in a new type of static mixer." International Journal of Multiphase Flow **29**(5): 813-840.

## References

---

- Liu, Z. and R. D. Reitz (1997). "An analysis of the distortion and breakup mechanisms of high speed liquid drops." International Journal of Multiphase Flow **23**(4): 631-650.
- Luo, Hean, and Hallvard F. Svendsen. "Theoretical model for drop and bubble breakup in turbulent dispersions." AIChE Journal-American Institute of Chemical Engineers **42.5** (1996): 1225-1233.
- Mäkelä, J. S., et al. (2008). "Properties of preliminary breakdown processes in Scandinavian lightning." Journal of Atmospheric and Solar-Terrestrial Physics **70**(16): 2041-2052.
- Meijer, H. E. H., et al. (2012). "On the performance of static mixers: A quantitative comparison." Progress in Polymer Science **37**(10): 1333-1349.
- Nachtigall, S., et al. "Analysis of drop deformation dynamics in turbulent flow." Chinese Journal of Chemical Engineering.
- Napper, D. H. (1977). "Steric stabilization." Journal of Colloid and Interface Science **58**(2): 390-407.
- Napper, D. H. and A. Netschey (1971). "Studies of the steric stabilization of colloidal particles." Journal of Colloid and Interface Science **37**(3): 528-535.
- Nazir, A., et al. (2013). "Droplet break-up mechanism in premix emulsification using packed beds." Chemical Engineering Science **92**: 190-197.
- Nere, Nandkishor K., Ashwin W. Patwardhan, and Jyeshtharaj B. Joshi. "Liquid-phase mixing in stirred vessels: turbulent flow regime." Industrial & engineering chemistry research **42.12** (2003): 2661-2698.
- Paglianti, A. and G. Montante (2013). "A mechanistic model for pressure drops in corrugated plates static mixers." Chemical Engineering Science **97**: 376-384.
- Pal, R. (2000). "Shear Viscosity Behavior of Emulsions of Two Immiscible Liquids." Journal of Colloid and Interface Science **225**(2): 359-366.
- Peng, S. J. and R. A. Williams (1998). "Controlled Production of Emulsions Using a Crossflow Membrane: Part I: Droplet Formation from a Single Pore." Chemical Engineering Research and Design **76**(8): 894-901.
- Sahu, A. K., et al. (1999). "CFD modelling and mixing in stirred tanks." Chemical Engineering Science **54**(13-14): 2285-2293.

## References

---

- Schuch, A., et al. (2014). "Production of W/O/W double emulsions. Part I: Visual observation of deformation and breakup of double emulsion drops and coalescence of the inner droplets." Colloids and Surfaces A: Physicochemical and Engineering Aspects **461**: 336-343.
- Tadros, T. (2004). "Application of rheology for assessment and prediction of the long-term physical stability of emulsions." Advances in Colloid and Interface Science **108–109**: 227-258.
- Tadros, T. F. (1994). "Fundamental principles of emulsion rheology and their applications." Colloids and Surfaces A: Physicochemical and Engineering Aspects **91**: 39-55.
- Thakur, R. K., et al. (2003). "Static Mixers in the Process Industries—A Review." Chemical Engineering Research and Design **81**(7): 787-826.
- Tidhar, M., et al. (1986). "Characteristics of a motionless mixer for dispersion of immiscible fluids—II. Phase inversion of liquid-liquid systems." Chemical Engineering Science **41**(3): 457-462.
- Van den Akker, H. E. A. (2006). The Details of Turbulent Mixing Process and their Simulation. Advances in Chemical Engineering. B. M. Guy, Academic Press. **Volume 31**: 151-229.
- Walstra, P. (1993). "Principles of emulsion formation." Chemical Engineering Science **48**(2): 333-349.
- Zhang, L., et al. (2015). "A study of mixing performance of polyacrylamide solutions in a new-type static mixer combination." Chemical Engineering and Processing: Process Intensification **88**: 19-28.
- Hirschberg, S., et al. (2009). "An improvement of the Sulzer SMX™ static mixer significantly reducing the pressure drop." Chemical Engineering Research and Design **87**(4): 524-532.
- Ascanio, G., et al. (2004). "Measurement of Power Consumption in Stirred Vessels—A Review." Chemical Engineering Research and Design **82**(9): 1282-1290.
- Kumaresan, T. and J. B. Joshi (2006). "Effect of impeller design on the flow pattern and mixing in stirred tanks." Chemical Engineering Journal **115**(3): 173-193.
- Uppal, A., et al. (1974). "On the dynamic behavior of continuous stirred tank reactors." Chemical Engineering Science **29**(4): 967-985.

## References

---

Pacek, A. W., et al. (1998). "On the Sauter mean diameter and size distributions in turbulent liquid/liquid dispersions in a stirred vessel." Chemical Engineering Science **53**(11): 2005-2011.

Kumar, R. "Dispersion in stirred vessels." Journal of the Indian Institute of Science **72.3** (2013): 235.

Freudig, B., et al. (1999). "Dispersion of powders in liquids in a stirred vessel." Chemical Engineering and Processing: Process Intensification **38**(4-6): 525-532.

Lagisetty, J. S., et al. (1986). "Breakage of viscous and non-Newtonian drops in stirred dispersions." Chemical Engineering Science **41**(1): 65-72.

Coroneo, M., et al. (2011). "CFD prediction of fluid flow and mixing in stirred tanks: Numerical issues about the RANS simulations." Computers & Chemical Engineering **35**(10): 1959-1968.

Hobbs, D. M. and F. J. Muzzio (1997). "The Kenics static mixer: a three-dimensional chaotic flow." Chemical Engineering Journal **67**(3): 153-166.

Byrde, O. and M. L. Sawley (1999). "Optimization of a Kenics static mixer for non-creeping flow conditions." Chemical Engineering Journal **72**(2): 163-169.

Martínez, J., et al. (2015). "Influence of spatial discretization schemes on accuracy of explicit LES: Canonical problems to engine-like geometries." Computers & Fluids **117**: 62-78.

Jalali, A., et al. (2014). "Accuracy analysis of unstructured finite volume discretization schemes for diffusive fluxes." Computers & Fluids **101**: 220-232.

# Ringraziamenti

Sono arrivato al termine di un lungo percorso iniziato ormai 6 anni fa, pieno di sacrifici, lunghe giornate passate a studiare e di progetti sempre in attesa di essere consegnati. Ma, allo stesso tempo questi sono stati anni pieni di gioie e di soddisfazioni, gli anni della maggiore libertà e delle responsabilità, gli anni in cui ho conosciuto tanti nuovi amici con cui spero di continuare a condividere preziosi momenti. Questa tesi poi è il frutto di una meravigliosa esperienza all'estero durata 6 mesi, in Inghilterra, all'università di Birmingham. Ho sempre desiderato fare un'esperienza di questo tipo ma, non ho mai avuto davvero la forza di partire, il coraggio di andare in un posto dove non sarei stato in grado di comunicare. Alla fine le circostanze sono state tali da non poter dire di no, sono partito e tornato più determinato di prima, più consapevole dei miei mezzi e più ricco dentro. Infatti, in questi mesi spesi a Birmingham ho conosciuto molti ragazzi unici nella loro semplicità, provenienti da tutto il mondo che hanno saputo condividere con me le loro esperienze, le loro aspirazioni e anche le loro passioni.

Questa stupenda occasione di crescita mi è stata data dalla prof. dell'università di Pisa Elisabetta Brunazzi che non smetterò mai di ringraziare e dall'Ingegnere Federico Alberini che mi ha accolto nel suo ufficio a braccia aperte. Federico mi ha presentato tutti, mi ha sostenuto in tutto il mio lavoro di tesi e si è rivelato un valido collega e ancor più importante un amico sincero pronto a mettere in secondo piano anche il proprio lavoro per aiutarmi. Grazie Fede, non avrei mai potuto fare quello che ho fatto senza di te.

Chi però mi ha davvero portato fin qui, chi mi ha indirizzato sempre nel seguire le mie passioni sono i miei stupendi genitori, che insieme alle mie sorelle sono sempre state lì a fare il tifo per me. Papà, mamma gran parte di quello che ho imparato nella vita lo devo a voi e adesso non trovo nemmeno le parole giuste per ringraziarvi, ma sono sicuro che quando leggerete queste righe capirete tutto.

E' arrivato il momento di ringraziare la mia metà, la donna che ha sopportato tutte le mie discussioni da Ingegnere, che mi ha dato la serenità per andare avanti e mi è stata accanto. Tu che mi sei stata vicina anche quando eravamo lontani, passando un'intera estate con me in Inghilterra. Grazie Erica, grazie amore.

Infine, ma non per importanza, ringrazio tutti gli amici con cui ho avuto la fortuna di vivere qui a Pisa: Gianluca l'amico di una vita sempre lì, ovunque io fossi, Maurizio collega e fratello allo stesso tempo (quante ne abbiamo passate insieme), Sabino giocatore incallito di calcetto, Matteo, ragazzo davvero generoso, Manuele il perfezionista, Calogero e tutti gli altri. Tutti voi avete reso ogni mio giorno più leggero, nonostante lo studio e i problemi della via quotidiana.